Title

Compositional Analysis of Lacquer Alterations in Post-Angkorian Buddha Statues and a Novel 3D Approach to Their Conservation

Author

McGough, Jennifer

Publication Date

2023

Peer reviewed|Thesis/dissertation

UNIVERSITY OF CALIFORNIA

Los Angeles

Compositional Analysis of Lacquer Alterations in Post-Angkorian Buddha Statues and a Novel 3D Approach to Their Conservation

A thesis submitted in partial satisfaction of the requirements for the degree Master of Arts in Conservation of Cultural Heritage

by

Jennifer Rebecca Lee McGough

2023

ABSTRACT OF THE THESIS

Compositional Analysis of Lacquer Alterations in Post-Angkorian Buddha Statues and a Novel 3D Approach to Their Conservation

by

Jennifer Rebecca Lee McGough

Master of Arts in Conservation of Cultural Heritage

University of California, Los Angeles, 2023

Professor Ioanna Kakoulli, Chair

The Middle Period of Khmer history (15th to 19th century) was an age of transformation at Angkor, where heavy royal reinvestment of the formerly Hindu site with Theravada Buddhism's iconography and religious practices led to an era of reconstruction and pilgrimage to the site of Angkor Wat. Many of the Buddha statues collected and venerated in Preah Pean, on the second floor, and in Bakan at Angkor Wat have since been relocated to alternate storage or display. These include both stone and wooden statues, many of which still retain remnants of their decorative lacquered surfaces. It is evident that many of these statues have undergone historic instances of repair and relacquering during their veneration, as well as iconographic modification.

Current knowledge about the materials used in the historic restorations of these states is mainly derived from limited epigraphic evidence during the period combined with Cambodian lacquer traditions and international lacquer research. Given the variation in lacquer types and origins, material additives, fillers and bulking agents, and pigments across regions, this project

aimed to augment the understanding of traditional Cambodian lacquer use by identifying the components of lacquer layers used on these statues. The first stage of the project involved a visual survey of the collection aided by handheld digital microscopy and ultraviolet-induced visible fluorescence *in situ*, followed by the compositional analysis of samples taken from three stone and three wooden statues using portable X-ray fluorescence (pXRF), cross-sectional microscopy, and pyrolysis-gas chromatography/mass spectrometry (Py-GC/MS).

The primary binding agent for the analyzed layers was found to be thitsi lacquer, with layers of shellac and pine resin also present in a few samples. Drying oil was the most frequent additive to the lacquer mixtures, while carbohydrate and proteinaceous additives were not present. Cinnabar (HgS, mercury sulfide) and carbon black were identified as primary colorants for red and black, respectively, but the possibility of iron oxides (hematite or magnetite) could not be ruled out.

Compositional analysis was followed by the exploration of a potential treatment method for lacquered objects using modified fused deposition modeling 3D printers. An open-source design for paste extruders was fabricated and used to replace the standard extruders on commercially available 3D printers, allowing for the printing of non-standard, viscous mixtures.

The thesis of Jennifer Rebecca Lee McGough is approved.

Thiago Sevilhano Puglieri

Min Li

Ioanna Kakoulli, Chair

University of California, Los Angeles

2023

Table of Contents

List of Figures

List of Tables

Acknowledgments

I would like to start off by expressing my heartfelt thanks to my thesis advisor, Dr. Ioanna Kakoulli, for her help, support, and eternal patience through this process, made all the more difficult by a worldwide pandemic. I would also like to thank Dr. Christian Fischer, who was my co-advisor in all but name. I am so grateful for your continued support through every rabbit hole and hurdle we came across. My committee members, Dr. Thiago Sevilhano Puglieri and Dr. Min Li, also have my thanks for their patience and comments.

There are also so many others that made this work possible. I am eternally grateful to the Cambodia Ministry of Culture and the Angkor Conservation Offices for allowing me to conduct this work and the l'École française d'Extrême-Orient, Siem Reap for hosting me throughout the project. I want to thank Dr. Sophie Biard and Ms. Hang Chansophea, both of whose companionship and guidance helped me navigate both Cambodia at large and this project. They made the experience unforgettable and truly helped me find my direction throughout the work both there and on my return to the US. I'd also like to thank Eric Stocker and everyone at the National Museum of Cambodia – thank you for welcoming me into your workshops, for sharing your knowledge and expertise, and your patience at my endless questions!

At UCLA, I'd like to thank the rest of my department for their support: Glenn Wharton, Ellen Pearlstein, and Alice Paterakis. The biggest thank yous must also go to William Shelley for his flexibility as we tried to obtain strange materials during a strange time, Deidre Brin for being my enthusiastic partner in crime as we wrestled the printers into submission, Doug Daniels for being a fantastic board to bounce ideas off of and for helping with 3D scanning, and Shaharoh Chism for her help in all the logistical issues that crept up near the end.

Outside of UCLA, I want to thank Dr. Catherine Matsen at the Winterthur/University of Delaware Program in Art Conservation, who not only provided me access to the equipment necessary to complete my analyses but also valuable mentorship as I explored my data. Similarly,

thank you to Dr. Michael Schilling at the Getty Conservation Institute for his endless patience and eagerness to share his knowledge with student. I have learned so much from you both!

Last but not least, thank you to my beloved family and friends. To my dear parents who have supported me since day one and whose love and inspiration have led to me to where I am today – Thank you. To my friends in LA and around the world that have been by my side through thick and thin – Thank you. To my cohort that laughed and cried with me every step of the way – Thank you, and we made it.

Thank you all so very, very much.

1. Introduction

The conservation of Asian lacquerware represents a complex challenge for conservators and researchers. On most objects, the lacquer is stratified with each layer often featuring a specific formulation based on working properties for an intended function. Additives that affect these working properties can greatly contribute to lacquerware deterioration; therefore, understanding their composition is integral to designing conservation treatments that address the appropriate variables.

Within the last two decades, scientific inquiry into this subject has expanded significantly, spearheaded in regions where lacquer traditions continue to thrive and grow, such as Japan, China, and Thailand. Yet, lacquer traditions existed across all of East and Southeast Asia, including regions like Cambodia that experienced a modern decline in its practice and cultivation. While lacquerware from neighboring regions has received more attention, these cultures have left traces of their lacquer history in archaeological and historical records. They did so through objects with preserved decorative surfaces and repairs, as well as inscriptions documenting its symbolic use. Scientific evaluation of these objects will undeniably augment the wider corpus of knowledge on Asian lacquer history and use, as well as provide important insight into the continued care and preservation of these objects in collections residing both in their home countries and abroad.

Conservation treatments of these objects also present complications. Lacquered objects in their native communities have traditionally been repaired using lacquer itself. While this method can be the most aesthetically, culturally, or spiritually appropriate, lacquer remains a difficult material to process and apply by conservators that have not trained in the art. Novel technologies such as additive manufacturing (3D printing) provide a promising solution by allowing for predictable replication of workflow and customizable application, which could increase the accessibility of this material type for use by a larger number of conservators worldwide.

2. Research Scope and Significance

The scope of the thesis is twofold: 1) to analyze scientifically decorative lacquered surfaces and lacquer repair materials applied to post-Angkorian Buddha statues from the understudied Preah Pean[1] collection from Angkor Wat and now at the Angkor Conservation Offices and 2) to explore the application of modified 3D printers in the conservation of large-scale lacquered objects. It aims to identify the most practical printers in terms of versatility, applicability, and accessibility, followed by the fabrication of a working modification for printing non-standard substances.

The Preah Pean collection has never been evaluated using pyrolysis-gas chromatography/mass spectrometry and contemporaneous documentation of the craft from the period is limited, so this thesis is a first step towards understanding the scope of materials used in alterations applied to such statues during this period in Cambodia. This part of the thesis is further completed in two phases: the first consists of an observational study identifying material morphology of the collection at Angkor Conservation Offices followed by analytical analyses completed on samples taken from six of the statues.

[1] The Preah Pean collection is alternatively referred to as “the Cruciform Gallery” or “The Hall of a Thousand Buddhas”.

3. Part 1: Compositional Analysis of Post-Angkorian Lacquered Buddha Statues

3.1 Background

Lacquer in modern vernacular has grown to encapsulate almost any natural or synthetic organic film-forming coating used as surface varnishes for wood, metal, etc. In East and Southeast Asia, however, lacquer refers specifically to naturally produced, film-forming tree sap that polymerizes by enzymatic reactions into a durable, glossy coating (Figure 1). While this material has been historically referred to by a variety of generic names in the West, including “Asian lacquer,” “oriental lacquer,” or the Japanese-derived “Urushi”, it has a specific designation in each of its native cultures. As mentioned, Japan calls this material “漆” / ”うるし” (urushi), but it is “生漆” (shengqi) in China, "sơn mài” in Vietnam, “ម្រ័ក្ស” (mreak or mrāk) in Cambodia, “รัก” (rak) in Thailand, and “thitsi” in Burma to name a few (Lu & Miyakoshi, 2015). The history of this material spans thousands of years of use, either functionally as a protective coating or adhesive, or as a decorative surface. As knowledge of the material grew over time, lacquer masters across cultures developed complex recipes and new techniques to produce lacquerware exhibiting colored, incised, textured, gilded, or inlaid surfaces, the results of which have survived into the modern age.

Figure 1: Stepwise lacquerware construction display at Artisans D'Angkor in Siem Reap, Cambodia

3.1.1 Lacquer chemistry

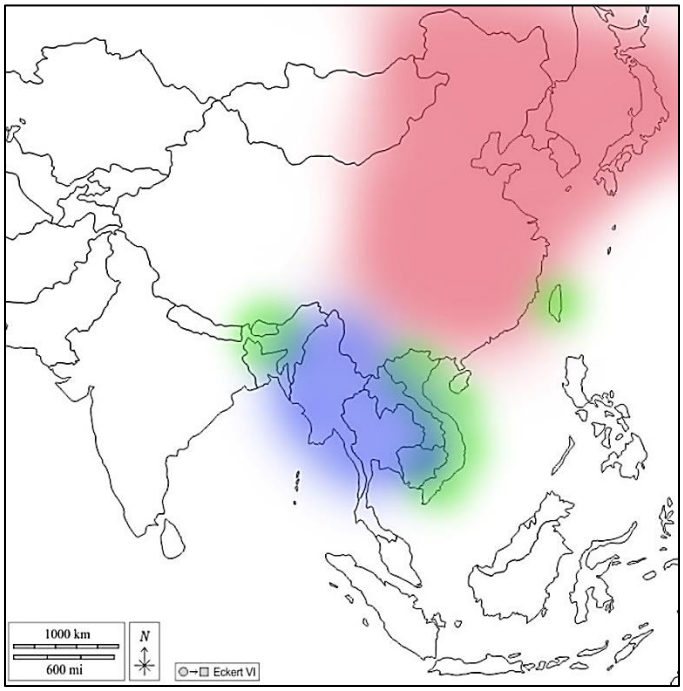

Figure 2: Map of general lacquer tree grown distribution by catechol identifiers - Urushiol (red), Laccol (green), and Thitsiol (blue).

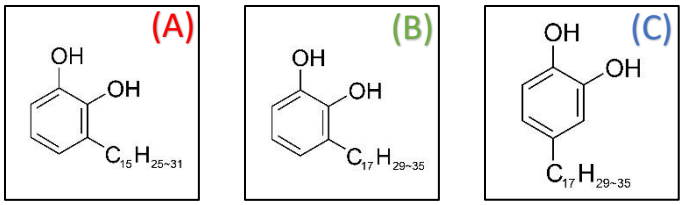

Figure 3: Molecular structure of (A) Urushiol, (B) Laccol, and (C) Thitsiol

Lacquer trees belong to the Anacardiaceae family, which includes roughly 600 species internationally. Most of these species (Figure 2) grow in the subtropical climate of Southeast Asia and some in the evergreen forests of East Asia (Lu & Miyakoshi, 2015). Chemical studies of sap taken from trees used in modern lacquer production combined with characterization of historic and ancient lacquerware has identified four of these species as traditional sources, regionally differentiated and distinguishable by their primary film forming catechol derivatives (Figure 3) (Lu & Miyakoshi, 2015; Schilling et al, 2016). *Toxicodendron vernicifluum* (previously classified as *Rhus vernicifera*) grows in East Asia, throughout China, Japan, and Korea. It's characterized by Urushiol, a blend of 3-substituted catechol derivatives featuring n=15 carbon chains with 0-3 olefins. Toxicodendron succedanea (previously classified as Rhus succedanea) is mainly harvested across Vietnam and Taiwan and has the principal component, Laccol, a blend of 3-substituted catechol derivatives with n=17 carbon chains accompanied by 0-3 olefins. *Gluta usitata* (previously classified as *Melanorrhoea usitata*) and *Gluta laccifera* both grow in Southeast Asia. The former is harvested mainly in Myanmar, though it has also been found in Cambodia, Laos, and Thailand. *Gluta laccifera*, on the other hand, is primarily found and harvested in Cambodia, but also grows in Thailand and Vietnam (Heginbotham & Schilling, 2009;

Szczepanowska & Ploeger, 2019). Both species' characteristic component is Thitsiol, a mixture of mainly 4-substituted and some 3-substituted catechol derivatives with n=17 carbon chains (Lu & Miyakoshi, 2015).

Raw lacquer sap is made up of three main components aside from the aforementioned characteristic primary catechol derivative. Laccase—an enzyme containing about 55% protein and 45% carbohydrate, with a 0.23% concentration of copper—is the catalyst for polymerization. 1-5% of the lacquer is made up of glycoproteins, which are roughly 10% carbohydrates and 90% proteins composed of 15 amino acids. Lastly are polysaccharides, which act as a dispersing unit for the laccase and catechol derivatives.

The collected lacquer latexes are water in oil emulsions, where the water phase is generally composed of 20-30% water, 5-6% polysaccharides, and roughly 1% of the laccase enzyme. The catechol derivatives make up the bulk of the lipid component (60-70%), with an additional 2-3% glycoproteins (Szczepanowska & Ploeger, 2019).

3.1.2 Lacquer curing mechanism

Lacquer curing can take up to 2 months in higher relative humidities (RH), but improper environments can lead to resin that never cures. The ideal environment is about 80% humidity and 30°C (E. Stocker, personal communication, September 15, 2022).

The mechanism for curing is a two-step oxidation process. The first step is the laccase-catalyzed oxidation in which the lipid components are catalyzed by the laccase enzyme to form quinone radicals. Radical transfer occurs to form dimer, trimer, tetramer, oligomers. This is then followed by auto-oxidation of the side chains when the catechol monomer concentration is less than 30%, with cross-linking occurring when the peroxy radicals formed by reaction with oxygen attach to other double bonds or allyl radicals in other side chains. This reaction is inhibited, however, by the antioxidant phenolic hydroxyl groups of the catechol ring, which are reduced by the catalyzed polymerization and obstruct contact with the unsaturated side-chains, which causes the slow cure rate of lacquer (Webb, 2000; Ishimura & Yoshida, 2015; Lu & Miyakoshi, 2015).

Lacquer film, once cured, is composed of densely packed grains. Spherical particles of polymerized urushiol form. Figure 4 shows the structure of these particles, which are coated with a layer of polysaccharides with the glycoproteins acting as an adhesive between the particles and providing an oxygen barrier, contributing the durability of cured lacquer (Obataya et al., 2002; Mcsharry et al., 2007).

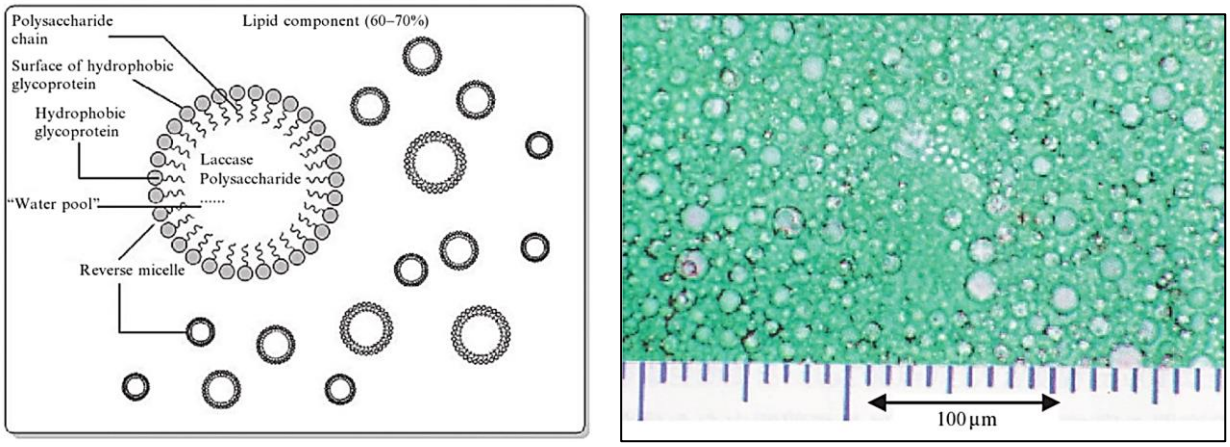

Figure 4: (Left) Diagram of grain micelle structure and (Right) photomicrograph of lacquer sap demonstrating granular structure. Images from Lu & Miyakoshi, 2015.

3.1.3 Harvesting the raw materials

Collecting lacquer sap is similar to the process for collecting gum or tapping syrup. The basic principle involves incising the trunk and collecting the exuded sap in a container. Trees can typically flow for about 20 hours before the incision seals.

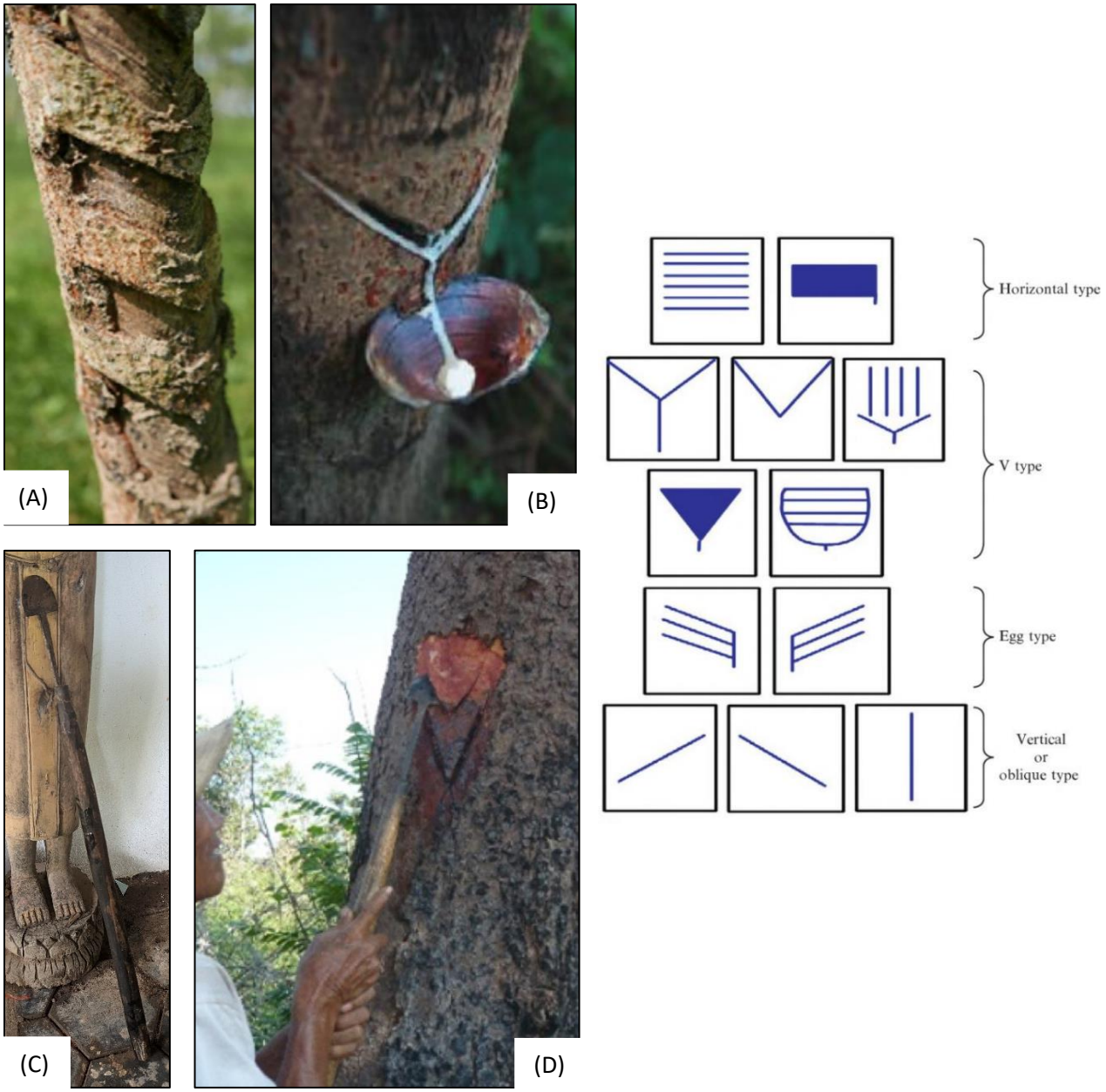

Figure 5: (Right) Diagram of harvesting cuts for lacquer trees. (Left) Elements of the harvesting process. Old, closed chevron cuts are visible on (A), which (B) shows a fresh V type cut actively producing the white sap into a seashell collection dish. A half-moon bladed instrument used in Cambodia (C) is used for cutting V-shapes into the trunk (D). Images from Lu and Miyakoshi, 2015; Szczepanowska and Ploeger, 2019; and author.

Detailed practices for harvesting lacquer differ between regions. Types of incisions for tapping can be seen in Figure 5. In general, the horizontal type is popular in Japan and sometimes in Vietnam; V and egg in China, Vietnam, Cambodia, and Myanmar; Vertical and oblique in Thailand and Myanmar. The incision releases the sap, but the shape provides a channel to direct

the flow into collection vessels, which can be cups, leaves, bamboo containers, etc. (Lu & Miyakoshi, 2015).

Multiple factors may also contribute to the yield and quality of the sap produced, including but not limited to tree age, growth environment, and collection season. Sap can only be harvested from adult trees in which the laticiferous canals are fully developed. These canals are specialized cells that contain latex and contribute to the specialized production of metabolites for the tree. The larger these canals are, the better and higher quality sap the yield (Zhao et al., 2013). This means that lacquer trees are generally tapped between 5-15 years old.

The exact age can also depend on the region and type of lacquer produced. In Japan, where lacquer is actively cultivated, trees are tapped only once at 10 years old for the highest quality sap, then cut down and replaced (E. Stocker, personal communication, September 15, 2022). In China, whose production is largest in the world, providing 85% of the global output, several germplasm varieties of Toxicodendron vernicifluum are cultivated, such as “Dahongpao”, “Gaobachi”, and “Huangmao Guizhou” (Bai et al., 2022). These varieties are tapped at different times based on their rate of bark growth, which is related to the rate of laticiferous canal development (Zhao et al., 2013). For example, the sap from HuoYanzi can be collected after only 5 years of growth, while Gaobachi varieties develop slower and need 10 years before tapping (Lu & Miyakoshi, 2015).

Cambodia, on the other hand, does not have widespread cultivation of lacquer trees in modern times. The practice has faced a great decline because the income obtained from selling traditional lacquered objects did not compensate for the cost of producing lacquer and lacquerware objects (Ly, 2021). No organized groves exist for lacquer sap collection and only a few households in the villages of Trea and Pralay in Kampong Thom province, central Cambodia, continue to practice their traditional lacquer work. Most known and tapped lacquer trees grow at the base of mountainous regions and grow within or alongside other cultivated landscapes, such as rice fields, or in forested areas. Lacquer collectors must travel from tree to tree to obtain the

Figure 6: Saps from the three catechol types. Image from Lu et al, 2013.

sap, so the overall yield is quite low. The trees themselves are also older, harvests beginning when they reach about 15 years. The sap of trees that produce thitsi lacquer slightly differ from urushi or laccol (see Figure 6). It is usually thicker and more viscous than urushi or laccol, flowing less readily from incisions (E. Stocker, personal communication, September 15, 2022).

The season for harvesting may also vary slightly between regions as environmental changes affect tree growth. Higher temperatures and sun increase yield, while rain, low temps, and reduced sun can reduce it. Generally speaking, however, lacquer trees are tapped during the peak of leaf growth, which is associated with promoting the assimilation of laccase, the enzyme responsible for the unique curing mechanism of lacquer, between June and October (Lu & Miyakoshi, 2015). As mentioned previously, depending on the tree, some can be tapped repeatedly, and some only once.

3.1.4 Refinement and application

Refining sap varies based on local techniques and the extent of such processing depends on the intended use for the lacquer. Raw lacquer is used as an adhesive for assembling tools, coating household items as a protective layer, and caulking material for boatmaking in Cambodia (Sitha, 2002). For lacquerware objects in Japan, raw lacquer is also applied as a surface coating to reinforce the substrate and smooth out the surface (Lu & Miyakoshi, 2015). However, the water in oil emulsion is not a stable state. If left in its raw form, lacquer can precipitate an aggregated

plant gum (Kumanotani, 1995). Refining the lacquer removes impurities and increases its overall stability, and is generally used for the decorative finishing layers on most lacquerware.

Figure 8: Brushes used to apply lacquer layers.

Universal refinement begins by first filtering to remove wood chips, leaves, insects and other impurities. The lacquer can then be used in its raw state or further processed. In Japan, lacquer is matured for roughly a year before any additional processing is conducted and the matured lacquer is called *ki-urushi* (Mcsharry et al., 2007). After this aging period, the Japanese termed *kurome* treatment can be applied. The lacquer is stirred for 30 minutes at room temperature, followed by heated stirring for an additional two hours at a temperature no greater than 45°C to avoid deactivating the enzyme. *Kurome* results in the evaporation of water, polymerization of urushiol, and reaction of the urushiol with glycoproteins, making it more stable overall (Kumanotani, 1995). In Cambodia, a similar method of "cooking" lacquer has been documented in the creation of performance masks (Figure 8). Raw lacquer is placed into a large pot and heated until the water evaporates and the lacquer is "dry," after which point additives are mixed in (Sitha, 2002).

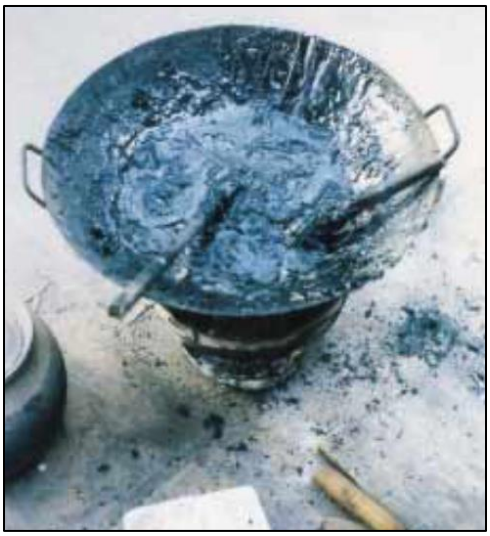

Figure 7: Cooking lacquer with local resin additives in Cambodia. Image from Sitha, 2002.

Like refinement, the specificities of application method vary from region to region but the general principle is relatively similar as it depends

primarily on natural limitations of the material. Usually, the intended form of the lacquerware object is first created out of a substrate material such as wood, stone, plant fiber, clay, etc. The lacquer is then applied by brush (see Figure 7) in thin successive layers. Because the curing process requires contact with oxygen and humidity, the most external parts of a layer will begin to cure first. Therefore, thick layers may result in incomplete curing once the external surface is sealed. Each layer is sanded or polished before the next layer is added. Additives to the lacquer recipes also tend to follow the same pattern. Thicker filled materials are added to lower levels, particularly the ground and build-up layers, which tend to be uncolored, since they are not visible in the final product. Finer inclusions are added to layers closer to the external surface to begin smoothing it out, while the final ones are generally unadulterated by fillers. These finishing layers can include decorative elements, such as pigment. The external surface can also be further modified with added gilding, inlays, or molded appliques depending on regional, cultural, or spiritual preferences (Webb, 2000; E. Stocker, personal communication, September 15, 2022).

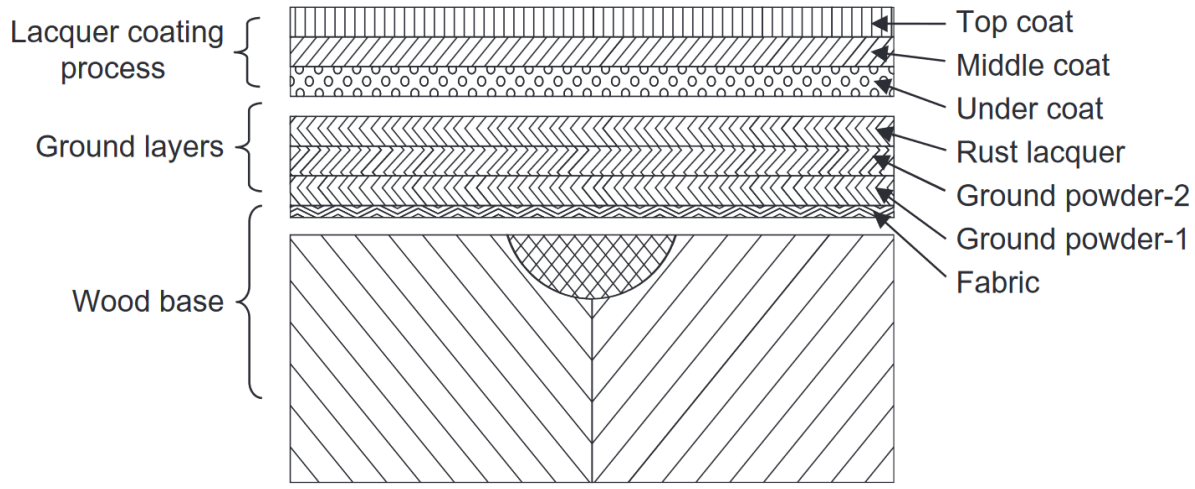

Figure 9: Example of Japanese-style lacquer layer buildup. Images from Lu and Miyakoshi, 2015.

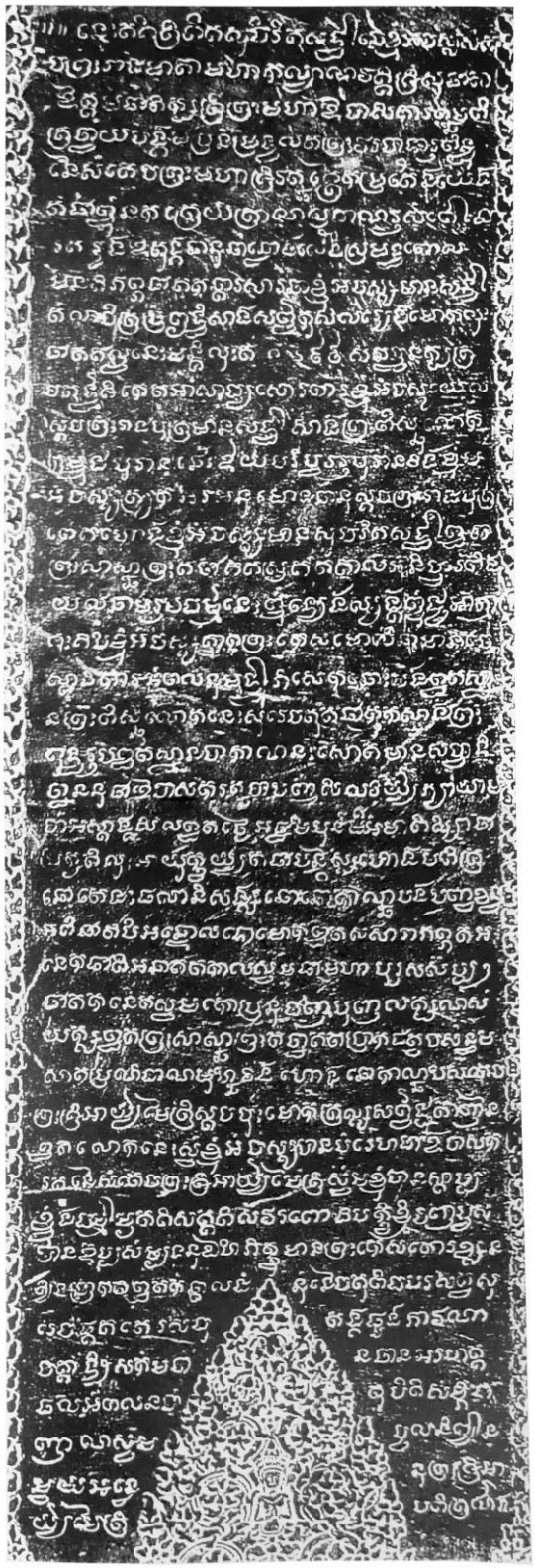

Figure 10: Inscription from Preah Pean describing the Queen Mother adding her burned hair to lacquer used to restore the Bakan Buddha statues. Image from K. 303, IMA 2 – APSARA 2013.

3.1.5 Additives

Additives for lacquer vary depending on region, function, and use. Bulked lacquers have a variety of uses, from functional caulking to smoothing ground layers for decorative lacquerware, and their composition can change drastically from region to region or even object to object. In Myanmar, wood sawdust is documented for utilitarian uses of lacquer, such as waterproofing objects. Meanwhile, Japan is well known for is used of gradated clays (*tonoko* and *jinoko*) in the preparation of hollow-form lacquerware objects (E. Stocker, personal communication, September 15, 2022). Calcium carbonate (crushed shell) has also been used in lacquer “mortars” (hard bulked layers) in Cambodia to relacquer statues (Ly, 2021). Given the relative expense of true lacquer and since these bulked layers tend to be visually hidden beneath the finer decorative layers, other materials have served as additives in East Asia, not only for their working properties but also for cost-saving measures. These include various alternative binders (e.g., blood, animal glue, *funori* seaweed adhesive, starch pastes) as well as drying oils (e.g., tung, peanut, rapa, sesame), which also have the added benefit of increasing lacquer plasticity and gloss (Schellmann,

2011). For molding compounds used to create appliques or other decorative elements in Cambodia, lacquer is cooked following the aforementioned method and mixed with fillers such as *pheh* (ash) made from burnt *cham boeung* (rice-straw) or *sleuk tnaut* (palm leaves from *Borassus flabellifer*) (Sitha, 2002). This has also been observed in Myanmar for ceremonial objects, such as statues (Szczepanowska & Ploeger, 2019). Other burned materials have been incorporated into lacquer recipes as well, some as a black pigment and others as spiritual offerings. Epigraphical inscriptions at Angkor Wat's Preah Pean include an account by the Queen Mother describing the later phenomenon, in which her cut hair was burned and mixed into the lacquer used to restore the Bakan statues of Buddha as a sign of her devotion (see Figure 10).

There are limited other natural pigments used in traditional lacquer production due to the material's naturally acidic nature, meaning organic dyes and pigments will break down. Other mineral pigments used throughout history, such as lead white, azurite, or malachite, also decompose in this environment. These reactions can further hinder the lacquer curing process, as decomposition can raise the overall pH of the lacquer and deactivate the catalyzing laccase enzyme (McSharry et al., 2007). Therefore, the most frequently used colorants were generally limited to carbon/bone black and magnetite (Fe_3O_4, iron oxide) for black, hematite (Fe_2O_3, iron oxide) and cinnabar (HgS, mercury sulfide) for red, and orpiment (As_2S_3, arsenic III sulfide) for yellow (Mcsharry et al., 2007; Szczepanowska & Ploeger, 2019). Black could also be obtained as a chemical reaction with iron hydroxide or iron acetate added during the refinement process (McSharry et al., 2007; Liu et al., 2023)

3.1.6 Deterioration

Lacquer's popularity as a coating and decorative material in the East and Southeast was not only for its aesthetic qualities, but also for its protective ones. Once fully cured, newly applied lacquer is tough, insoluble, and chemically stable. Organic substrates used to produce the object's form are relatively protected from environmental fluctuations, moisture, and pest intrusion.

Yet, over time, the protective qualities of this coating are affected by natural deterioration mechanisms. These fall into two categories: chemical and physical. The chemical deterioration of lacquer involves the breakdown of its existing chemical bonds and the formation of new ones via reactions with the environment, reducing its overall stability. Physical deterioration of lacquer arises from mechanical influences that lead to surface and structural damages. These types of degradation are often interrelated and can exacerbate each other.

The primary agent for the chemical deterioration of lacquer is light. Light exposure causes oxidation, chain scission, and cross-linking that affects the gloss, transparency, and color of the lacquer. Surfaces will dull and grow opaquer, while colors fade or become less distinct. It can also cause extensive embrittlement and micro-cracking throughout the surface (Webb, 2000; Webb et al., 2016). The photooxidation of the surface makes it more soluble in water, so contact with liquid can cause color change and tidelines. Oils, including those from hands, can cause additional microcracking and etch permanent fingerprints into the surface. These reactions turn the previously resilient coating highly sensitive, leaving it vulnerable to further damage from physical means. The embrittled surface is easily scratched or chipped, so handling or other mechanical manipulations can easily lead to flaking, loss, or abrasion (see Figure 11).

Of course, deterioration of the decorative surface also reduces its protective quality. Previously encapsulated substrates are now exposed to environmental fluctuations, which can cause a variety of issues depending on the substrate material. Organic materials like wood and plant fibers are highly susceptible to humidity, causing dimensional change as the plant structure adapts to varying moisture contents. Such deformation can place additional stress on the overlying lacquer which cannot swell or shrink to the same degree. This structural incompatibly may lead to delamination of the coating from the substrate, cracking, or losses. Inorganic materials like stone or ceramic may also have similar physical damages, though resulting from different means. Depending on the source, natural clay and stone often contains soluble salts that

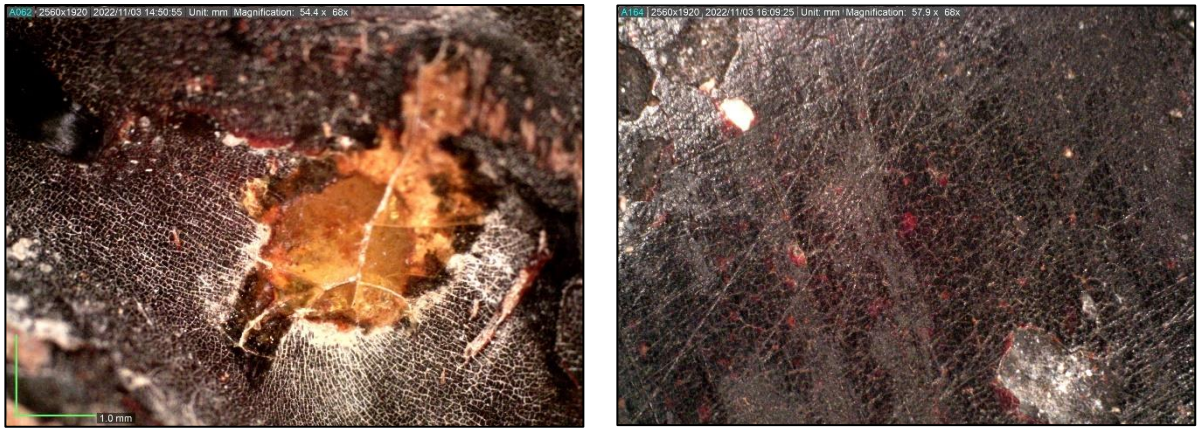

Figure 11: (Left) Microcracking exacerbated by differential shrinkage of resin droplet on lacquer surface. (Right) Increased transparency of and scratches on aged lacquer.

solubilize and recrystallize with fluctuations of humidity. The impermeability of the lacquer coating in comparison with the surrounding material can cause the salts to recrystallize just below the surface as the humidity drops, creating shearing losses and delamination of the lacquer (Webb, 2000).

The formulation of each layer may also have an effect on how and to what extent the lacquer degrades. This topic is an ongoing question for researchers, because—as seen from the previous section—the types and amounts of additives in lacquer recipes can differ greatly. Some modern studies have looked into pinpointing the different effects of additives, such as Han et al. (2023) who found that iron contributed to a loss of gloss and increased blanching, cinnabar led to pitting of the surface and darkening from chemical darkening of the pigment, and different formulations affect the width and extent of microcracking differently. It is because of this variation of material and resultant degradation that understanding the composition of lacquer layers is imperative to the continued preservation of lacquerware in cultural heritage.

3.1.7 Lacquer use on Middle Period statues at Angkor Wat

The Middle Period of Khmer history—spanning from the 15th to 19th century—was marked in Angkor by grand transformations. During this time, there was heavy royal reinvestment of the formerly Hindu site with Theravada Buddhism's iconography and religious practices. Inscriptions made in this period describe an era of reconstruction and pilgrimage to the site of Angkor Wat. Two inscriptions in the northwestern wing identify King Ang Chan as the patron of narrative panels completed in this area in 1564 AD. Inscriptions in Preah Pean and Bakan recount additional restorations and alterations at the temple, notably the modification of the central sanctuary. Additional inscriptions carved in not only Khmer but also foreign languages—for example, Japanese and Arabic—are visible in Phnom Bakheng and Preah Pean, indicating both the domestic and international draw this site had for pilgrims and merchants. The accumulation of sculptures (see Figure 12) in the Buddhist halls of Angkor Wat are linked to these pilgrimages (Thompson, 2004).

Figure 12: Historic photo of Preah Pean Buddha statues in situ, c. 1930. Image from l'École Française d'Éxtrême-Orient CAM05055.

Many of the Buddha statues collected and venerated in Preah Pean, on the second floor, and in Bakan at Angkor Wat have since been relocated to alternate storage or display, mainly at the Angkor Conservation Office (ACO)

and at the National Museum of Cambodia in Phnom Penh. Others are now displayed in Preah Norodom Sihanouk Museum and Angkor National Museum. These include both stone and wooden statues with varying levels of preservation, many of which still retain remnants of lacquer. It is evident that many of these statues have undergone historic instances of repair and reconstruction in line with the efforts described in the aforementioned inscriptions, as well as iconographic modification as the site shifted into Theravada Buddhism; however, contemporary research into these methods of restoration and the materials used is lacking.

Current knowledge about the materials is mainly derived from the limited epigraphic evidence combined with Cambodian lacquer traditions and international lacquer research. While the collection has been evaluated and catalogued numerous times since its initial discovery in Angkor Wat, the inventories that include notes on the objects' conditions and materials are based almost exclusively on visual data. Madeleine Giteau (1975) describes the technique of manufacture and the methods of historical repair found on both stone and wooden statues dating from the middle period, as well as commenting on the practice of adding new layers of lacquer and gilding to venerated statues. She also describes the resinous adhesives found on some of the statues housed at ACO, but no analysis was completed on any of the materials. In 2012, Runkel et al published a compositional analysis of the pigments found in multiple 9^{th} to 10^{th} century Khmer brick temples. Similarly, the same year Uchida et al (2012) published an analysis of polychromy found on the walls of Preah Pean. Both of these analyses provide insight into the coloring substances used in Cambodia before and during the middle period. While this may identify certain pigments and binders that may have been available for use in the restoration of statues, none of them are specific to the statues themselves or lacquer technology that may have utilized pigment or binder additives in their formulations. In fact, lacquer is not found or evaluated in either publication. Southeast Asian lacquers have been catalogued and characterized in technical studies completed by Heginbotham and Schilling (2009) and by Szczepanowska (2019), but neither were in reference to statuary. In 2003, an important conservation treatment was carried

out on the statue of Ta Reach at Angkor Wat by the German Apsara Conservation Project (GACP) in which the lacquered surface was treated. This intervention involved extensive collaboration with local communities where a clear preference for original, local, and natural materials was emphasized. As a result, this treatment was the first attempt to use natural lacquers in stone conservation work in Angkor, but compositional analysis of the pre-existing lacquered surface was not completed within the scope of the work (Warrack, 2011; Warrack, 2013; Ly, 2021).

That is not to say that, overall, knowledge of techniques of lacquerware production and repair from this period have entirely disappeared. Traditional lacquer artists continue to produce lacquerware and train artisans, using methods and recipes such as those described by An Sitha (2002) in the production of lacquer masks (Figure 13). Similarly, the material is still used to create functional lacquerware (*khmuk mreak khmer)*—such as household utensils and coated baskets—in the rural areas of mountainous regions where the lacquer trees (*dam kroeul)* naturally grow. Conservators at the ACO have also used traditional methods of cooking and bulking tree sap and lacquer to repair losses in wooden statues (C. Hang, personal communication, October 4, 2022). Similarly, one of the Buddha statues at Pre Rup temple in Angkor was treated in 2020 by a Cambodian conservation team and supervised by a lacquer conservation specialist from Stocker Studio in Siem Reap province, Cambodia. Raw lacquer mixed with petrol was used as a mastic to fill the losses and subsequent layers of polished lacquer were built up until a final iron oxide pigmented layer of *chrey krem* (*Ficus benjamina*) was used to tone it (Ly, 2021).

Figure 13: (Left) Mask by An Sitha. (Right) Buddha figurine by Stocker Studios.

While compositional analyses have not been previously conducted on the statues from Preah Pean, other statues dating to the same period or reflecting similar historical interventions from other sites in Cambodia have been evaluated. In 2000, the stone conservation workshop at the National Museum of Cambodia initiated a project to study and restore a Buddha Statue from Wat Kampong Luong in Angkor Borei, Southern Cambodia. While the Indian-style statue is dated to the Pre-Angkorian Phnom Da period (6th century), it has undergone various alterations and additions later in its history, including modification of the cranial protuberance, reshaped hands, and reformed facial features. Study of the stratigraphy of the successive layers revealed, below the recent layers of overpainting, thick layers of coatings and lacquers corresponding to phases of major additions and remodeling. The hard black mortar was analyzed and found to be a traditional mixture of crushed shell, rice starch, and palm sap. Further below, in contact with the stone, there were remnants of old black coatings and red lacquers much finer in thickness (Porte, 2002; Ly, 2021). However, the type of lacquer in these layers and their individual compositions

were not studied. Another study was completed on a single sample from a Cambodia-attributed wooden Buddha dating to the 16th century using Py-GC/MS. This sample showed the distinct markers for thitsi lacquer, with a high likelihood for added drying oil with no added proteinaceous no polysaccharide materials (Tamburini et al., 2017).

Yet, it is important to note that the international origins of many visitors to Angkor Wat during the middle period may have brought the influence of foreign lacquerware technology and new materials that could also have been adapted to the repair and modification of the statues at Angkor. Evidence of such knowledge exchange may already be visible in the losses on some of the seated stone Buddhas, where layers of textile can be seen beneath the raised lacquer surface (see Figure 14). This is a technique similar to the Japanese dry lacquer method of *kanshitsu* (E. Stocker, personal communication, September 15, 2022) and could have been adapted for use on the statues in order to modify the original figures seated on Nagas to align with later Buddhist iconography.

Figure 14:(Left) Buddha statue with evidence of textile alterations. (Right) Enlarged chest area with clear textile layers beneath lacquer losses.

3.2 Materials and Methods

3.2.1 Phase 1: Visual survey

3.2.1.1 Ultraviolet (UV)-induced, visible fluorescence photodocumentation

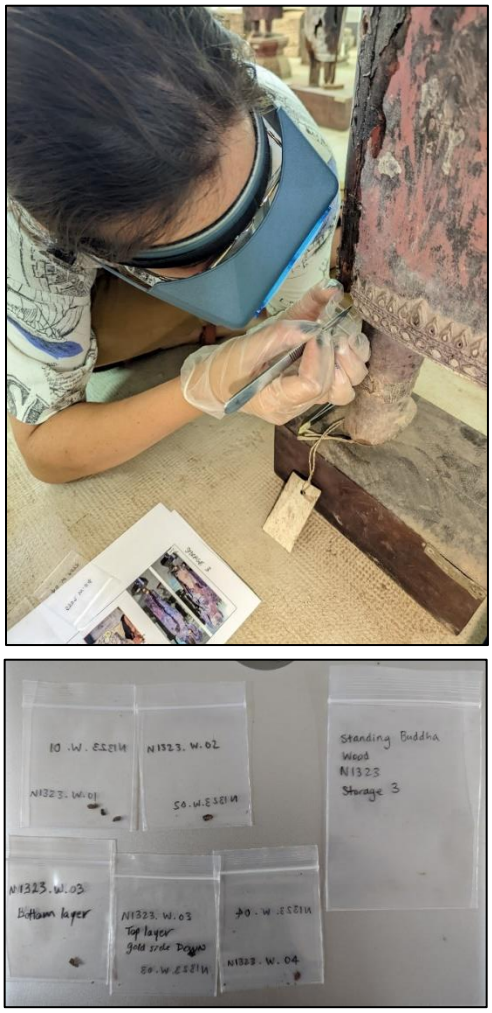

Figure 15: (Top) Sampling for Py-GC/MS. (Bottom) Bagging samples for transport.

The ultraviolet (UV) fluorescence photography conducted during this survey was done *in situ.* The warehouses housing the collection are very open, with grated windows that cannot be closed and have no covering. With no ability to control the general lighting, fluorescence was attempted in localized areas using draped fabrics or other light-blocking materials to reduce overall brightness, but it was rare to have complete darkness. The interaction between UV light and the materials on the surface was analyzed using UV-triggered visible fluorescence imaging to glean insights into surface properties. UV illumination was provided by a handheld UV flashlight with wavelength peaks at 395 nm. Photos, where possible, were taken using a Google Pixel 6 phone camera (50 MP, f/1.9, 25mm (wide), 1/1.31", 1.2µm, Dual Pixel PDAF, Laser AF, OIS).

3.2.1.2 Digital photomicroscopy

Portable digital photomicroscopy was completed with a Dinolite Edge Digital Microscope (Model: AM73915MZT). This was used to study surface morphologies of the statues, particularly in areas of loss where underlying materials were visible. It was also used to study lacquer layers where loss revealed multiple iterations of relacquering. Visuals were tracked and images taken using the DinoCapture 2.0 software by AnMo Electronics Corp.

Figure 16: Sampled Buddha statues from left to right: 2051, N509, 2259/N165, 5509, N1323, N1420.

3.2.1.3 Sampling

Six statues (Figure 16) were selected to sample for subsequent destructive material analysis[2]. The locations of sampled surfaces are listed in alongside cross section images in Appendix A. Particular care was taken to sample only small amounts of surface material with no damage to the statue's structure (see Figure 15). The location selected for sampling on each statue was representative of the materials in that section, but preference was given to areas of limited visibility, such as along pre-existing loss edges or on the back and bottom of the statue, as these are actively venerated icons.

Samples measured roughly 3-4 mm^2 in size. 2 mm^2 is generally sufficient to obtain enough material for pyrolysis-gas chromatography/mass spectrometry (Py-GC/MS); however, a slightly larger sample was required to account for inevitable material loss during transportation, as an attempt to maximize retrieval of degraded layers that escaped visibility in digital microscopic observation, and to allow for the mounting of cross sections. Samples were stored in labeled plastic bags and transported in a foam-padded plastic box to reduce vibrations and potential material loss (see Figure 15).

[2] Destructive analysis refers to scientific processes that require or result in damage to the object and/or destruction of a sample taken from the object in order to obtain an analytical result.

3.2.2 Phase 2: Material Analysis

3.2.2.1 Portable X-ray fluorescence (pXRF)

All samples were analyzed with X-ray fluorescence spectrometry (XRF) at the UCLA/Getty Conservation training laboratories. Each sample was placed inside an open ended XRF sample cup sealed on one side with Prolene® 4.0µm thin film. Spectra were collected with a handheld Bruker Tracer III-SD portable X-ray fluorescence spectrometer at 40 kV and 5.5 µA for 180 seconds with no vacuum and no filter. Spectrum interpretation was completed with the S1PXRF (version 3.8) software and overlayed with related spectra for comparative visualization using the Artax 7 software, both from Bruker. Given the small size of the samples, each sample was analyzed at least twice, once on either side – top: most external layers; bottom: lowest layers adjacent to substrate. Some samples had separated along layer interfaces during removal from the statues resulting in 34 separate "samples". In these cases, the top and bottoms of each part was analyzed. For evaluation in excel, the two spectra for each sample were overlayed and averaged to determine the relative intensity of each element.

It must be noted that the Bruker Tracer III-SD has a 10mm spot size for analysis, which is larger than most of the samples. In addition, since only the coatings and repair materials were sampled, most of the samples were relatively thin, likely lacking the infinite thickness[3] of ideal pXRF samples. As a result, X-rays were likely lost from the sample and it is probable that there is underreporting of some elements.

3.2.2.2 Cross-sectional analysis

A stratigraphic sample was removed from larger sample specimens with a scalpel under a stereomicroscope. These were mounted in Technovit 2021 LC Fast resin and cured in a Technotray® POWER oven for approximately 20 minutes. Mounted samples were subsequently wiped down with acetone to remove tacky surface resin, cut with a jewelers saw, and hand-

[3] Infinite thickness is the minimum thickness a sample must be in order to absorb all the x-rays of the primary x-ray beam emitted from an XRF instrument.

polished with increasing grades of 1500- 12,000 grit micromesh to reveal the stratigraphy of the sample.

Cross-sections were examined at the Winterthur/University of Delaware Program in Art Conservation (WUDPAC) Science Laboratories using the Nikon Eclipse Ni microscope in reflected visible light and with Nikon BV-2A filter cube (excitation range: blue-violet, excitation filter: BP 400-440, dichromatic mirror: 455, barrier filter: LP 470). Images were processed with NIS-Elements AR version 5.00.00 64-bit and captured with a Nikon DS Camera Control Unit DS-U2, DS Camera Head DS-Fi1/DS-5M/DS-2Mv/DS-2MBW.

3.2.2.3 Pyrolysis-gas chromatography/mass spectrometry (Py-GC/MS)

Lacquers polymerize through an enzyme-catalyzed oxidation mechanism leading to the formation of films with a high level of cross-linking, which are insoluble in most solvents and difficult to analyze. Due to the insolubility and complex structure of the lacquer films, only solid-state methods have been applied to their characterization, and the only method capable of distinguishing these materials is pyrolysis-gas chromatography/mass spectrometry (Py-GC/MS).

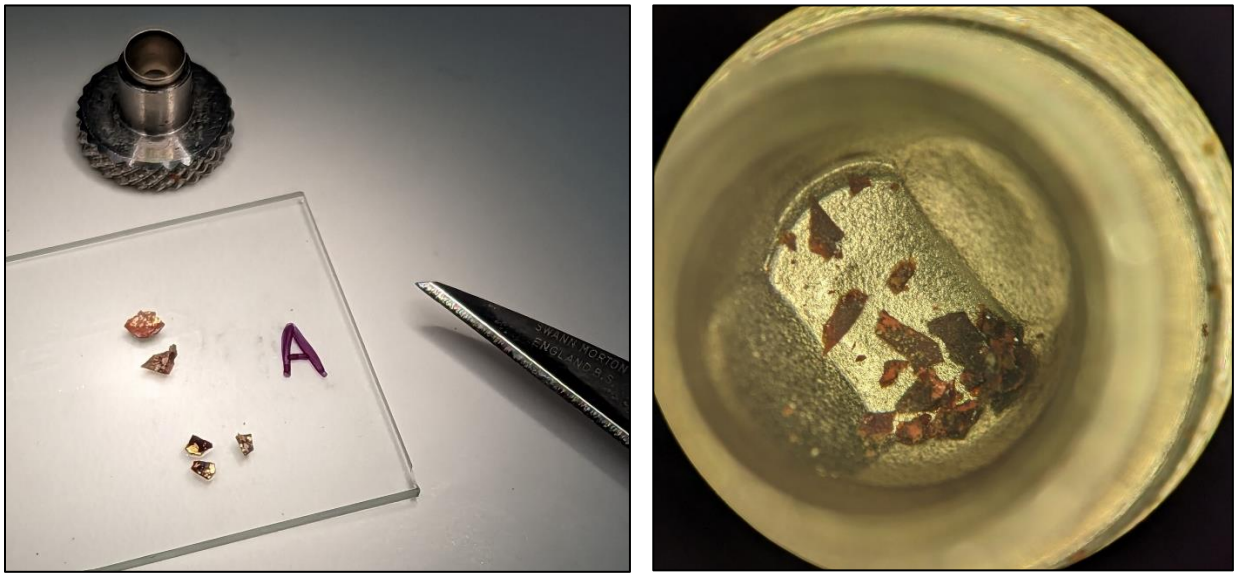

Figure 17: (Left) Samples glued to a glass slide before micro-excavation. (Right) Stereomicroscope view of excavated sample.

Each sample was micro-excavated prior to analysis in order to separate the ground layers from the lacquer layers (see Figure 17). Because each larger sample could yield anywhere from two to thirteen “sub-samples”, ten of the thirty large samples were selected for this analysis, resulting in 27 “sub-sample” runs. These samples were super-glued to glass slides to facilitate stability during excavation and the layers were removed under the stereomicroscope using a sharp scalpel in order to avoid contamination between the layers. Cross sections were consulted to differentiate layers, but in some cases multiple layers were removed together. These included samples in which there was an insufficient amount of material preserved in a layer to be analyzed alone. This was primarily in regard to the losses of degraded decorative layers. In other cases, sub-layering could not be distinguished even under magnification, particularly of the thicker black layers. Higher magnification combined with UV illumination was necessary to differentiate the minute differences within black strata, though sometimes the texture of layers within the black could be used to identify when an interface has been reached.

Samples were analyzed at the WUDPAC Science Laboratories by Py-GC/MS using TMAH (tetramethylammonium hydroxide) prior to analysis; this technique is also known as THM-Py-GC/MS (thermally-assisted hydrolysis and methylation – Py-GC/MS). The rationale for this approach was to convert carboxylic acids, alcohols and phenols to more volatile products prior to analysis.

Samples were placed into a 50μL stainless steel Eco-cup fitted with an Eco-stick, and 3μL of a 25% methanolic solution of TMAH (Sigma) was introduced for derivatization. After about one minute the cup was placed into the pyrolysis interface where it was purged with helium. Samples were pyrolyzed using a single-shot method at 600°C for 12 seconds. The Frontier Lab EGA/PY-3030D system was interfaced to a Hewlett-Packard 7820A gas chromatogram equipped with 5975 mass selective detector (MSD). A J&W DB-5MS Agilent 19091S-433 capillary column was used for separation (30m × 250μm × 0.25μm) with helium carrier gas set to 1.2 mL/minute. The pulsed

split injector was set to 280°C with a split ratio of 10:1 and 30 psi pressure for 30 seconds, with no solvent delay (18 psi). The GC oven temperature program was 40°C for 30 seconds then ramped at 6°C/minute to 320°C, followed by a nine-minute isothermal period. The MS transfer line was at 320°C, the source at 230°C and the MS quad at 150°C. The mass spectrometer was scanned from 33-550amu. Agilent MassHunter Workstation GC/MS Data Acquisition was used for sample acquisition. Data was interpreted with AMDIS software (version 2.73); the SCS_multi.csl calibration standard library was used to generate a calibration file and the data was then searched against the ESCAPE1549.msl mass spectral library, both provided by the Getty Conservation Institute. Results were tabulated and interpreted with the RAdICAL report template (v. June 2020).

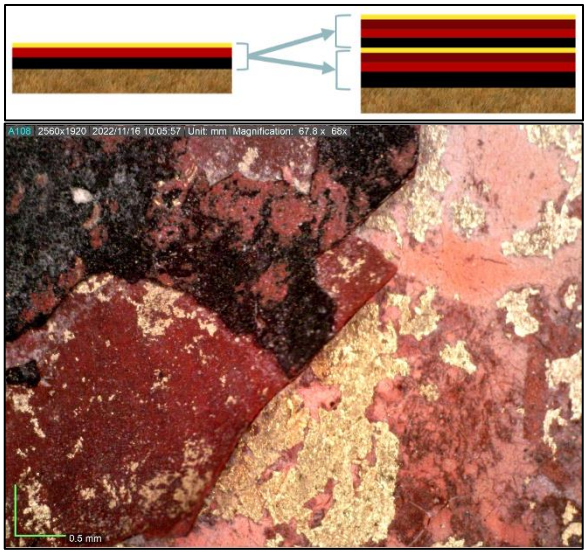

Figure 18: (Top) Diagram of repeating lacquered "sets." (Bottom) Photomicrograph of exposed lacquer "sets" from loss.

3.3 Results and Discussion

3.3.1 Phase 1: Visual survey

3.3.1.1 Surface-subsurface stratigraphy (layering)

Microscopic examination of the surfaces/subsurfaces showed a similar pattern for decorative lacquer application beginning with a layer of black, followed by red, and then gilding. The black appears to serve as a smoothing and priming layer, while the red gives color, either alone or through the gold. Gilding over red rather than black is known to provide a brightening effect to the gold color. The sampled Buddha statues predominantly displayed unique episodes of multiple relacquering, often occurring in grouped “sets.” These layers typically peeled away as a cohesive unit, with the weak pint commonly being the boundary between the gilding from one “set” and the subsequent layer of black from another “set” (see Figure 18). Such observations are consistent

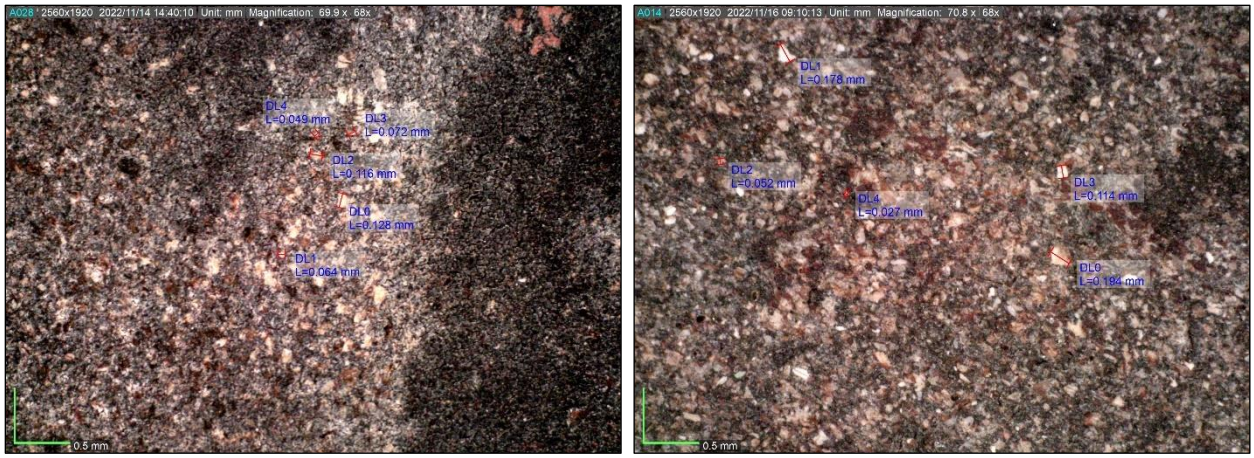

Figure 19: Photomicrographs with grain size measurements of angular white inclusions in potential ground layers from statues N1420 and N1323, respectively.

with epigraphical data that suggest stone sculptures were first coated with a lacquer mixture, followed by a layer of cinnabar-colored red, and finally gilding or other decorative elements. In most cases, each time the statue was relacquered, this entire “set” was repeated instead of reapplying single colored or gilded layers (Ly, 2021).

3.3.1.2 Ground layer

In addition to the decorative layers, a granular layer was identified directly above the substrate, particularly evident on wooden statues. This layer, usually grey-black in color, appears visibly coarse to the naked eye. Under magnification, it is further evident that there is sand mixed into the layer, with grains varying from 0.05-0.15mm for N1420 and 0.03-0.19mm for N1323. Many of these grains are irregular and have sharp edges, suggesting the use of crushed inclusions rather than natural silt or sand (see Figure 19); according to historic sources and analyses on similar objects, these inclusions could be of natural calcium carbonate, shell or bone origin. Calcium

Figure 20: Fluorescence of potential ground layer on sculpture N1323.

carbonate has historically been mixed with resins and other binders for construction, repair, or polychromy. In Europe, chalk[4] is a well-known preparatory ground layer for wooden polychrome statues. Cambodian history does not indicate this same material application; however, ground shell has been mixed into plasters for wall preparation, as well as in other contexts such as betel leaf recipes for consumption. It was also identified as an additive in the lacquer mortar on the statue restored at the National Museum of Phnom Penh (Porte, 2002). Alternatively, bone ash grounds are commonly used ground layers in lacquerware production from other regions, such as China (Webb, 2000). Conversations with conservator Marianne Webb in 2022 have further illuminated the utilization of bone grounds in areas that employ thitsi lacquers, of which Cambodia is a prominent producer. It is therefore not unlikely that these materials could also be crushed and mixed with lacquer to create a ground layer in these sculptures. The UV-induced visible fluorescence found that the grains fluoresce strongly in comparison the surrounding binding medium (see Figure 20).

Figure 21: Photomicrograph of multiple red layers visible along a crack.

3.3.1.3 Red layers

The studied statues displayed an observable variation in the intensity of red coloration between episodes of relacquering. In each case of


Figure 22: Visible light (left) and fluorescence (right) of overlapping surface layers on proper left sleeve of statue N1323.

[4] Naturally occurring calcium carbonate sedimentary rock

relacquering, the earlier red layers tend to be lighter in color and similarly fluoresces a lighter orange, while the later layers of red tend to be darker and fluoresce more red-orange (Figures 21 and 22). This could imply a difference in the composition of the pigment, perhaps related to the type or quality of pigment used. For instance, a more affordable or locally sourced pigment like red ochre (iron oxide) might be used instead of a more valuable imported pigment such as cinnabar. Furthermore, even when using the same type of mineral pigment, variations in shade could occur if the sources come from different regions.

That being said, some of the reds, such as on N1323 and N509 show larger distinct pigment particles visible in the later red layers, while the older red layers appear more homogenous with smaller particles that are not readily visible under magnification. Coloration can be affected not only by type of pigment but also in the pigment granularity, which can scatter light differently based on size and produce different hues of the same color. Therefore, larger particles of pigment bound in more lacquer may create a darker coloration than the same pigment with smaller particles bound in less lacquer.

There are some layers of red, however, that do not appear to be lacquer at all. This is mainly evident on statue 2259 but has also been seen on other statues in the larger corpus. The top coat of red is very dark, but under UV illumination, it reveals a bright green-yellow appearance (see Figure 23). Webb (2011) has described the autofluorescence of lacquer, in which newly applied lacquers to not appear to fluoresce while aged lacquers do. Generally, aged Asian lacquers fluoresce weak orange to bright yellow color. While UV-induced visible

Figure 23: Green-yellow fluorescence of red layers on statue 2259.

fluorescence examination provides only a qualitative evaluation insufficient for material identification, the stark contrast in this case points to a binding medium that is different from natural Asian lacquer.

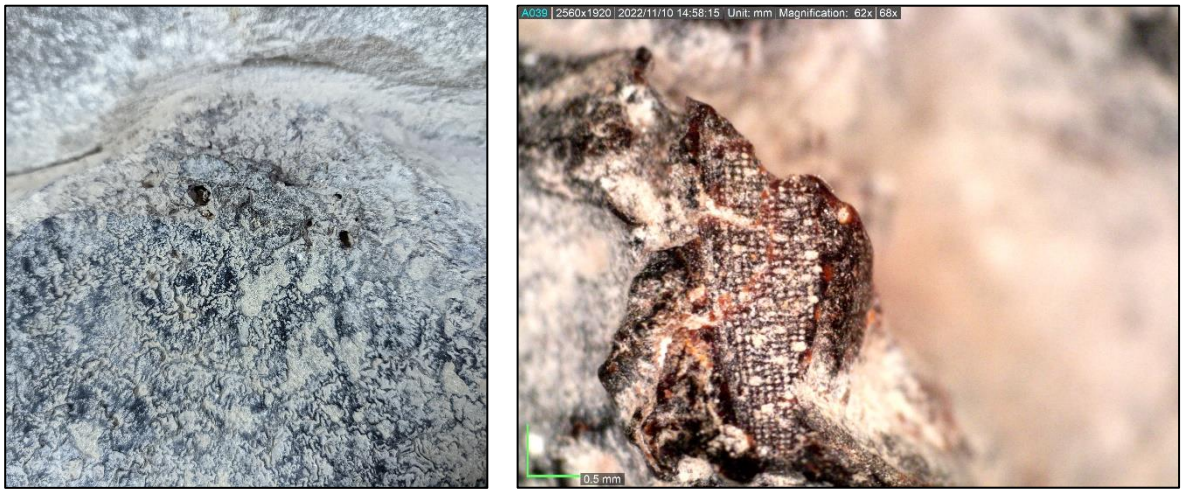

Figure 25: Detail image (left) and photomicrograph (right) of rice husk pseudomorphs on N509.

Figure 24: Detail image (left) and photomicrograph (right) of fibrous plant filler on N1323

3.3.1.4 Repair and modification materials

The six selected statues show clear evidence of historical repairs. Their morphologies are fairly distinct from the decorative surface layers. In general terms, the closer the fill material is to the surface, the smaller the inclusions tend to be. Large-scale fills appear to use roughly mixed plant materials as the predominant bulking agent, with or without sand. On N1323, this plant material

seems to be something that was quite fibrous, whereas on N509, clear pseudomorphs of rice husks are visible (see Figures 24 and 25). These are distinguishable from other types of grain husks because of the characteristic texture on the outer surface (Sung et al, 2009), as shown in the scanning electron micrographs (Figure 26).

Smaller, smoothing fills could contain a variety of silt or sand mixed in, while re-surfacing and molded ornamentations would have much smaller grains that may have been ash or fine silt/clay. Adhesives could vary depending on usage. Presumably for closer joins, the adhesives had fine silt/clay bulking agents similar to the latter, but for rough adherence such as on boards for repair, sand grains could be larger.

While most of these fillers seem to have been mixed with a material that fluoresced similarly to the overlying decorative layers, three statues (N509, 2259, and N1420) all displayed evidence of another resin that appears neon orange under UV light (see Figure 27). Although not conclusive by itself, this particular fluorescence is often indicative of shellac[5]. This is interesting and may be indicative of a later restoration material because, although there is a known and lengthy history of its use as a dye in Southeast Asia, there is little information on its use as a decorative or repair material on statues. However, based on these observations, it seems that it was used for the same applications as the lacquer repair materials, with similar inclusions.

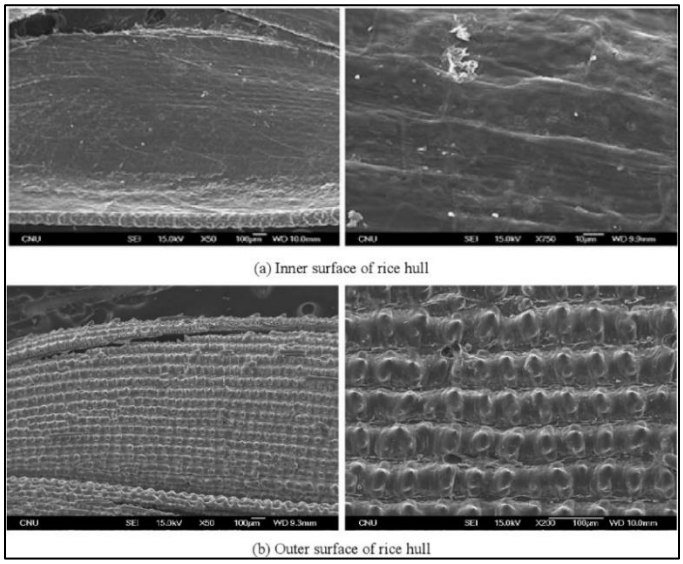

Figure 26: SEM images of rice husk morphology. Images from Sung et al, 2009.

[5] Shellac is a substance derived from natural stick-lac, which is a resin generated by the scale bug belonging to the Lacciferidae family and specifically the Kerria or Laccifera lacca species.

Figure 27: Fluorescences of non-lacquer material on (from top to bottom) N509, N1420, and 2259.

3.3.1.5 Condition survey and conservation history

The lacquer appears to have a better adherence to wooden substrates than stone. In fact, in many of the stone sculptures, lacquered surfaces seem to contribute to stone scaling. This is likely the result of soluble salt accumulation just under the surface. The lacquer layers, when stable, are not permeable to water; therefore, soluble salts would not be able to escape the substrate. Their subsequent crystallization just beneath the surface forces separation of the overlying material from the bulk of the substrate.

The lowest layer of black next to the ground or substrate often shows an interesting degradation phenomenon in which the layer has distinct spots of translucent red (see Figure 28). The layers of black higher up in the strata do not show this degradation feature. Discussions with Marianne Webb in 2022 indicated that this particular effect is unique to thitsi lacquers when applied over ground layers rich in bone. In these instances, the lacquer does not seem to adhere effectively to the bone-enriched substrate, and can preferentially detach in these areas. Another common degradation feature of all lacquers when exposed to light is their increased transparency. Unpigmented lacquer also appears black after layering and curing, but is naturally reddish in coloration. These spots of red therefore may be concentrations of bone in the ground that are visible through this aged layer, enhancing the natural red of the unpigmented layers.

This may also indicate a couple of conclusions that are not immediately obvious in visual observations. Firstly, the presence of this degradation phenomena in both stone and wooden statues implies that a ground layer may exist on the stone figures as well, or that the sandstone contains elements that mimic the effects of a bone ground. Secondly,

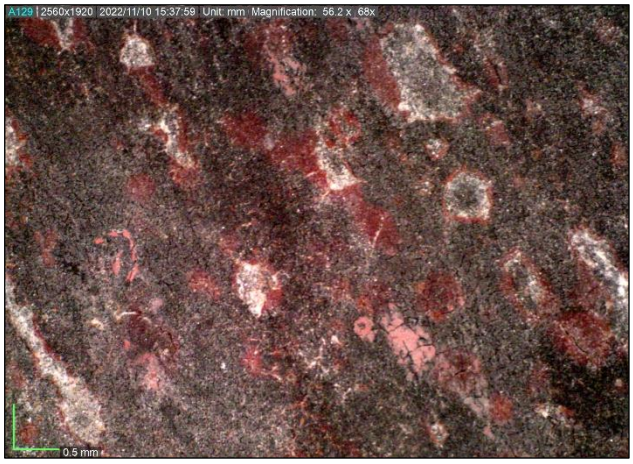

Figure 28: Photomicrograph of red spots on black lacquer layers.

the initial lacquering often involved the use of locally-produced thitsi lacquer, given that Cambodia is a natural source of this material.

3.3.2 Phase 2: Material analysis

3.3.2.1 Portable X-ray fluorescence (pXRF)

PXRF indicated a trace or low-intensity peaks of silica (Si), potassium (K), titanium (Ti), manganese (Mn), nickel (Ni), and copper (Cu) across every reading (Figure 29 as example). Their uniformity suggests that they are contaminants from the surrounding environment rather than purposeful additives. Given that the storage warehouse for these objects has open windows and housekeeping of the collection requires frequent dusting, it is logical to assume that these elements may be components of dust and soil from outside.

The higher intensities of iron (Fe) across the samples are more difficult to interpret. Cambodian soil naturally contains high levels of iron, which gives it a distinct red coloration. In fact, conversations with local stone and lacquer conservator Sok Soda in 2022 revealed that the soil itself has been and continues to be used as a pigment to produce red lacquer. Iron presence

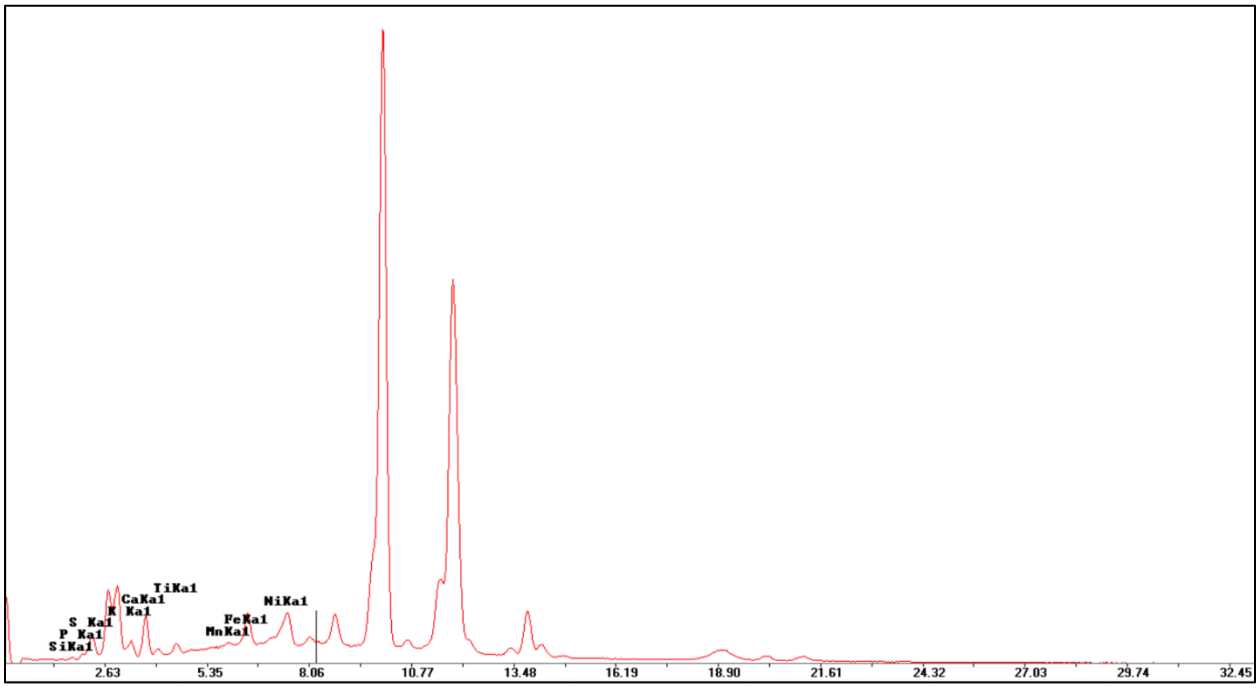

Figure 29: PXRF spectra for N1323-W-03 Top, showing trace elements.

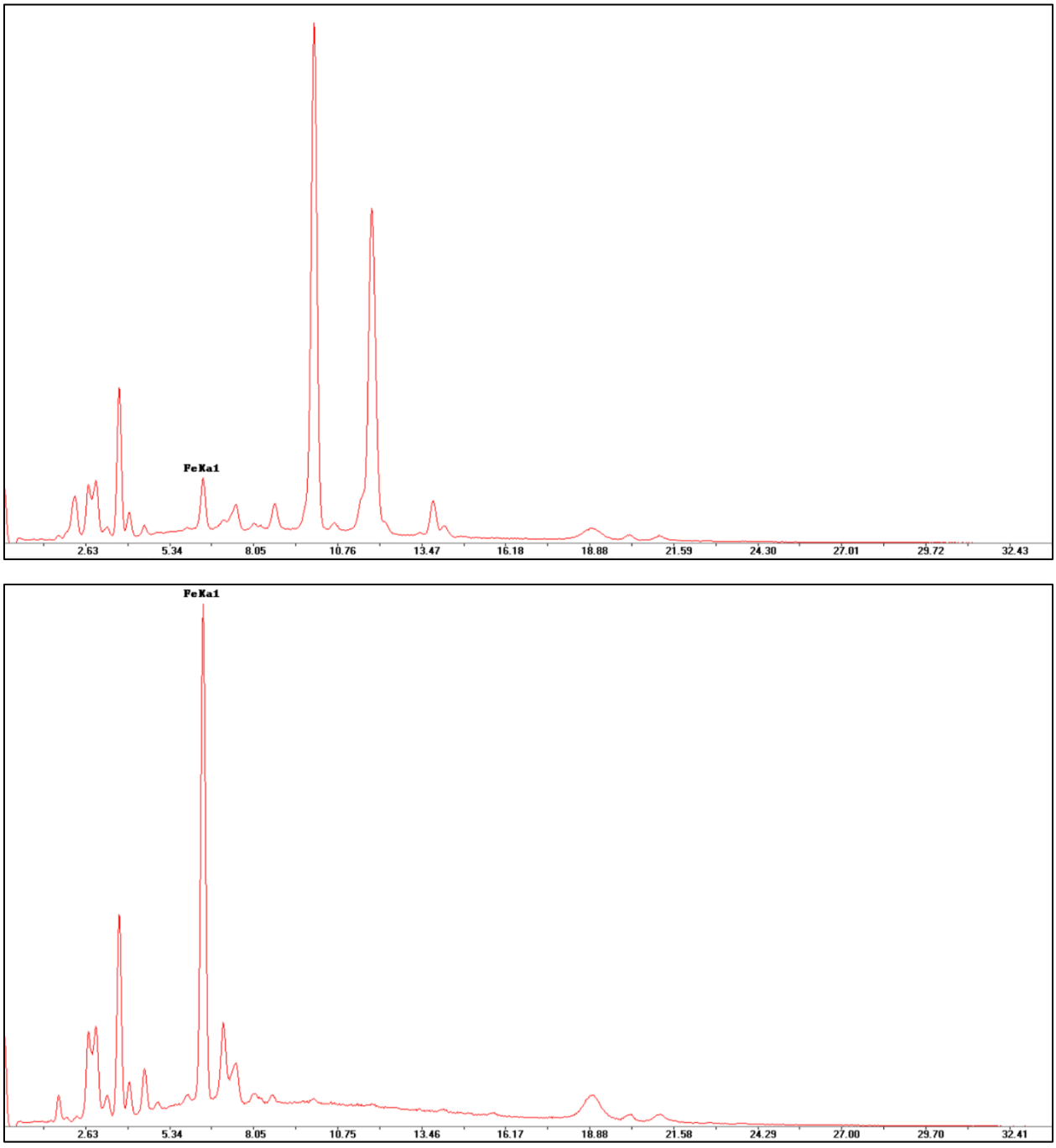

Figure 30: PXRF spectra for N1323-W-02 indicating iron (Fe) intensity when readings are taken of the bulk fill material (top) versus the surface layers (bottom).

is further complicated by the fact that black lacquers have also been colored using iron pigments or chemical reactions with ferrous compounds [6] (McSharry et al, 2007; Liu et al., 2023).

[6] Powdered magnetite is a black mineral pigment added to lacquers as a physical colorant, while iron (II) hydroxide and iron acetate are added to raw lacquer during the cooking or *kurome* refinement process as a chemical alteration to black. In China, historical records indicate that the latter additives were obtained by soaking iron

Determining the intentional addition of an iron-containing pigment solely based on the presence of iron (Fe) therefore proves challenging. However, it is worth noting that the peak intensities for iron don't display the same uniformity across samples as do the previously mentioned trace elements. This could suggest that, while the iron is a contaminant from the environment, it could also have been added in such quantities that its presence is much stronger in certain samples compared to others. F or example, for statue N1323, sample number 02 had separated into two sections during sampling. The surface layers retain a relatively low intensity peak of iron in comparison with the bulked material directly below it (Figure 30). This could indicate some type of added ferrous material into the bulked fill, though whether it is colorant or naturally occurring ferrous minerals in the sandy filler is impossible to determine with pXRF alone. Additionally, the dominance of the mercury (Hg) peak in the surface layers may also affect the counts for the iron, making them appear lower than they are.

A similar issue arises for the presence of Calcium (Ca), except in N1323 where the bottom and top layers of the same sample have distinctly different intensities of Ca. Analysis of sample 3 from the bottom up showed a much stronger presence of calcium than the reading taken from the top. When pXRF attenuation[7] is taken into account, the fact that the two sides have distinctly different intensities for calcium suggests that a calcium-based material was purposefully added to one of the bottom layers, resulting in the larger intensity (Figure 31). Combined with the morphological and UV observations from phase 1, this could suggest a calcium-based ground,

scraps in rice vinegar (Liu et al, 2023). Japanese terminology also refers to this latter type of black lacquer as *roiro-urushi* (McSharry et al, 2007).

[7] Attenuation refers to the reduction in intensity of X-rays as they pass through a material. This reduction can be due to several phenomena, including absorption, scattering, and reflection. The extent of attenuation depends on the energy of the X-rays and the composition and thickness of the material they are passing through. Therefore, when using pXRF on a layered sample, the attenuation of X-rays by upper layers can affect the measurement of deeper layers, resulting in spectral differences when a sample is measured from opposing sides.

such as ground shell or bone ash. Shell is composed of calcium carbonate while bone is calcium phosphate. Differentiation between the two is difficult for these samples using pXRF, as carbon and oxygen are not detectable by pXRF and all samples had a minor presence of phosphorous,

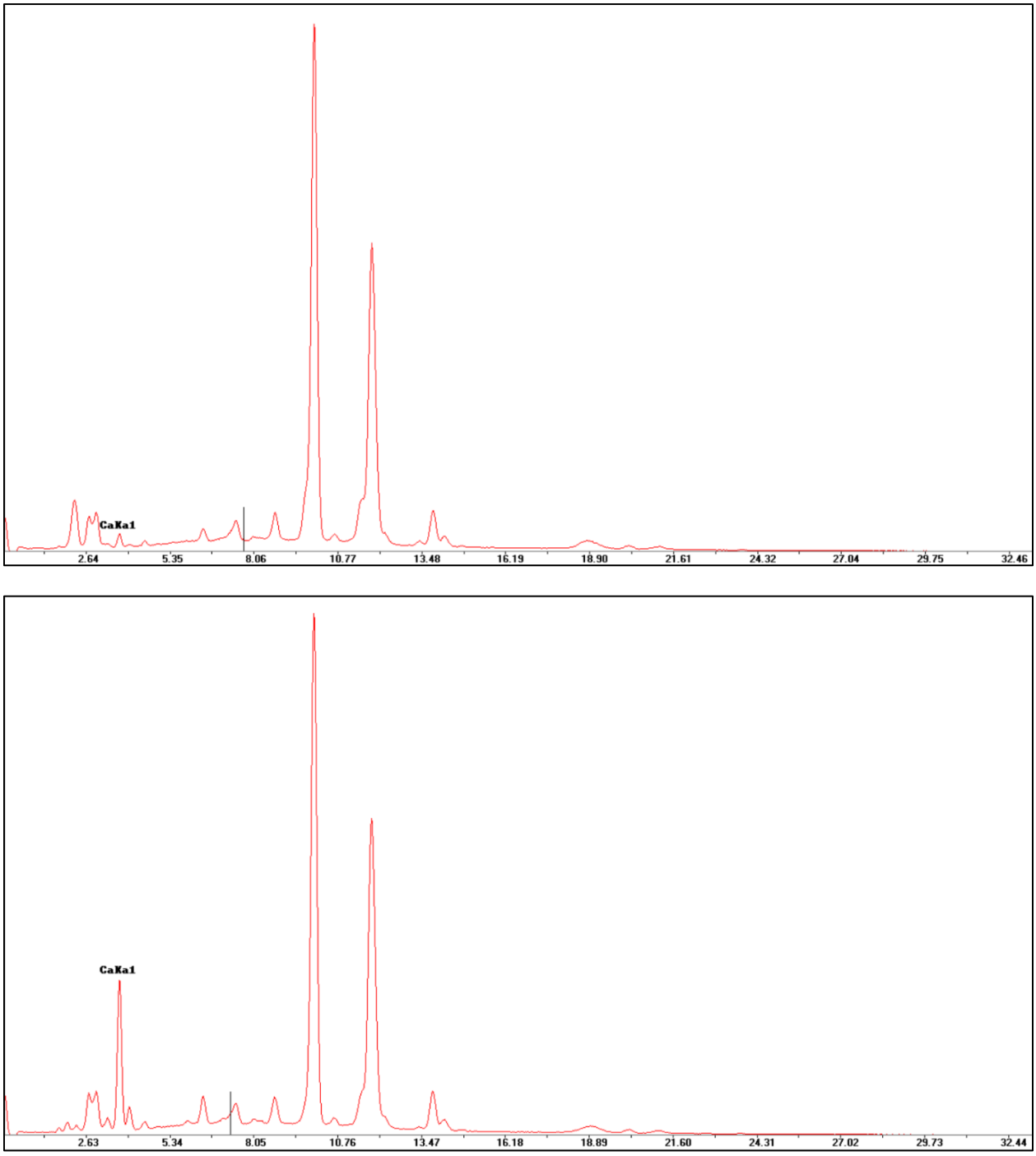

Figure 31: PXRF spectra of N1323-W-03 showing differences in calcium (Ca) intensity when readings are taken from the top (top) of the sample versus the bottom (bottom).

although the lack of variation in the phosphoric peak in itself may suggest it is a trace contaminant rather than added bone ash. The aforementioned pattern of detection that suggests calcium in the ground layer appears in six of the other samples that showed stronger calcium intensities when taken from the bottom; however, it must be mentioned that there were also three other samples that showed this same differentiation in reverse. The remaining samples all had calcium but with no notable contrast between top and bottom.

The presence of gold (Au) is consistently observed in cross-sections where at least one-layer exhibits gilding. Nonetheless, in sample 2259-S-01, the presence of gold was accompanied by markedly elevated intensities of both copper (Cu) and lead (Pb), seen in Figure 32. This suggests the possibility of a copper-gold alloy being used for the manufacture of this particular foil. In contrast, other occurrences of gold did not exhibit similar coinciding intensities or any other indication that would imply the use of an alloy rather than a pure metal.

The most prominent, and perhaps anticipated, peaks were those of mercury (Hg) (Figure 33 for example). These peaks align with cross-sections that show red layers, pointing to the likely

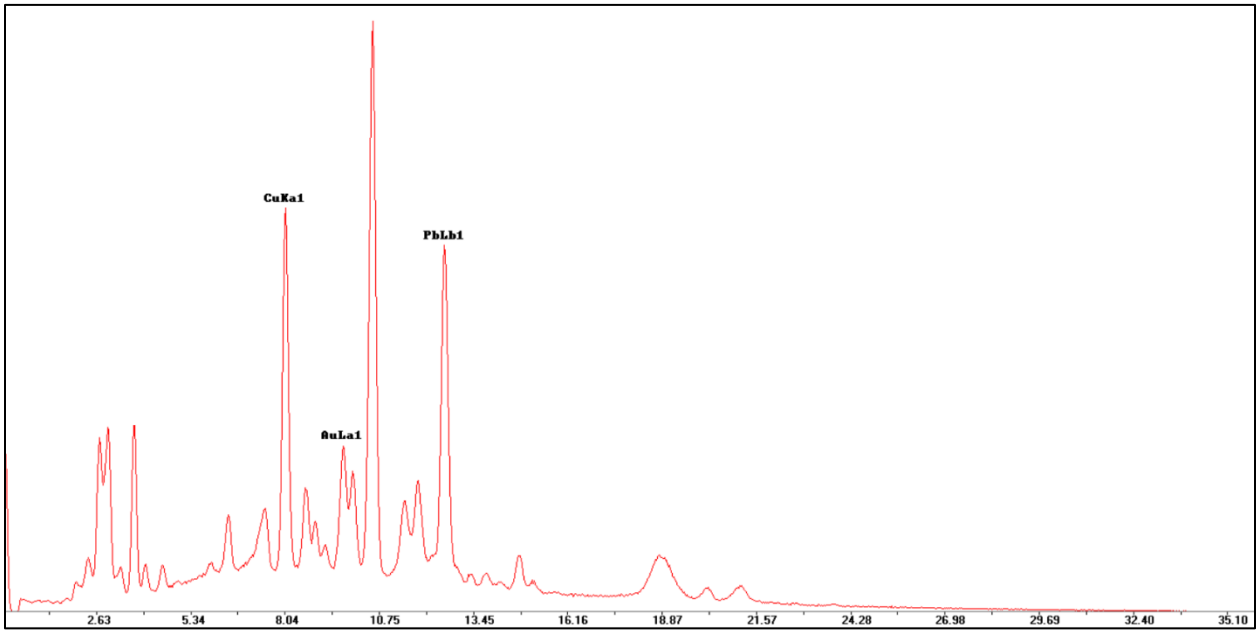

Figure 32: PXRF spectrum of 2259-S-01 showing potential gold alloy in gilding.

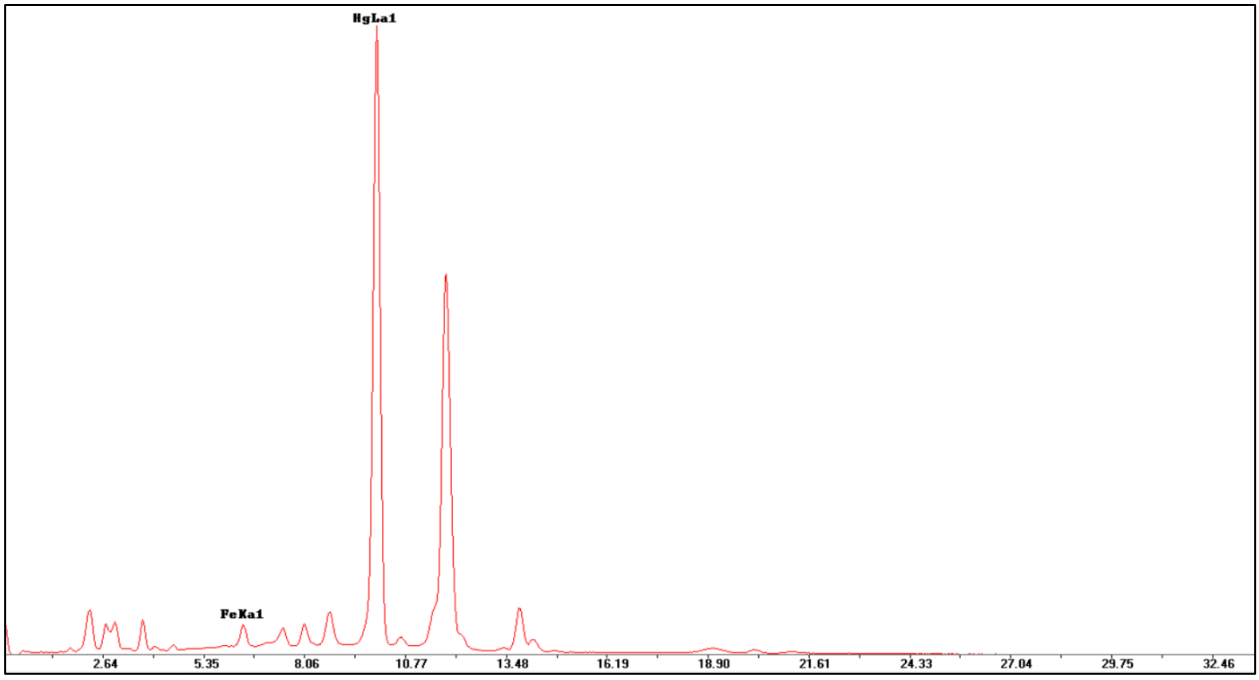

Figure 33: PXRF spectrum of N509-S-02 Lac Layers showing an example of mercury (Hg) presence as an indicator of cinnabar pigment.

use of cinnabar (mercury sulfide) as the red pigment. However, these data are insufficient for distinguishing between multiple red layers within a single sample, especially when those layers could originate from different pigment sources, such as cinnabar and iron oxide.

3.3.2.2 Cross-sectional analysis

The cross-sectional analysis revealed a highly complex stratigraphy that was impossible to fully evaluate by hand-held digital microscopy. While the aforementioned lacquer "set" remained true (black, red, and sometimes gold), the bulking, repair, or ground layers showed additional layers that were difficult to distinguish without UV illumination (Figure 34).

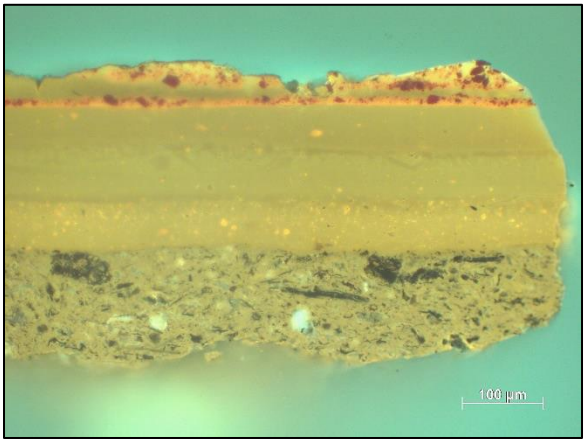

Figure 34: Photomicrograph of 2051-S-02 cross-section, 20x magnification and 430nm UV reflectance illumination.

Across all samples, there is a high variation in the total number of layers, ranging from 2 to 13 (not accounting for "single layer" bulk material samples). The higher number of total

layers represents as many relacquering interventions rather than a complex stratigraphy from a single lacquering episode. Additionally, this variance in the number of layers can even occur on samples taken from the same statue, evidence of preferential repair and recoloring of the most spiritually prominent parts of the figure—namely, the face, chest, and arms/hands. This is particularly apparent on three of the statues. N1420-W-02 from the statue's back has five total layers with a single lacquer "set". Conversely, N1420-W-01 and N1420-W-03 from the face and shoulders, respectively, both have six layers including two lacquer "sets," indicating relacquering. Similarly, N1323 has only three layers total including a single "set" on its back (N1323-W-04), but thirteen layers total on the robes of the proper left arm (N1323-W-03) including three, possibly four "sets". Lastly, 2259 has only two layers with one "set" on the back (2259-S-04), but the face (2259-S-01) and the chest (2259-S-02) have ten total layers with two "sets" and six to seven total layers with two to three "sets", respectively.

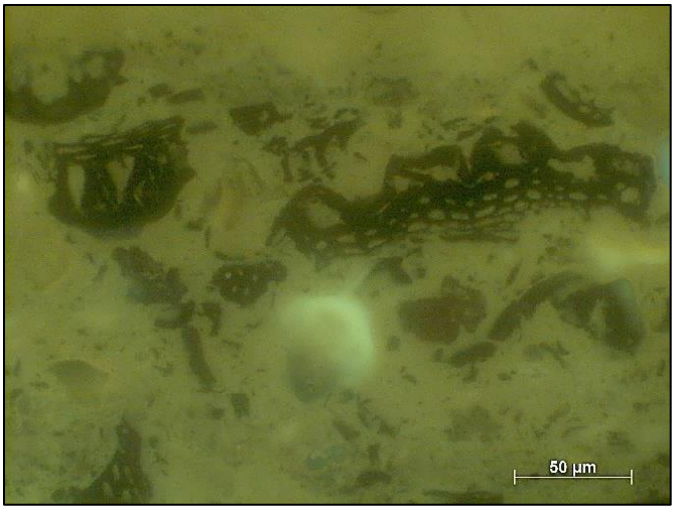

Figure 35: Photomicrograph of N509-S-04 cross-section, 50x magnification and 430nm UV reflectance illumination.

The morphological makeup of each layer is clear in cross section. Surface layers (the decorative layers of black, red, and gold that make up a "set") do not have visible inclusions aside from red, angular pigment particles. Layers further down are bulked fill or ground layers, differentiated from one another by unique mineral or botanical inclusions of gradated size (see example in Figure 34). The layers closer to the external surface have finer and more homogenous inclusions that appear mineral in nature (e.g., fine sand), whereas those closer to the substrate have rougher inclusions such as larger minerals of varied size and shape alongside botanical remnants (Figure 35). These botanical inclusions retain visible plant morphology, many of which appear structurally similar to a monocot grass (e.g., cereal stalk).

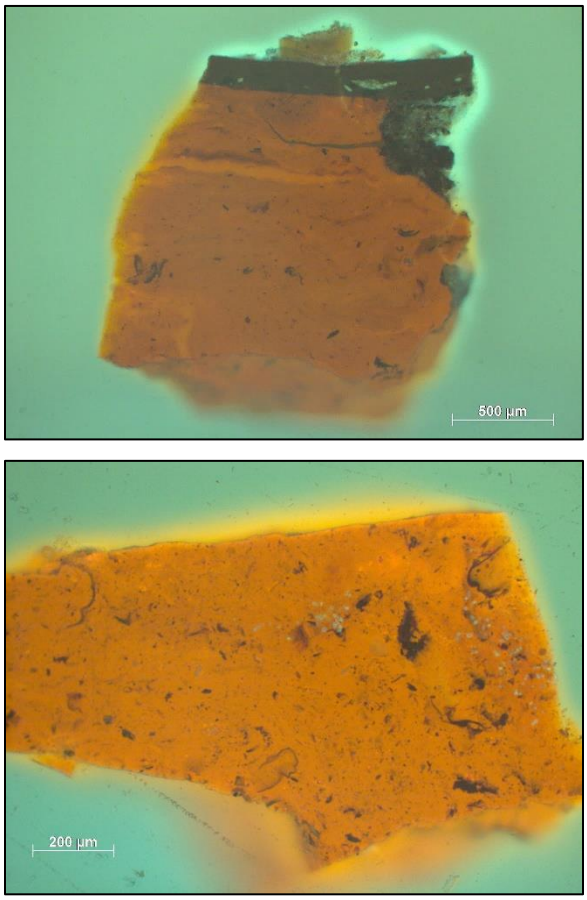

Figure 36: Bright orange fluorescence evident in photomicrographs of 2259-S-02 (top) and N509-S-01 (bottom).

All cross sections were illuminated in UV, with 430nm showing the clearest delineation of layers. UV illumination also provided clear, qualitative differentiation of certain layers when compared with the relatively uniform fluorescence of others. These are not evaluative, merely indications for further study. Most layers on all samples had a mild fluorescence (as a note, in images, the fluorescence appears brighter as magnification increases). The exceptions to this observation include 2259-S-02 and N509-S-01 (red), seen in Figure 36. Both of these stone statues have layers that were strongly fluorescent and bright orange in color, distinctly different from other materials. 2259-S-02 also has a black layer that quenches in UV, as compared to most black layers that still have mild fluorescence in UV. The red layers on 2259-S-(03-05) and one of the red layers on 2259-S-02 also fluoresce much brighter than any other layers, as does the resin sample from N509-S-03 and the bottom bulk N1323-W-01.

3.3.2.3 Pyrolysis-gas chromatography/mass spectrometry (Py-GC/MS)

The Py-GC/MS analysis provided a comprehensive view into the organic components of the lacquer layers. Of the 26 pyrolyzed samples, 24 were processed successfully while two were inconclusive

Anacards

Across all but three of the 24 successful runs, lacquer was detected as the primary resin component. Determining the identity of the Anacard is relatively straightforward. As elucidated by Schilling et al (2016), the three lacquer types can be differentiated by the formation of homologous series of marker compounds including catechols, phenyl catechols, phenols, phenyl phenols, alkyl benzenes, and hydrocarbons. For urushi and laccol, the amounts of these are similar, but each series has a maximum side chain length and most abundant member. In urushi, the maximum side chain length is 15 carbons with the most abundant member having seven carbons. In laccol, this changes to 17 carbons and nine carbons, respectively. Thitsi, however, stands out more distinctly due to the high levels of alkyl benzenes. The RAdICAL report template presents the marker compounds as stacked area graphs called "gestalt graphs" that allows for easy visualization of these differences (see Figure 37).

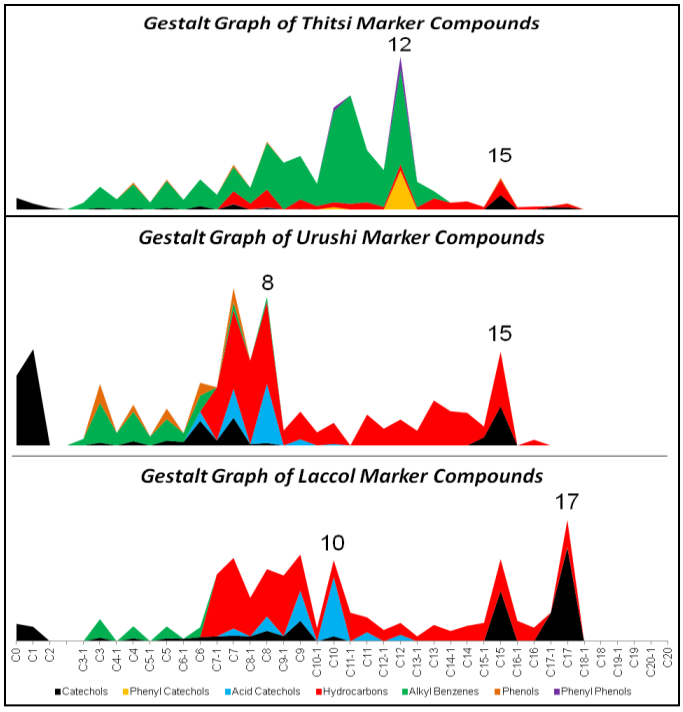

Figure 37: Example Gestalt graphs for lacquer types. Image from Shilling et al, 2016.

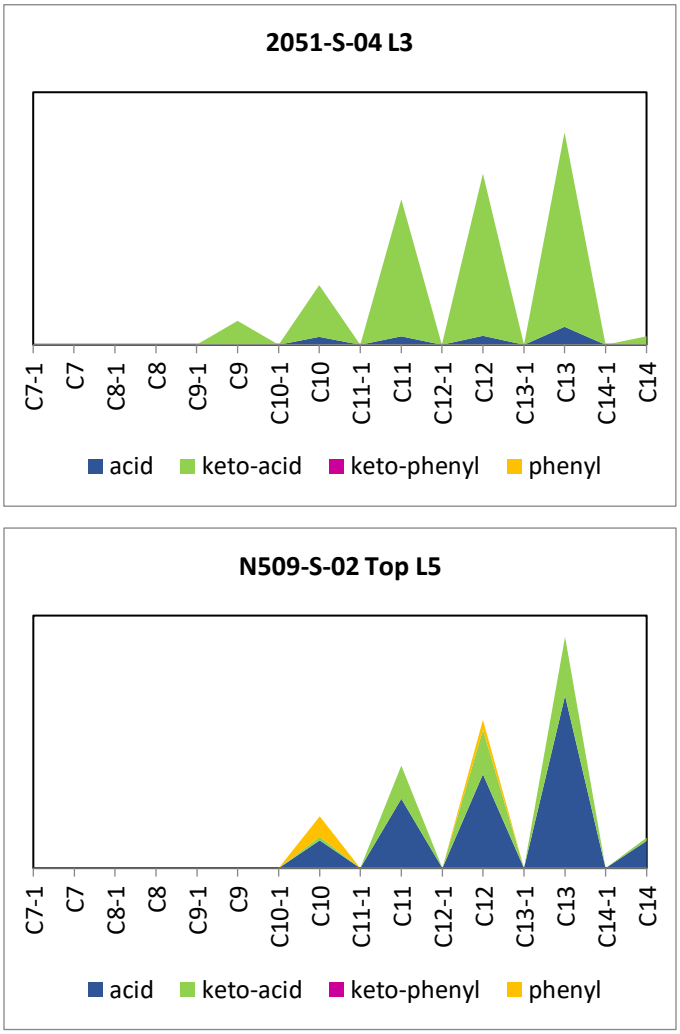

Figure 38: Thitsi Gestalt graphs reflecting the relative aging by the formation of acid catechols.

Aged lacquers also develop acid catechols (C8 mazzeic acid for urushi and thitsi, C10 arlenic acid for laccol) formed by oxidation of the unsaturated side chains of substituted catechols. These are visible in the gestalt graphs as well. In thitsi, these aging products are difficult to visualize in the overall graph, so a secondary gestalt graph (see Figure 38) gives a zoomed in view of their formation. Essentially, the more acid catechols are present, the more aged the layer.

Based on the analysis results, all the samples identified as lacquer were further categorized as thitsi lacquer. However, there were significant variations in the extent of aging among these samples. Sample 2051-S-04 was perhaps the most well preserved overall with very low formation of acid catechols, suggesting the surface lacquering was completed more recently than other statues. Interestingly, the top layers of 5509-W-03 don't appear particularly aged, yet the bulked layer used to create the molded applique beneath it appears highly aged (Figure 39). This would suggest that the lacquering of the surface was completed far later than the original fabrication of the surface decorations.

The rest of the samples are relatively consistent in terms of lacquer aging. All show signs of acid catechol formation, but the rations decrease slightly as the layers get lower down. This is likely because the overlying layers somewhat shield the lower strata from light and humidity until they begin to break down.

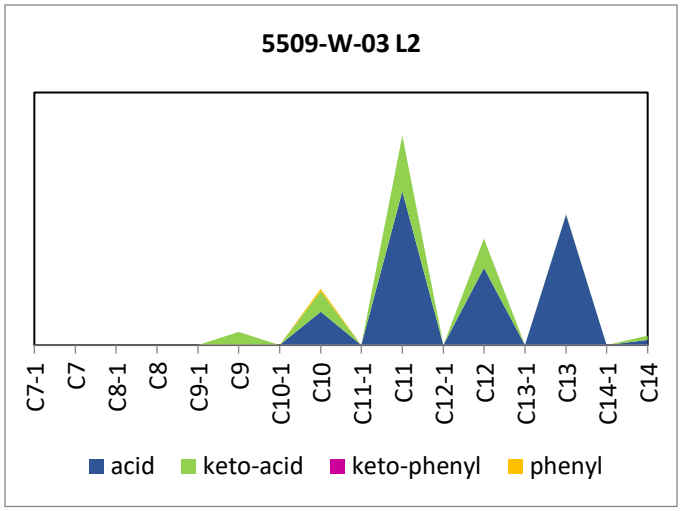

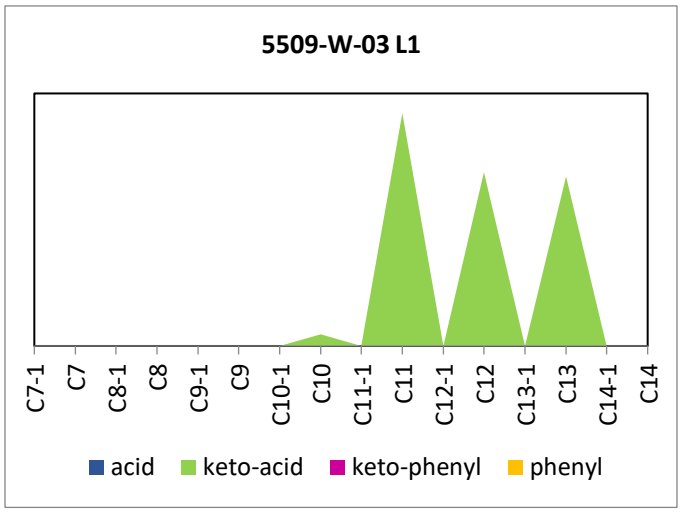

Figure 39: Thitsi Gestalt graphs showing the aging difference between the bulked applique material (top) and decorative lacquer (bottom).

Resins

For the three layers where lacquer was not detected, two were found to be composed entirely of shellac, and the third was a mixture of pine resin and camphor. Both of the shellac layers were thicker bulking or adhesive layers in sample N509-S-01 and sample 2259-S-02 (see Figure 40). The combined pine resin and camphor resins were detected in the decorative surface layers (layers 1-4) of sample 2259-S-02, suggesting variations in the finish layer or a modification in the gilding process for that particular statue (see Figure 41). These findings all align with anomalous fluorescences noted in the cross-sectional observations.

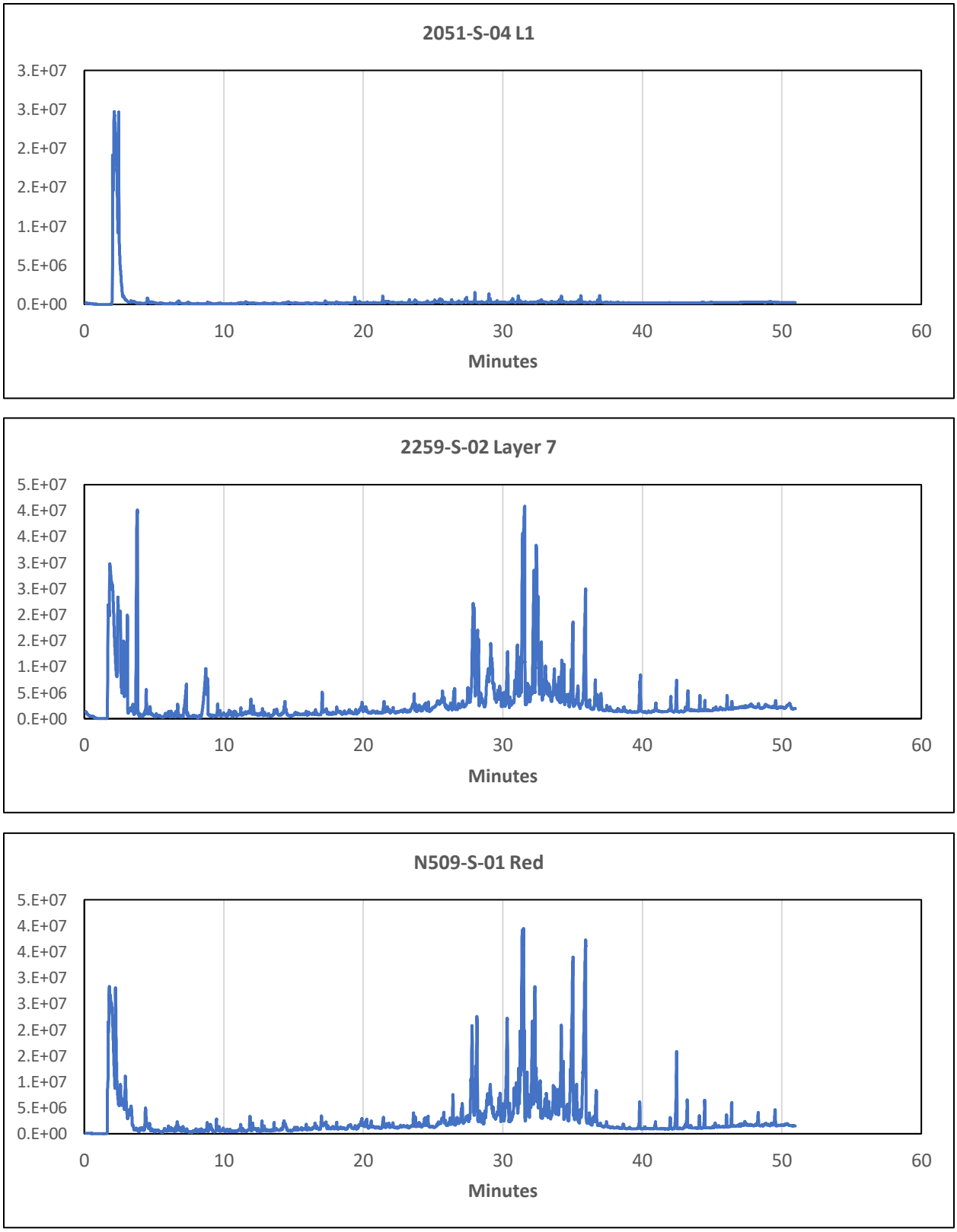

Figure 40: (Top) Example Py-GC/MS chromatogram of a thitsi lacquer undiluted by other resins. (Center and Bottom) Py-GC/MS Chromatograms of layers made out of shellac.

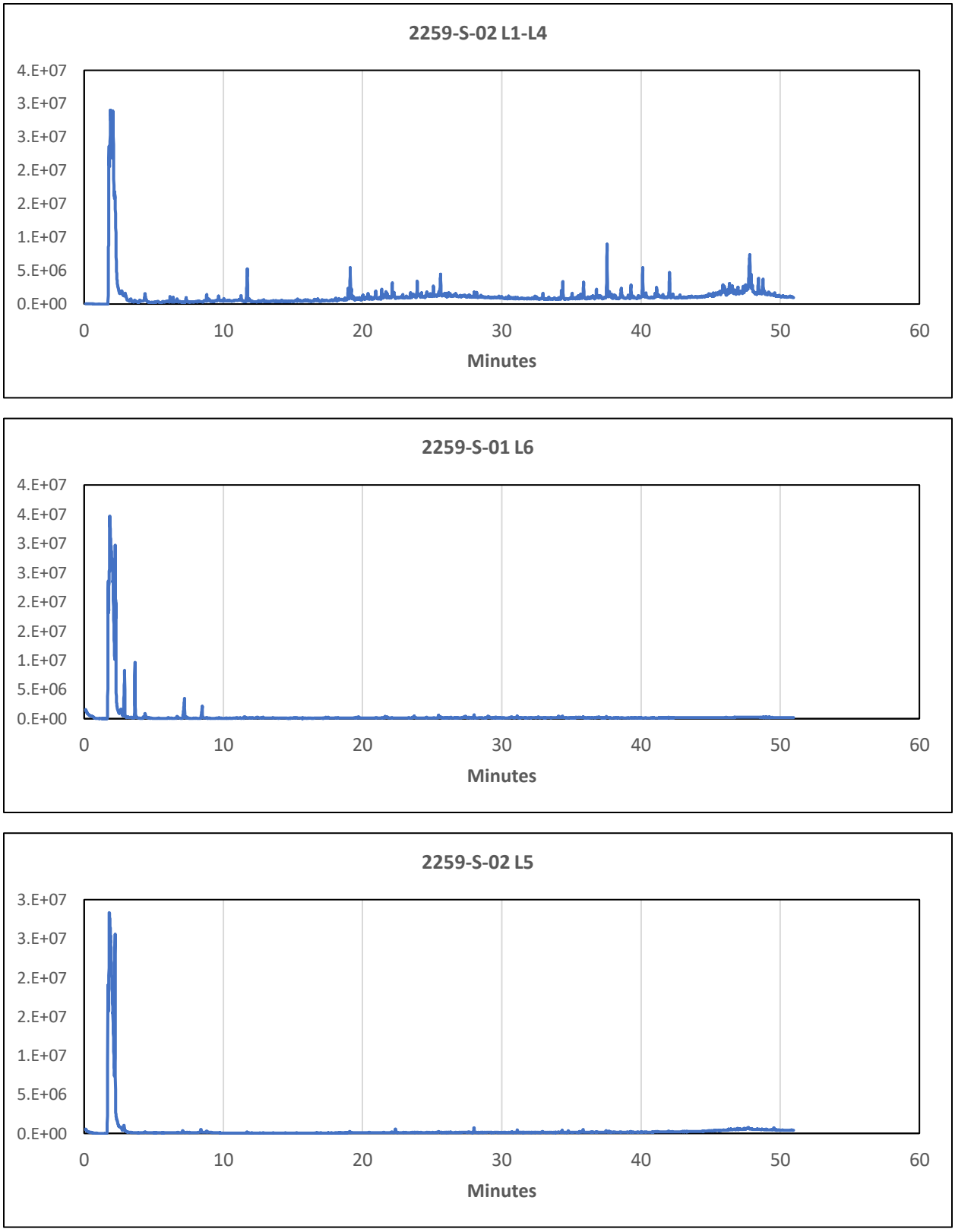

Figure 41: Py-GC/MS Chromatograms of pine resin and camphor mixture layers (top) followed by two pure pine resin layers (center and bottom).

Pine resin was also detected in conjunction with thitsi lacquer for layer 6 of 2259-S-01 and layer 5 of 2259-S-02 (see Figure 41). While there had been no historic documentation of pine resin being mixed with lacquers in Cambodia, nor was it brought up as a potential additive in conversations with conservators or artists, the practice has been noted as a common in neighboring Vietnam and modern Cambodian lacquer artists do have mixtures of lacquer including resins from Dipterocarps, which is explored further later in this section (Szczepanowska & Ploeger, 2019).

Similarly, while shellac has been well documented as a coating commonly used in furniture, musical instruments, and other objects in Europe and farther west, it is less discussed as alternative material to or one used in conjunction with lacquer in East and Southeast Asia (Derry, 2012; Caruso et al., 2014). In Cambodia, current knowledge of the material revolves mainly around its use as a dye, as well as some applications of its resin as an adhesive; however, it has not been previously noted on post-Angkorian Buddha sculptures in the region (C. Hang, personal communication, October 4, 2022). However, compositional evidence has been found in other regions. In China, lacquered, inlayed mirrors (Jinyin pingtuo 金银平脱) from the Tang dynasty (618-907 AD) have been found to contain shellac coatings overlaying the lacquered layers (Hu, 2017; Wang et al., 2020). Japanese export lacquers from the mid-1700s have also been found with shellac layers. Some of these may have been contaminants from later restorations, but in at least one case the shellac was in a protected location that suggested purposeful application by the original artisan (Heginbotham & Schilling, 2009).

The single instance of camphor is interesting. Camphor occurs as both a solid resin and oleoresin from *Cinnamomum camphora,* the production of which has been historically noted in China. Its presence has been detected previously, though very infrequently, in lacquer compositions from Japan and China by its marker compounds camphor and camphene, and historical texts mention its addition to thin lacquer before application (Heginbotham et al., 2016).

In this case, however, camphor is detected as an additive to pine resin rather than lacquer, but its plasticizing properties can be assumed to apply to other resins as well. Given that the pine resin-camphor mixture was applied as the colored lacquer layers rather than as part of the lower bulking layers—as the pine resin has been detected in other samples—it may be that the camphor was added specifically to influence the aesthetic qualities of the resin so it could be better applied as a decorative layer.

An observation worth noting for Cambodian lacquerwares is the absence of any dipterocarp markers in the materials. Cambodia is a large producer of *chor chong* and *chor toeuk* and it is an important cottage industry in the region (Dyrmose et al., 2017). The former is a hard resin collected from the tops of the Dipterocarp trees common in Cambodia, mainly *dam pcheuk* (*Shorea obtuse*) and *dam chor chong* (*Shorea vulgaris*). It is yellow in color and brittle. The latter is an oleoresin harvested from the trunks of Dipterocarp trees by carving a hole and lighting a fire to promote secretion, mainly from *dam trach (Dipterocarpus intricatus), dam chheou teal (Dipterocarpus alatus), dam theng (Dipterocarpus obtusifolius),* and *dam khlong (Dipterocarpus tuberculatus).* This wood oil resin is sticky, elastic, and brown (Schmid, 1963; Sitha, 2002). The two are often mixed together and used similar to lacquer in functional aspects (e.g., adhesives or boat pitch) (C. Hang, personal communication, October 4, 2022). Both have been documented as lacquer additives in modern lacquerware production of Khmer masks with *chor chong* facilitating pouring and solidification in the mask mold and *chor toeuk* granting greater elasticity (Sitha, 2002). The lack of markers for any of these materials suggests that these types of resins were more used for mold-made objects like masks rather than decorative surface layers or on spiritual icons. They may also be a modern additive developed after the decline of lacquer production in the region. Alternatively, there are several instances where samples indicated multiple markers across various resin types at relatively high counts. This may be an indication of a resinous component in the lacquers that does not currently have adequate reference in the

database. Given the wide variety of trees that produce *chor chong* and *chor toeuk*, it is not unlikely that the database for dipterocarps is incomplete; however, previous studies using this process have identified dipterocarp resins so the complete lack of *any* dipterocarp markers suggests, if there is an unidentified resin, it is of different origin (Heginbotham & Schilling, 2009).

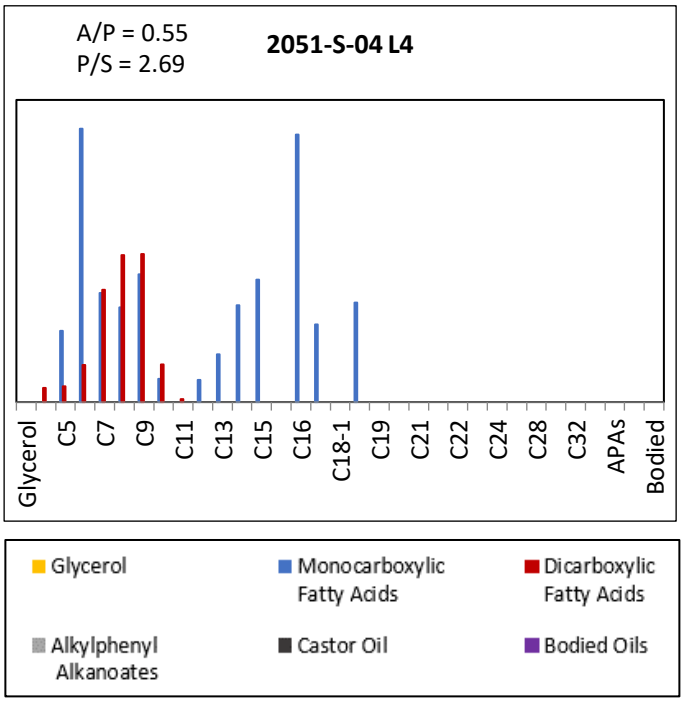

Figure 42: Bar graph showing added drying oil in a lacquer mixture.

Oils and fatty acids

Among the 24 samples studied, all but five showed the presence of drying oils, which were often added to lacquers for a number of potential reasons. Oils were usually easier to obtain than the lacquer itself, meaning the addition of oils could reduce the overall production cost of the lacquer. The addition of oil could also soften and dilute the lacquer, making it easier to apply and glossier once cured. This gloss was a result of a slowed curing time, allowing a better leveling of the layers (Heginbotham et al., 2016). This is particularly true for thitsi lacquers, as they tend to be thicker than urushi or laccol varieties. It has also been noted that oils were sometimes added to the lacquers for storage, perhaps for its slowing effect on curing in order to avoid premature oxidation (Szczepanowska & Ploeger, 2019).

Oils are generally made up of glycerol esters of fatty acids. These appear as marker compounds in the form of methyl esters of monocarboxylic and dicarboxylic fatty acids, methyl ether derivatives of glycerol, and alkylphenyl alkanoates (Schilling et al., 2016). In the RAdICAL template, presence of oils is determined by the presence of dicarboxylic acids and

Table 1: Interpretation of A/P and P/S ratios for oils and fatty acids. Table from Schilling et al, 2016.

	Material	***A/P***	***P/S***	***Characteristic compounds***
drying	Tung oil	High	1 - 1.2	
	Heat-bodied tung oil	High	1 - 1.2	Alkylphenyl alkanoates (APAs)
	Linseed	High	1.2 - 2.5	
	Sesame oil	High	1.5 - 2	Contains sesamin (unique to sesame oil)
	Rapa oil	High	2 - 3	Dicarboxylic fatty acids (abundant C_{11}, C_{12}, C_{13}); high MW fatty acids ($C_{22\text{-}1}$, C_{22}, $C_{20\text{-}1}$, C_{20}, $C_{24\text{-}1}$, C_{24})
	Tallow tree oil	High	~ 3	
	Perilla oil	High	2 – 4	
non-drying	Blood	Low	~ 2	Phosphate, cholesterol, and unverified markers for blood and protein
	Animal glue	Low	~ 4	Pyrrole, diketopyrrole, and unverified markers for protein
	Urushi	Low	~ 2	Anacard markers (C_{15} catechols and hydrocarbons, Mazzeic acid)
	Laccol (Arboretum)	Low	~ 7	Anacard markers (C_{17} catechols and hydrocarbons, Arlenic acid)
	Thitsi (Strahan)	Low	~ 7	Anacard markers (C_{15} catechols and hydrocarbons, alkylphenyl catechols, alkyl benzenes, Mazzeic acid)

monocarboxylic acids together. These are visualized in a bar graph (Figure 42) for easier identification.

Ideally speaking, two fatty acid peak area ratios, A/P (dimethyl azelate to methyl palmitate) and P/S (methyl palmitate to methyl stearate), can be used for oil or fatty acid identification. As drying oils age, they produce high levels of azelaic acid. This leads to higher A/P ratios than other oils and fats, such as those from animal glues or blood. Realistically, however, A/P ratios generated through Py-GC/MS can vary quite a bit based on the instrument conducting the analysis (M. Schilling, personal communication, August 3, 2023). Interpretation for oil identification would then rely on alternative elements. For non-drying oils and fats, the lower A/P ratio would occur *in addition to* identifying markers of proteinaceous additives for a confident

Table 2: Py-GC/MS results for oils and fatty acids.

Sample #	***Layer #s***	*Layer(s) Description*	***Anacard/Resin***	***Oils/Fatty Acids***
2051-S-04	1	B1	Thitsi	Drying oil (P/S: 1.93)
2051-S-04	2	R2	Thitsi	Drying oil (P/S: 1.23)
2051-S-04	3	B2	Thitsi	Drying oil (P/S: 1.68)
2051-S-04	4	B3	Thitsi	Drying oil (P/S: 2.69)
2259-S-01	2, 3	B1 and B2	Thitsi	Drying oil (P/S: 1.83)
2259-S-01	4	[G2/S2?] R1	Thitsi	None detected
2259-S-01	5	B3	Thitsi	Drying Oil (P/S: 1.69)
2259-S-01	6	B4	Thitsi/Pine	Drying oil (P/S: 2.48)
2259-S-02 Top	1, 2, 3, 4	R1, B1, R2, R3	Pine/Camphor	None detected
2259-S-02	5	B2	Thitsi/Pine	None detected
2259-S-02	7	B4	Shellac	None detected
5509-W-03 (molded)	1	R1, B1	Thitsi	None detected
5509-W-03 (molded)	2	B2	Thitsi	None detected
N509-S-01 Black	n/a	B1, B2, B3	Thitsi	Drying Oil (P/S: 4.22)
N509-S-01 Red	n/a	B1	Shellac	None detected
N509-S-02 Top	1	G1, S1, R1	Thitsi	Drying oil (P/S: 2.92)
N509-S-02 Top	2, 3, 4	B1, B2, B3	Thitsi	Drying oil (P/S: 2.13)
N509-S-02 Top	5	B4	Thitsi	None detected
N509-S-02 Bottom	n/a	Fabric and B5	Thitsi	Drying oil (P/S: 1.59)
N1323-W-03 Top	1, 2	R1, B1, G1, R2, B2	Thitsi	Drying oil (P/S: 0.89)
N1323-W-03 Top	3	G2, R3	Thitsi	Drying oil (P/S: 1.07)
N1323-W-03 Top	4	B3	Thitsi	Drying oil (P/S: 1.03)
N1323-W-03 Bottom	1, 2	G3, S1/B4, R4	Thitsi	Drying oil (P/S: 1.38)
N1323-W-03 Bottom	3	B5, B6	Thitsi	Drying oil (P/S: 1.31)

identification. Ideally for drying oils, the P/S ratio can be evaluated for identification; yet, in reality, many commonly used oils have overlapping P/S ranges (see Table 1) that hinder confident identification (Schilling et al., 2016). Additionally, other sources can produce fatty acids that affect the ratios, such as naturally occurring oils from the lacquers themselves or other additives such as wax (Heginbotham et al., 2016). For example, in the tested samples, only two layers were identified as having wax additives: N509-S-01 Black and Layer 1 of N509-S-02 Top. These two

also correlate to the two largest ratios of P/S, suggesting that the wax additives may be contributing factors.

That being said, there are some takeaways from the distribution of P/S ratios (see Table 2). The lacquer "sets" present on N1323 show correlations in their P/S ratios that appear to indicate potentially different oils used in each round of application but which remained consistent within a certain round of relacquering. The upper or most recent set has a P/S of 0.89, the middle set has P/S of 1.03 and 1.07, and the lowest set has P/S of 1.38 and 1.31. The first two sets appear to fall in the range of tung oil, albeit perhaps from different sources. Alternatively, each layer of 2051-S-04 has a different P/S ranging from 1.23 to 2.69, suggesting a different oil could have been used for each individual layer.

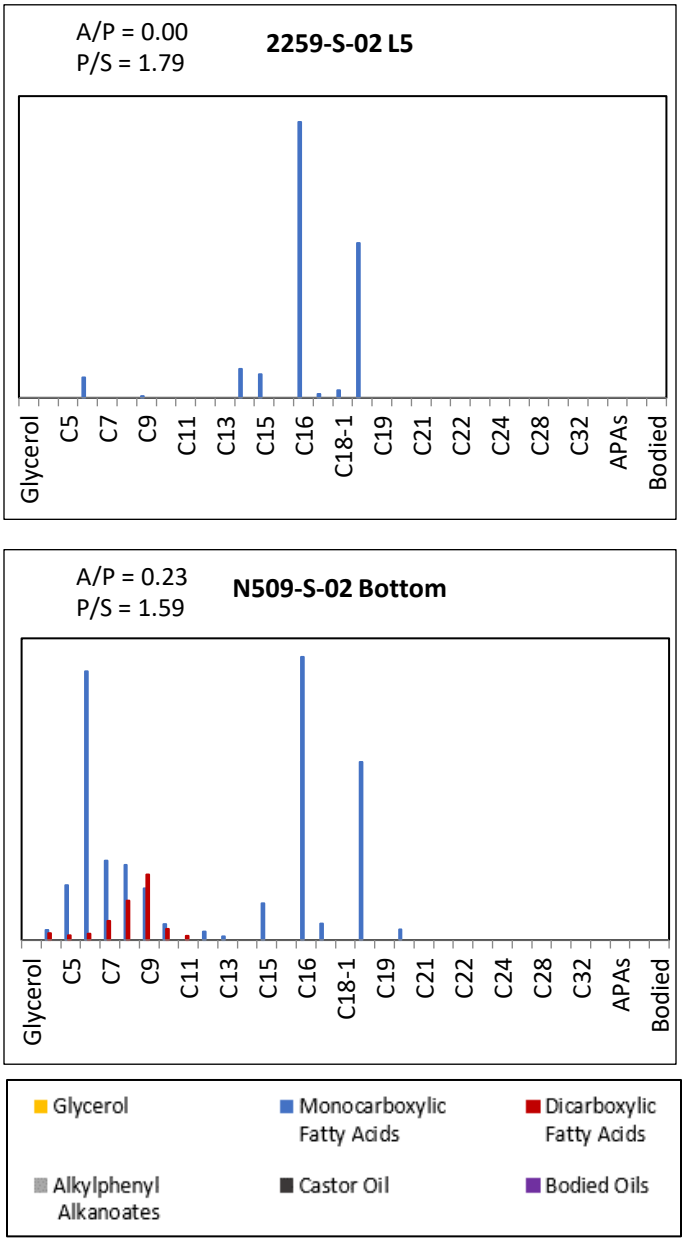

Figure 43: Py-GC/MS bar graphs showing high C16 and C18 monocarboxylic acid in samples both without (top) and with (bottom) the presence of added drying oils.

It should also be noted that, regardless of oil presence, all tested samples show a distinctly high count of C16 monocarboxylic acid and all but three show generally high counts C18 monocarboxylic acid (see Figure 43). It is unclear what is contributing to the spikes of these compounds, as they do not coincide with a pattern among oil ratios, nor to the main type of resin media.

Pigments and other additives

As mentioned previously, there are a limited number of colorants that can be successfully used to blacken lacquer: carbon/bone black or magnetite pigment and iron hydroxide or iron acetate chemical alteration. Py-GC/MS is suited to the detection of organic components, and as such is more conducive to the identification carbon or bone black pigments. Obtaining carbon black requires the burning of a material to create soot. The process of burning and collecting this soot can affect the final formulations of the pigment; however, Shilling et al (2016) have found that certain polycyclic aromatic compounds that are present in blackened lacquers and not in natural lacquers stand as probable marker compounds for soot (see Table 3).

Table 3: Key marker compounds for soot with example positive identification, N509-S-03.

Soot	*RI*	*Peak Area*	*Match*	*RI-RI(lib)*
Fluoranthene	2071	0		
Cadalene	1683	700517	79	0.7
Pyrene	2070	0		
Cadinene	1417.6	75523	71	-8.4
Indeno[1,2,3-cd]pyrene	3262	0		

These markers alone are not sufficient to differentiate the type of carbon black, but when they occur in conjunction with other markers, a more confident identification can be made. Often markers from Pinaceae resin will coincide with soot markers, but when trimethyl phosphate is noted instead, the soot is likely bone black. General soot markers were identified on six of the individual layers, all aligning with samples containing black layers. Of those, two occurred alongside Pinaceae markers; however, one of those layers, 1-4 of 2259-S-02 Top, was also identified as pine resin, so the Pinaceae markers are likely mostly from that. Instead, the soot

Table 4: Py-GC/MS results for pigments.

Sample #	***Layer #s***	*Layer(s) Description*	***Anacard/Resin***	*Pigment*
2051-S-04	1	B1	Thitsi	None detected
2051-S-04	2	R2	Thitsi	Sulfur (Cinnabar)
2051-S-04	3	B2	Thitsi	None detected
2051-S-04	4	B3	Thitsi	None detected
2259-S-01	2, 3	B1 and B2	Thitsi	None detected
2259-S-01	4	[G2/S2?] R1	Thitsi	Sulfur (Cinnabar)
2259-S-01	5	B3	Thitsi	None detected
2259-S-01	6	B4	Thitsi/Pine	None detected
2259-S-02 Top	1, 2, 3, 4	R1, B1, R2, R3	Pine/Camphor	Soot, Sulfur (Cinnabar)
2259-S-02	5	B2	Thitsi/Pine	Soot
2259-S-02	7	B4	Shellac	None detected
5509-W-03 (molded)	1	R1, B1	Thitsi	Soot?
5509-W-03 (molded)	2	B2	Thitsi	Soot
N509-S-01 Black	n/a	B1, B2, B3	Thitsi	None detected
N509-S-01 Red	n/a	B1	Shellac	None detected
N509-S-02 Top	1	G1, S1, R1	Thitsi	Sulfur (Cinnabar)
N509-S-02 Top	2, 3, 4	B1, B2, B3	Thitsi	None detected
N509-S-02 Top	5	B4	Thitsi	Soot?
N509-S-02 Bottom	n/a	Fabric and B5	Thitsi	Soot
N1323-W-03 Top	1, 2	R1, B1, G1, R2, B2	Thitsi	Sulfur (Cinnabar)
N1323-W-03 Top	3	G2, R3	Thitsi	Sulfur (Cinnabar)
N1323-W-03 Top	4	B3	Thitsi	Sulfur (Cinnabar)
N1323-W-03 Bottom	1, 2	G3, S1/B4, R4	Thitsi	Sulfur (Cinnabar)
N1323-W-03 Bottom	3	B5, B6	Thitsi	None detected

from this layer is likely bone black, as it is also the only one to coincide with the presence of trimethyl phosphate.

The pXRF data had also indicated the presence of mercury in many of the samples. This presence of mercury is reflective of the red pigment, cinnabar, which can be further corroborated from the Py-GC/MS data. When mercury sulfide is pyrolyzed in the presence of TMAH, it forms dimethyl sulfide and mercury vapor. The mercury vapor occurs early in the chromatogram and can be difficult to detect without a closer look through an extracted ion chromatogram, but the dimethyl sulfide is easily detectable. In the case of these samples, dimethyl sulfide was detected in eight of the layers coinciding with red layers in all but one (Table 4). Layer 04 of N1323-W-03

Top is described as a black layer, but is just under the red layer in Layer 3, so it is likely that some cross contamination of the layers occurred during sampling in which some of the red layer ended up in the black. These positive identifications of dimethyl sulfide also align with the pXRF data for samples with mercury detected.

The pyrolyzed samples showed no evidence of protein or carbohydrate additives. The only other additive that was found were the two aforementioned layers with wax markers.

3.4 Conclusions and Further Research

The collection of post-Angkorian Buddha statues from Preah Pean have a complex history of pilgrimage and alteration. They provide a fascinating look into not only lacquer traditions for spiritual statues, but also how these traditions may have changed over time with episodes of relacquering and repair, as well as how they may have been influenced by practices and materials brought by foreign visitors. Initial observational analysis conducted the collection surveyed the morphology of repair and decorative materials; pinpointed the practice of lacquered “sets” of black, red, and gold layers; and identified the potential for shell or bone grounds. Compositional analysis conducted on samples taken from six of the collection’s statues expanded on these initial findings to identify specific components in the lacquer recipes.

Py-GC/MS identified thitsi lacquer, local to Cambodia, as the main resinous component of the majority of tested layers, with pine resin and shellac being rare alternatives. Drying oils appear as common additives to the thitsi, with tung oil identified specifically in at least two samples, making up anywhere from about 1/8th to 1/3rd of the total composition of thitsi lacquer mixtures.

Most of the red decorative layers were identified as cinnabar (mercury sulfide) through pXRF and Py-GC/MS, with pXRF adding the potential for iron oxide (red layers) or iron oxide (black) as well. Black layers, for the most part, appeared to be unadulterated with pigment; however, a few indicated the presence of carbon black with one instance of bone black, specifically.

Carbohydrate and protein additives commonly found in urushi or laccol lacquer mixtures were not found in any of these layers. Ultimately, this study provided an insightful first look into the lacquer formulations used in this collection. Further study with additional instrumentation and full analysis of the remaining samples will certainly broaden our understanding of how these formulations changed across the collections and over multiple interventions.

The pXRF data indicated the presence of both iron (Fe) and mercury (Hg)-based red pigments, the latter also confirmed by Py-GC/MS analyses, suggesting the use in the lacquer formulations of red ochre and cinnabar respectively. XRF analyses have also detected calcium (Ca) in the samples and suggested that the calcium distribution may differ between layers.

Additional analysis using scanning electron microscopy/energy dispersive spectroscopy (SEM-EDS) would add a great deal of data by providing elemental mapping of the strata. This may show the distribution of these inorganic components within the different layers to help identify pigment use and ground composition. SEM-EDS can also identify layers of gilding that may be difficult to pinpoint in cross sectional analysis and may have been missed in original observations, as well as provide information on the identity of the mineral makeup of additives in lower filler layers.

While Py-GC/MS is currently the most effective method of differentiating organic components in lacquer mixtures, additional Fourier-transformed infrared spectroscopy (FTIR) could provide comparative data for the identification of alternative resins such as the pine and shellac. Alongside SEM-EDS, FTIR can assist in differentiating calcium carbonate versus calcium phosphate grounds (shell versus bone grounds, respectively) and note the presence of other additives like silicate materials (e.g., ashed rice husk).

Overall, only ten of the 30 total samples were analyzed through Py-GC/MS. Completing analysis of the remaining twenty would provide additional comparative material that would shed light not only on the variety of materials used across statues, but also on the repair and relacquering history of a single statue.

4. Part 2: 3D Printing as a potential treatment for lacquered objects

4.1 3D technologies in conservation

The integration of 3D printing into the sphere of conservation and museology presents an intriguing blend of tradition and technology. Museums have been at the forefront of leveraging this innovation, often capitalizing on 3D printing as an educational medium. Replicas, meticulously crafted using 3D printers, have emerged as a tool in museum education departments. These tangible reproductions have provided visitors, especially students or visually impaired guests, with a unique opportunity to interact, handle, and engage with museum objects without jeopardizing the integrity of the original piece (Figure 44).

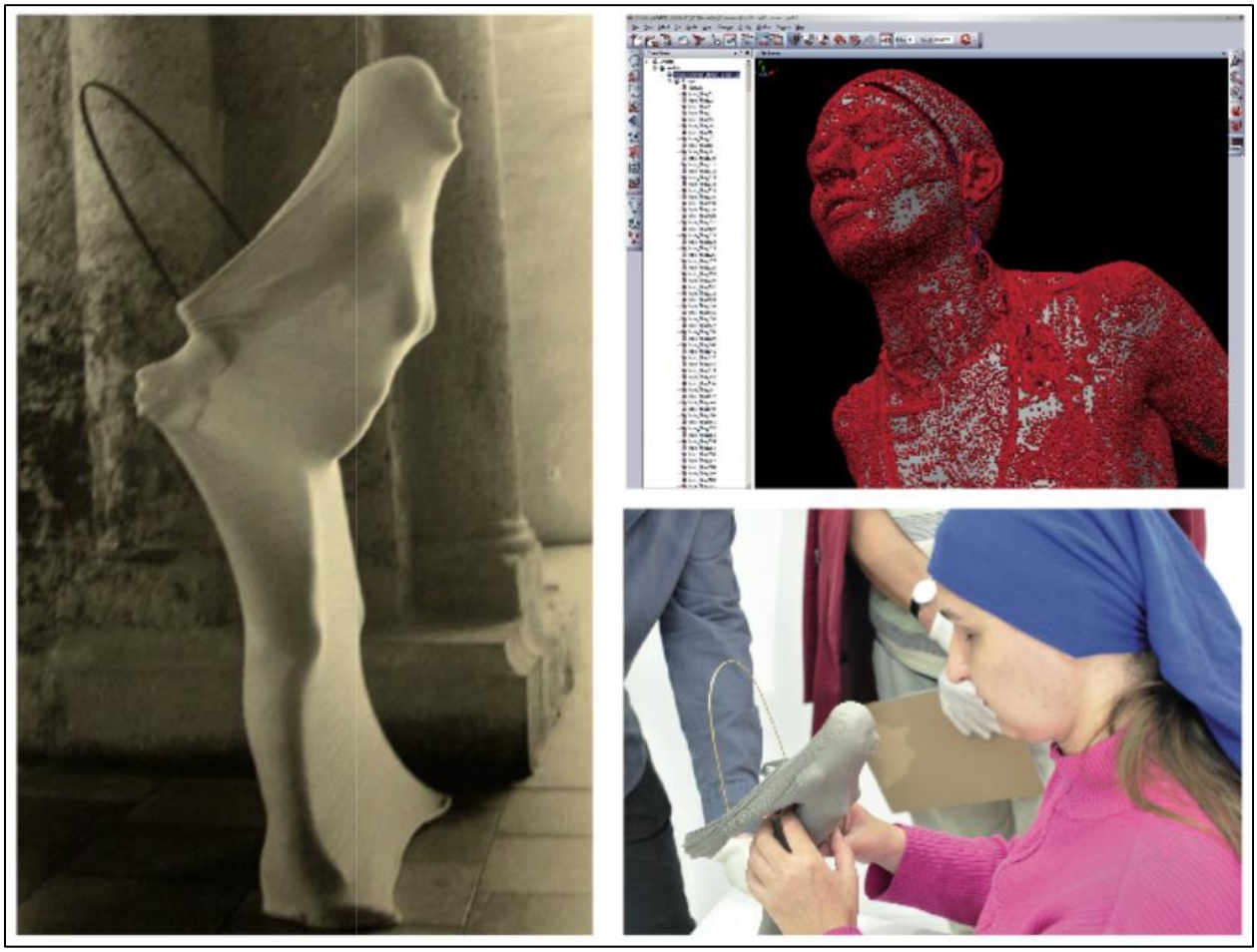

Figure 44: 3D modeled and printed reproduction of Untitled Photograph by Lotte Hendrich-Hassmann, 1982 to facilitate handling y visually impaired museum visitors. Images from Neumüller et al, 2014.

Printing has also been used as a tool in mountmaking, particularly for international collections or loans when the objects are not readily available (Neumüller et al. 2014; Cooper, 2019). Traditionally, creating custom mounts for artifacts involved a labor-intensive process, occasionally necessitating direct handling of the artifact, which could pose risks. With the introduction of 3D printing, mountmakers can tailor precise mounts without ever touching the actual object. This not only ensures the safety of the artifact but also results in mounts that perfectly contour the object, offering optimal support and aesthetic appeal (B. Farrar, personal communication, February 15, 2020).

While 3D technologies have been applied to conservation in a variety of ways, treatments using 3D printing have focused primarily on two aspects: creating customized supports or detachable fills. Supports can be made both externally—such as those employed by mountmakers—or internally, as described by Arbace et al (2013) in their restoration of a terracotta

Figure 45: Fitting sherds reconstructed through 3D printing. Images from Burgess, 2018.

statue. Although fills and reproduction elements have been used for the conservation treatment of various objects (Figure 45), most applications are on ceramic reconstruction (Lee & Wi, 2015; Burgess, 2018; Garland et al., 2018).

All these methods are based on 3D data capture using photogrammetry or structured light scanning in order to obtain an accurate model to print. These techniques also allow the replication of decorative elements, reducing guesswork or inaccuracies in reproductions. For example, Henriques (2020) applied this methodology to the restoration of missing elements of a frame belonging to an 18th century painting of D. José, Prince of Brazil, from the National Palace of Queluz, Portugal. Existing elements of the frame were scanned to obtain their model and reproduced by 3D printing for areas of loss (Figure 46). These treatments, however, generally use printers as is, working within the confines of common printable materials.

Figure 46: Reconstructed frame element from 3D scanning and modeling (left) followed by printing and adhering (right). Images from Henriques, 2020.

4.2 Additive manufacturing and printer selection

Additive manufacturing, the industrial term often interchanged with 3D printing on the commercial scale, builds objects by methodically adding material in layers until the desired form emerges. While a large number of industrial methods exist, there are five main types of additive manufacturing available for smaller scale fabrication that would be applicable to conservation, each with distinct features and advantages (Figure 47):

1. **Material extrusion: fused deposition modeling (FDM) or fused filament fabrication (FFF)**

   The most widely used form of commercial printer, FDM operates by extruding a solid thermoplastic filament through a heated nozzle. This molten material, upon being deposited on the build platform, cools and solidifies, creating the object. Dimensional accuracy for this method hovers around +/- 0.5%, with a variance of +/- 0.5 mm at the lower end. Depending on printer brand, layer heights can vary between 50 and 400 microns.

2. **Vat polymerization: stereolithography (SLA) and digital light processing (DLP)**

   The second most widely used form of commercial printer, these methods leverage a light source to selectively cure a vat of photopolymer resin. While SLA employs a precise laser point to essentially “draw” each layer, DLP adopts a voxel approach, curing entire 3D layers simultaneously. The dimensional accuracy stands at +/- 0.5%, reaching a lower limit of +/- 0.15 mm. With layer heights ranging between 25 and 100 microns, it produces high resolution prints. SLA and FDM stand out as the most affordable and user-friendly techniques, suitable for desktop usage and cost-efficient scaling.

3. **Powder bed fusion: metal laser sintering (DMLS); selective laser melting (SLM); and electron beam melting (EBM)**

   This technique utilizes a thermal source to weld powder particles together, layer by layer. Most commonly, thermoplastic powders, such as Nylon, serve as the primary material. The method boasts a dimensional accuracy of +/- 0.3%, with a lower limit of +/- 0.3 mm.

4. **Material jetting: material jetting (MJ) and drop on demand (DOD)**

   MJ and DOD deposit droplets of material selectively on a build plate. The droplets, made from photopolymers or wax, cure upon light exposure. What sets material

jetting apart is its capability to print diverse materials in a single object. This variety ensures that support structures might differ from the actual object structure. The dimensional accuracy is impressive at +/- 0.1mm. DOD finds specific utility in wax casting. The layer height varies between 16 and 32 microns.

5. Binder jetting

In this method, a liquid bonding agent is deployed to bind specified regions of a powder bed, fusing them together. It combines facets of selective laser sintering and material jetting. Depending on the choice between metal or sand as a substrate, dimensional accuracy varies: ±0.2 mm for metals and ±0.3 mm for sand. Layer height is contingent on the material, with full-color models typically at 100 microns, metal parts at 50 microns, and sand-casting mold materials lying between 200-400 microns.

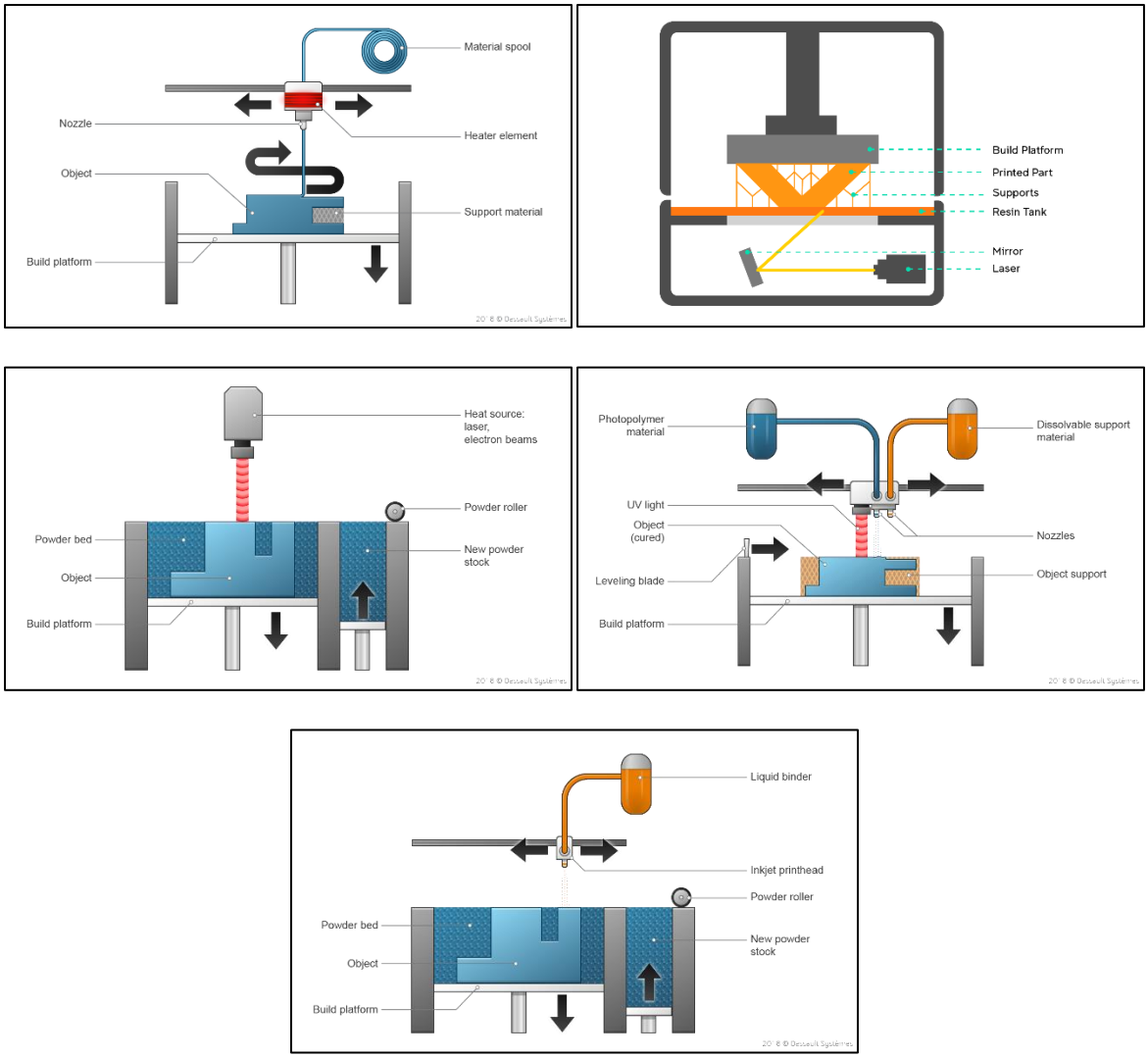

Figure 47: Diagrams for each 3D printing method. From left to right - FDM, SLA, Powder Bed Sintering, Material Jetting, and Binder Jetting. Images from Dassault Systèmes, 2023 and UNSW Making, 2023.

Figure 48: Test print showing layer resolution of FDM vs SLA printers. Images from MANUFACTUR3D, 2018.

Among the many additive manufacturing techniques available, FDM/FFF (Fused Deposition Modeling or Fused Filament Fabrication) and SLA/DLP (Stereolithography and Digital Light Processing) emerge as frontrunners in terms of accessibility. Their dominance in the 3D printing communities is due to the fact that they offer a balance between affordability and functional utility, making them a favorite for both hobbyists and professionals alike.

In contrast, other methods, such as Binder Jetting and Powder Bed Fusion, have limited commercial appeal. Their application leans heavily towards industrial sectors, where large-scale rapid prototyping is the primary focus. The cost factor associated with these methods, owing to the sophisticated technology and high-quality materials required, renders them unsuitable for everyday consumers. Additionally, the reliance on powder beds adds an additional variable to consider in terms of stability and reduces the versatility of this method for treatment solutions that require certain material qualities, such as translucency or texture.

When drawing a direct comparison between SLA and FDM, SLA distinctly boasts superior layer resolution (MANUFACTUR3D, 2018). This means the output from an SLA printer will often be smoother, with finer details sharply pronounced (Figure 48). However, this precision comes with its own set of challenges. SLA employs a unique mechanism where the object is printed upside-down using UV-cured resins. In order to devise unique formulations for printing with SLA, one needs to integrate UV-curing additives.

The challenge arises when we consider materials like lacquer, which are notably UV-sensitive. Preliminary curing with UV can have unintended consequences. Previous studies on attempts to directly UV cure lacquer films have highlighted an interesting anomaly: excessive exposure in the initial curing phases can lead to material deformation, such as warping or wrinkling (see Figure 49). This can be reduced by extended hydrogenation or mechanical polishing, but this would require extensive post-processing (Xia et al., 2010; Okino et al., 2016). Furthermore, the process encounters hurdles when attempting to incorporate additives into the resin formulation, such as pigments or bulking agents. These inclusions can obstruct the UV light's path, resulting in uneven or incomplete curing (D. Daniels, personal communication, May 19, 2022).

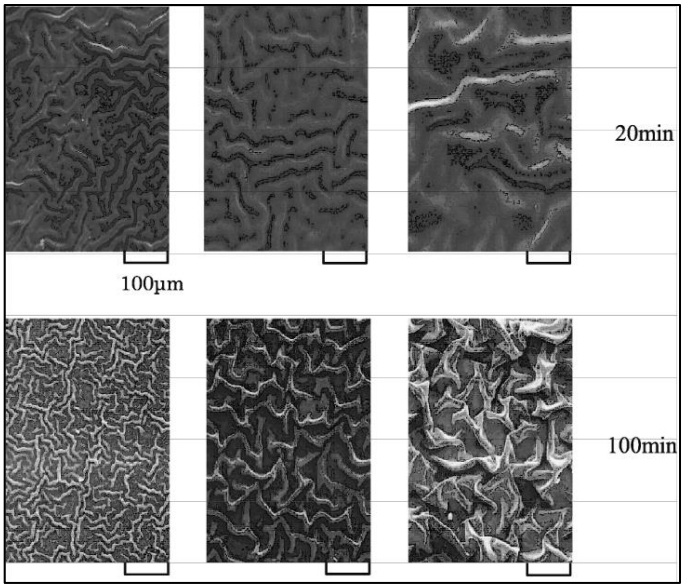

Figure 49: SEM micrographs of urushiol film deformations after UV irradiation. Images from Okino et al, 2016.

On the other hand, FDM may not match the finesse of SLA in terms of layer resolution, but it offers an unparalleled level of flexibility. It's a system more open to experimentation. Modifying the hardware, trying out novel materials, and even integrating unconventional components becomes feasible with FDM. This flexibility is pivotal, especially when working with unconventional materials, pushing the boundaries of what is traditionally achievable in the realm of 3D printing (MANUFACTUR3D, 2018).

Selecting an FDM printer for such use can be confusing, however. The market is packed with options ranging from beginner-friendly models to those tailored for professional use. Printers for beginners are tailored more for hobby and commercial use. They typically have a lower price point ranging from $200 to $2000. Printers closer to the higher end of this spectrum often overlap with lower-range professional printers, boasting a larger variety of printable material, larger build

volumes, more consistent layer resolution, and additional options such as dual extruders (extruders that can print two separate materials at once) and enclosed chambers (heated covers that allow for more consistent printing). Their advantages are not limited to cost, however; many of these “hobby” printers remain highly open source and have large communities online that provide prompt assistance on topics such as troubleshooting issues, calibrating print beds, or modifying hardware or G-code. Such support is crucial for newcomers and those looking to adapt printers for unconventional tasks. Examples of these beginner-friendly models include the Sovol SV06 ($280) and the Prusa i3 MK3S+ (Assembled: $900; Kit: $650). Conversely, professional printers geared towards manufacture and rapid prototyping come with heftier price tags that can range in the thousands, but they also promise better precision, speed, and robustness, with models like the UltiMaker S7 ($8400) and Delta WASP 2040 Industrial X ($6300). With the greater range of built-in options (e.g., multiple extruder head types, wider variety of printable materials, etc.) and robust designs, however, these machines tend to be less customizable in terms of hardware modifications.

For this project, availability was as much of a driving factor for machine selection as function was; however, practically speaking, printers available in Makerspaces and school labs tend to be in the middle to upper levels of beginner models and are the most conducive to modification. The Digital Archaeology Lab at the Cotsen Institute of Archaeology in UCLA provided access to their Lulzbot Taz 6 for use. Due to the time and access restrictions as a result of COVID, the author also purchased a kit for a second printer: Prusa i3 MK3S+ (Figure 50).

The Lulzbot Taz 6 was a reliable printer with 28cmx28cmx25cm build volume and 0.05mm-0.4mm layer resolution. It has automatic Z-axis leveling and comes with a TAZ Single Extruder Head v2.1 0.50mm nozzle, though additional extruder types can be purchased for the system. The printer prints through the Cura software, used by many brands of printer. Unfortunately, the Taz 6 is no longer manufactured, but has been replaced by smaller versions (Taz Mini 2) and upgraded versions (Taz Pro series and Taz Workhorse).

The Prusa i3 MK3S+ is arguably more open source than the Lulzbot. It is one of the earliest fully open-source designs created by Josef Prusa in 2012. It was originally intended to be self-replicable, meaning it had enough printable components that one could ostensibly build additional printers by printing those parts on the original. Today, this is perhaps even truer, with the hardware components like stepper motors and screw rods readily available in hobby shops online. It has a 25x21x21cm build volume and 0.05-0.35mm layer height. It has assisted Z-axis leveling and comes with a single extruder head, but, like the Lulzbot, additional extruder types can be purchased.

Building the Prusa was relatively straightforward, as the company includes a well-organized, detailed instruction manual with images combined with online chat assistance for any issues (Figure 51). All tools were included with the hardware and each item was clearly labeled. Because half of the parts are printed, however, there are at times issues in the fit of individual pieces. These are generally remediable with a sharp knife or, because the filaments are thermoplastic, a soldering iron.

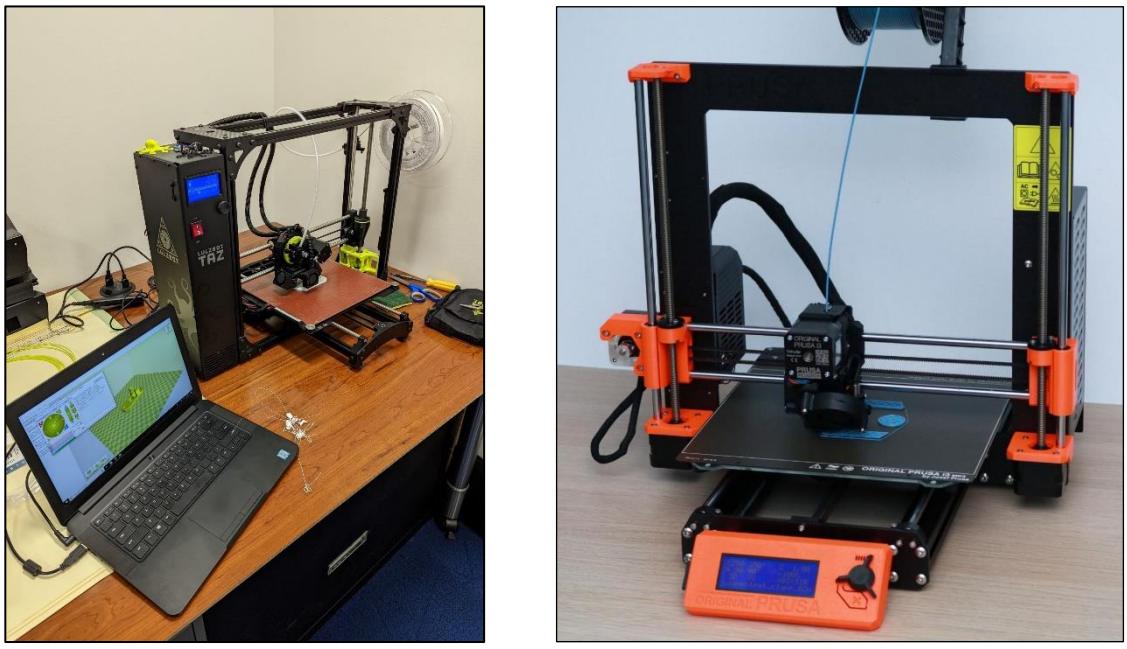

Figure 50: Lulzbot (left) and Prusa (right) used for this project.

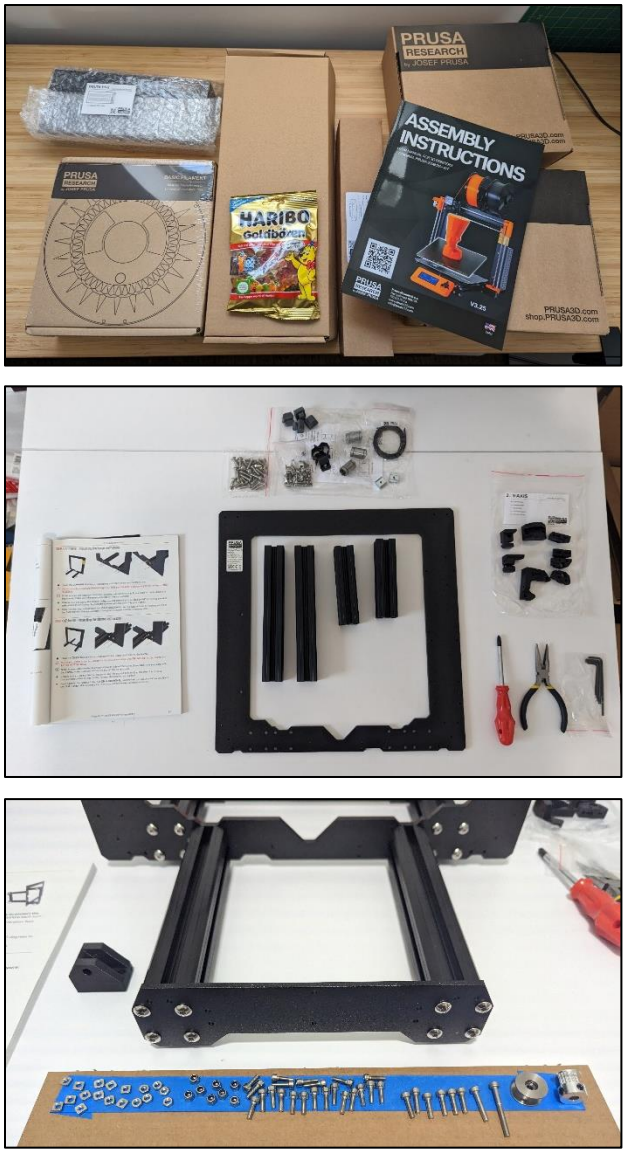

Figure 51: Images from Prusa kit assembly.

4.3 Paste extruder modifications

The modification challenge was straightforward: enabling thermal-free printing of non-standard materials. Paste printing is a commonly applied modification on FDM printers and has been used to print a variety of unique materials among hobbyists and for industrial fabrication, from edible pastes such as cheesecake and frosting to structural pastes such as concrete or clay (Lanaro et al., 2019; IDZone, 2019; Koumari, 2022; Lawless, 2023). While there are printers designed especially for varieties of paste printing, modifying a standard FDM printer is relatively straightforward. This technique replaces the heated extruder, which typically melts and dispenses the filament, with a paste extruder that uses pressure to expel viscous fluids and pastes. Various designs and models have already been created by other makers, inventors, or hobbyists and are available for free download from public databases such as Thingiverse, Lulzbot forums, Printables, GrabCAD, etc. The advantage here means the wheel didn't have to be reinvented; instead, the project could capitalize on the collective knowledge and experience of the 3D printing community.

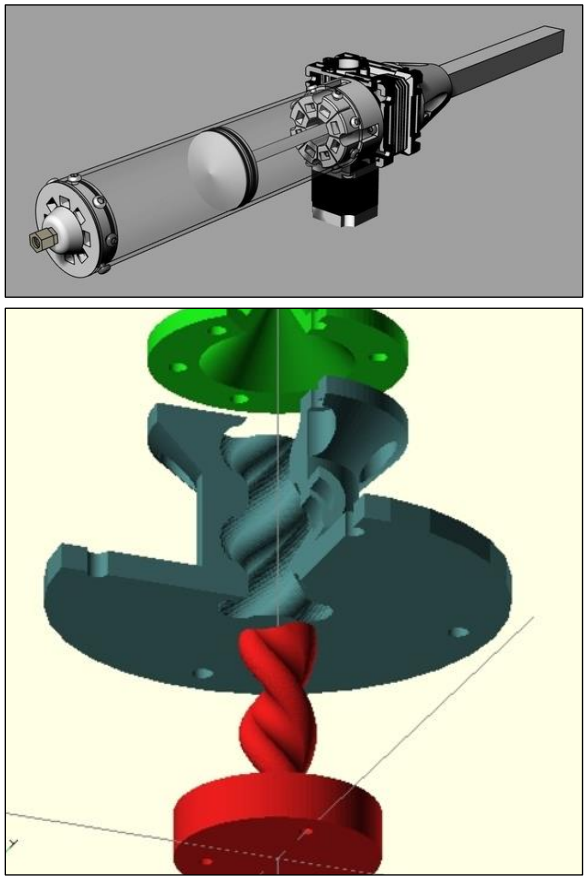

Figure 53: 3D models of plunger-type (top) and Moineau screw-type (bottom) paste extruders. Images from Thingiverse.com.

Most paste printers designed on these websites fall into two prominent categories: plunger-type and Moineau screws (Figure 53). Plunger-based extruders are more ubiquitous and have a better foundation of community-backed information and troubleshooting advice. They offer relatively reliable performance but have limited volume, given the need to pre-fill a finite, enclosed container before printing. Plunger type extruders are further delineated by screw-rod and belt-driven extruders (Figure 52). The former type tends to be external to the printer itself, using the rotating action of a threaded metal rod attached to a stepper motor to press a plunger down into a seated container. Because it is separate from the printer, this type of modification can be built to house varying container sizes for printable materials, as long as the motor is strong enough to power the compressive action. The printing material is fed through a tube from the mouth of the container to a nozzle mounted on the extruder platform.

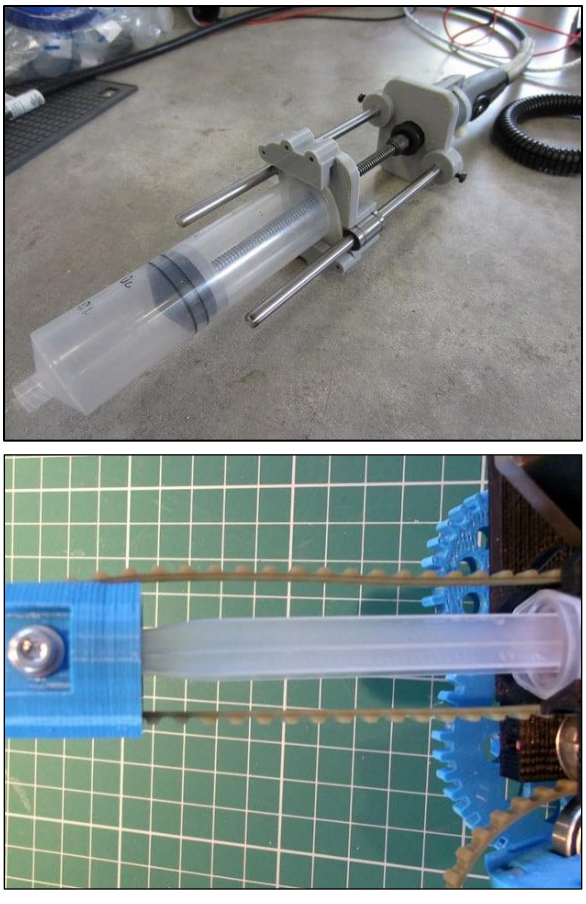

Figure 52: Screw-rod (top) and belt-driven (bottom) plungers. Images from Thingiverse.com.

The belt-driven types of extruders appear almost entirely based off of one 2012 design by UK online user RichRap, who created this type of extruder to sit directly onto the extruder carriage for a Prusa printer. Subsequent uploaders have built upon or redesigned elements to fit other printer carriages. Because of its early onset into the printing community, the RichRap extruder also has extensive calibration and test runs behind it, written up in blog posts and with instructive vides (Richrap3d, 2012).

Both types of plunger extruder have a mix of printable components and purchased hardware. The hardware elements for the original RichRap extruder are arguably easier to find and somewhat less expensive than the screw-rod style, but the difference is not large enough to be a defining factor for selection, especially given that any printer-specific hardware continues to become more affordable and accessible as 3D printing grows in the hobby field.

Moineau screws, while less well-tested, offer a continuous printing capability. The turning motion of the Moineau screw creates a constant extrusion pressure independent of container size, therefore a secondary loading method can be used to add printing material. In most tested cases, this tends to be a loaded syringe or larger plunger container that is manually controlled by the user. The models currently available online for this kind of extruder are constructed almost entirely by printed parts, making it far easier to replicate than the plunger type extruders (see Figure 54). However, constantly feeding material in while printing is relatively impractical and affects the extrusion rate and flow.

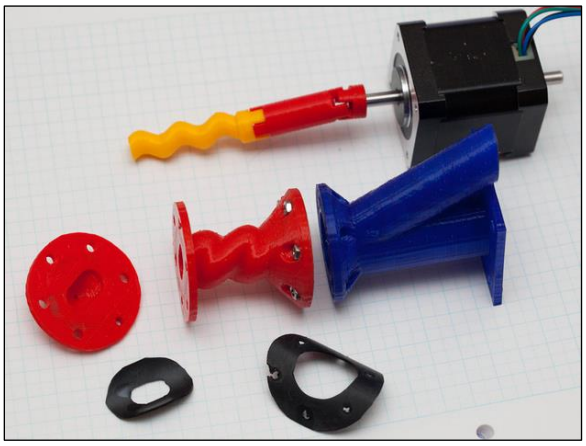

Figure 54: Printed Moineau screw paste extruder, disassembled. Images from Thingiverse.com.

Given the intended use of this type of modification, the free-standing screw-rod type of plunger extruder was selected for fabrication. Because its only points of connection to the printer are the stepper motor—used universally by FDM printers—and the printing nozzle, it can feasibly be attached to any printer on the market. While the

belt-driven/RichRap extruders appear well vetted, the most confident design is still made for the quick-release carriage attachment on a Prusa printer, making it less applicable for other brands. Moineau screw extruders were not chosen either due to the hands-on needs for adding printing material.

The model for the extruder was obtained from the Lulzbot forums, designed by user “bam” (*Open Source Syringe Pump - Filament*, 2014; *Index of /TAZ/Accessories/Halibut*, n.d.). Printable components for the modification were printed using the Lulzbot Taz 6. Syringes were provided by the UCLA/Getty Training Laboratories. Additional hardware was purchased from McMaster-Carr and Maker’s Tool Works (since closed).

4.4 Fabrication and Application

The extruder consisted of three printed parts: the motor mount, the pressure slider, and the syringe mount. All other components (see Table 5) were purchased. The stepper motor used was the original extruder motor removed from the Lulzbot Taz 6. The Taz 6 was able to print all three parts within a day, but scaling the model to the final print was difficult. Due to availability, the syringes sourced for this extruder were slightly smaller than the mount component. The model is directly scalable within the Lulzbot Cura software; however, scaling the entire model also reduces the diameter of the assembly holes for the other components. Therefore, electrical tape was used to bulk up the syringe for a snug fit.

M3 thermal inserts are essentially threaded cylindrical nuts with teeth on the external surface. Because the printed components are made from thermoplastics, a thermal insert can be pushed into a hole slightly smaller in diameter than itself using a soldering iron (Figure 55). This allows contact points for the screws and washers and is used to attach the motor and the threaded T-nut to the printed mounts.

Table 5: Components for fabricating the paste extruder.

Part Name	*Quantity*	*Purchased/Printed*	*Manufacturer*	*Part Number*
Motor mount	1	Printed	n/a	n/a
Syringe mount	1	Printed	n/a	n/a
Slider	1	Printed	n/a	n/a
Threaded rod	1	Purchased	Makers Toolworks	LEADSCREW-SINGLE
Threaded T-nut	1	Purchased	Makers Toolworks	LEADSCREW-SINGLE
10mm stainless rods	2	Purchased	Makers Toolworks	SHAFTING-10-SHORT
Z coupler	1	Purchased	Makers Toolworks	HELICAL-COUPLER
10mm Igus polymer bushings	4	Purchased	Amazon	n/a
608zz bearings	2	Purchased	Amazon	n/a
M3 thermal inserts	11	Purchased	McMaster-Carr	94180A331
M3x6 grub screw	4	Purchased	McMaster-Carr	91390A100
M3x12 socket head cap screw	11	Purchased	McMaster-Carr	91290A117
M3 washer	11	Purchased	McMaster-Carr	93475A210
NEMA17 stepper motor	1	n/a	n/a	n/a
Rubber feet	4	Purchased	Amazon	n/a
140cc syringe	Varies	Purchased	n/a	n/a
1/8” Teflon tubing, 10ft	Varies	Purchased	McMaster-Carr	5239K11
1/8” Luer lock male fitting	Varies	Purchased	McMaster-Carr	51525K33
1/8” Luer lock female fitting	Varies	Purchased	McMaster-Carr	51525K26
Luer lock nozzles (needle or plastic)	Varies	Purchased	McMaster-Carr	6699A6 and 6710A69

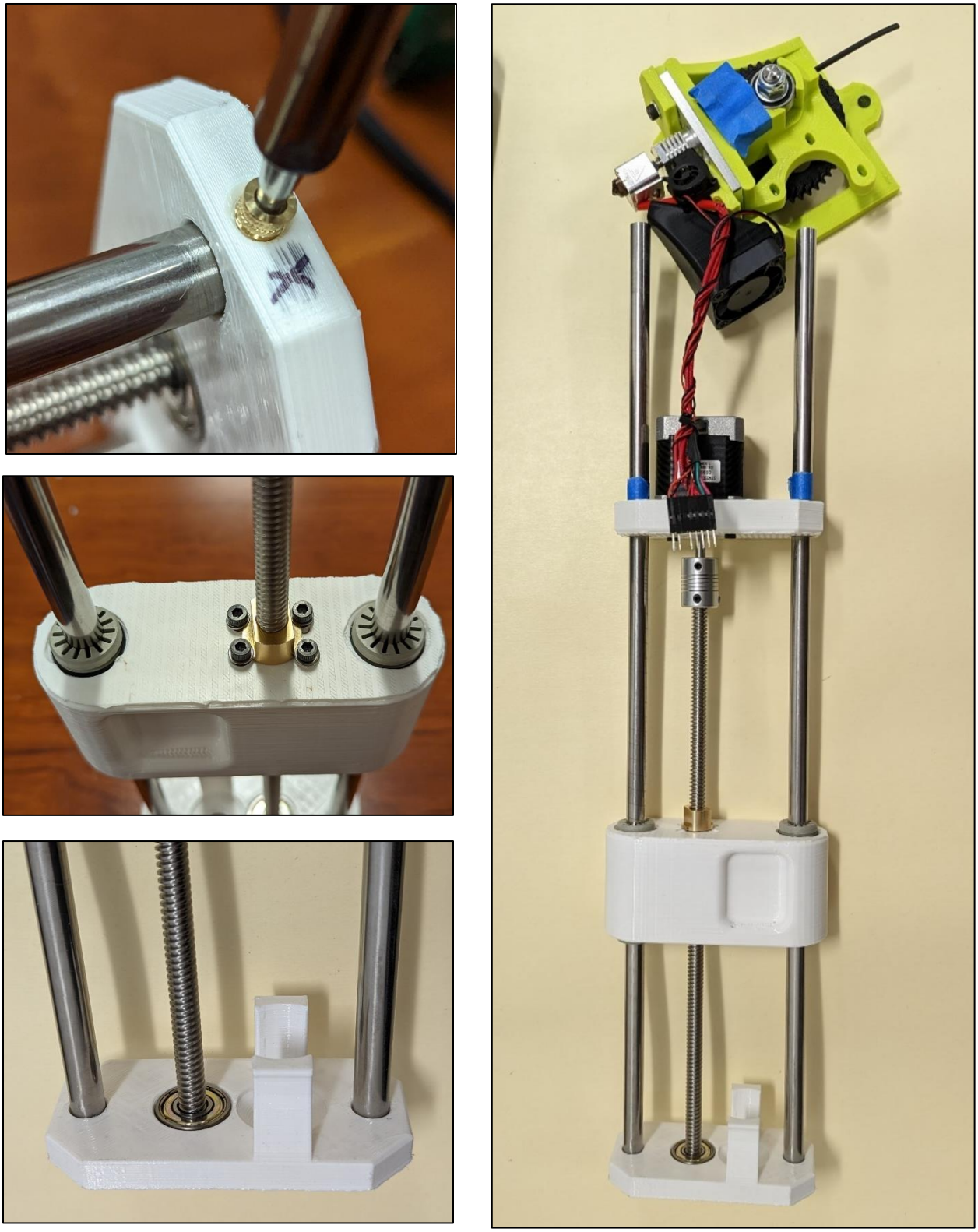

Figure 55: (Top left) Inserting an M3 thermal insert with a heated soldering iron. (Center left) Grey brushings pressure fit and T-nut secured with socket head cap screws. (Bottom left) Steel rods pressure fit and screw rod inserted into bearings. (Right) Paste extruder modification after assembly.

The polymer bushings are pressure fit into the slider component to allow for easy movement up and down the stainless rods, which are pressure fit into the motor mount and syringe mount on either end (Figure 55). The threaded rod is placed through the center of the three components, attached to the motor with the Z coupler. The rod diameter is larger than the rod attachment of the stepper motor, so the coupler acts as an adapter that centers the rotation on the threaded rod. At the base of the threaded rod, the two bearings act as friction reduction where it mounts into the syringe mount component.

The Luer lock system is the same as the syringe type locks that allow for interchangeable needles, so any nozzle that is compatible with a Luer lock syringe will be compatible as a printing nozzle, meaning the diameter of the extruded material can be controlled and changed easily. The male fitting is placed on the end of the tube that will attach to the syringe, while the female fitting will be places on the printing side. The nozzle head can then be attached to the extruder using zip ties or any other method that is available (Figure 56).

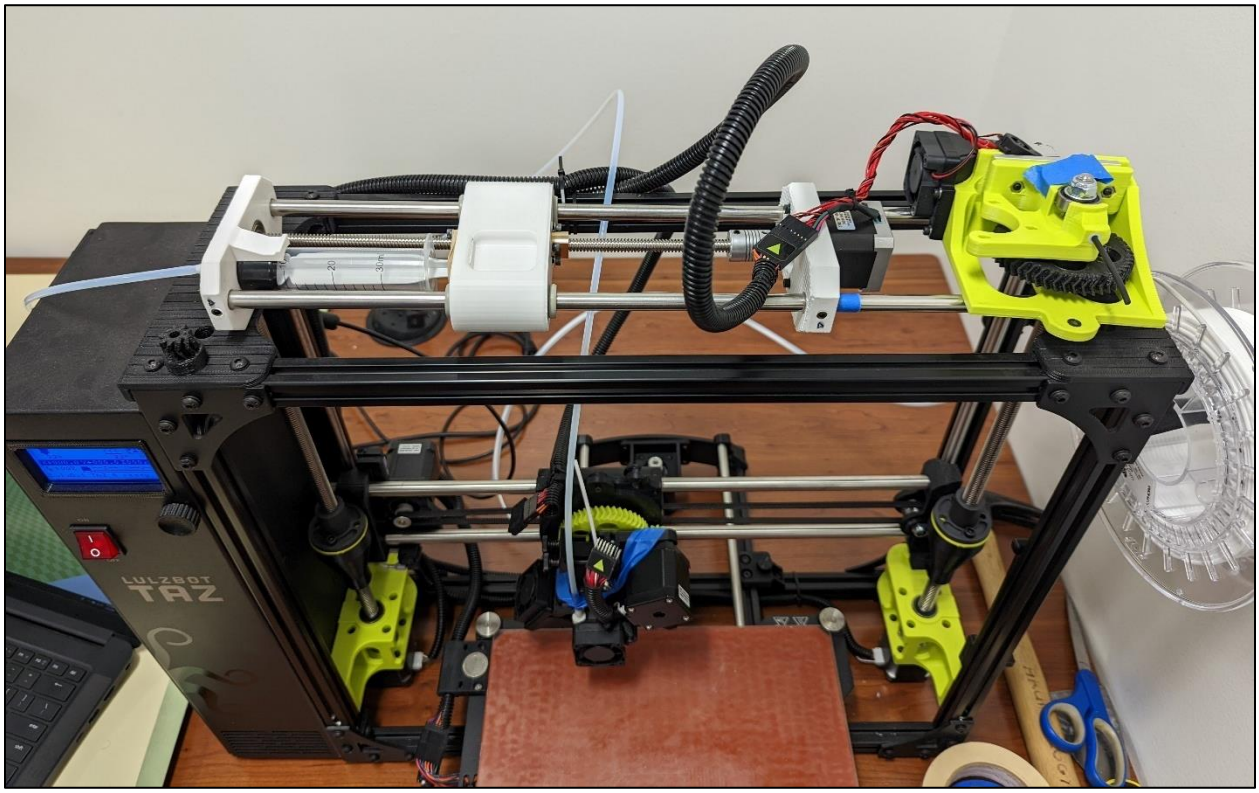

Figure 56: Modification assembled and connected to the printer for testing.

Figure 57: Lulzbot auto-leveling button and platform.

For the Lulzbot, because the extruder motor is already connected to the printer, no additional wiring is necessary. Cura software will control it as if it is connecting to the basic heated extruder. This makes it easy to adjust extrusion speed and positioning. Calibration, however, can be slightly difficult. Because the Lulzbot has an auto-leveler process, the nozzle of the extruder must press down on a button at the corner of the bed (Figure 57). While the extruder itself does not have to be removed to attach the paste extruder, this press can sometimes push the paste extruder up and out of alignment. Making sure the paste nozzle is mounted on the side away from the bed will avoid this accidental adjustment. Similar to the Lulzbot, the Prusa was also able to integrate the existing stepper motor into the paste modification. Unfortunately, less time was available to troubleshoot the Prusa, so successful printing was not achieved.

Because lacquer is costly in large quantities, fine clay slip was used as it is a known additive in lacquer and could be easily thinned with water to adjust its working properties. FDM printers also have a heated print bed, which is unnecessary for paste printing. This can be reduced, but not completely shut off within the printer settings; however, the G-code that controls the printer is easily editable using any text editing software, such as Notepad++. Within the code, “M140” sets the bed temperature and “S” indicates which temperature, so “M140 S0” will turn the heated bed off. This G-code edit should be applicable to any printer.

Initial tests of extrusion were promising, if flawed. A 0.33mm tip was used for the nozzle and the printer was able to dispense a line across paper that was taped to the bed (Figure 58). However, the nozzle quickly became clogged. Cutting the nozzle and increasing its diameter allowed for more consistent extrusion and less clogging but did not solve the issue entirely. Unfortunately, full experimentation for the printability of lacquer formulations across different printers could not be completed within the scope of this thesis, but with additional troubleshooting and experimentation, these preliminary findings show that modifying commercial FDM printers for alternative printing materials is a viable option and shows promise in the field of lacquer conservation.

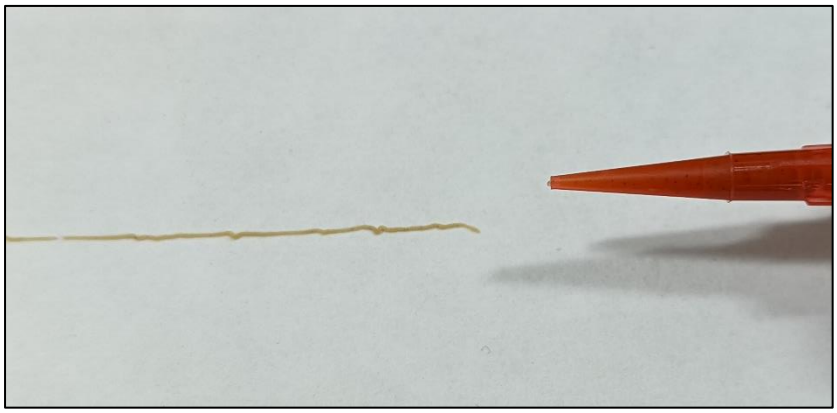

Figure 58: Nozzle size and resultant exuded line of material.

4.5 Conclusions and Further Research

The insight into lacquer formulations highlighted in Part I of this thesis, and their use in traditional conservation of spiritual statues gives rise to the potential application of novel 3D printing technology. Future work in testing printability will include fine-tuning the printing methodology and calibrating nozzles for layered printing. Identifying the exact material properties (e.g., viscosity, flow, cohesion of material vs adhesion of layers) necessary for optimizing the print will also be integral to designing lacquer compositions that are structurally sound, printable, and curable. The applicability of this instrument should also be considered in the wider field of conservation as it is not restricted to lacquer materials and can be applied to other conservation materials, such as Paraloid B-72.

The versatility FDM printers have in modification and adaptation allows for the printing of such bespoke paste recipes. Given the variance in lacquer recipes, the ability to alter formulation combined with the repeatability of printing methodology creates a unique opportunity to use paste

extruders to print lacquer formulations geared towards repairing large scale statuary. While full-scale testing of this technology is yet to be completed, preliminary tests of fabricated modifications have proved promising. In the future, it is not unlikely that historic traditions will meet modern ingenuity to create new ways of preserving the past.

Appendix A: Cross-sections

	Location Image	X-Section Image, 430nm UV [Top sections]	X-Section Image, 430nm UV [Bottom sections]	Total Layers: Description
2051-S-01		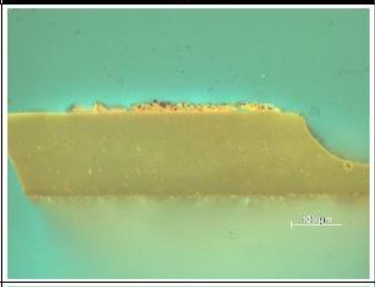	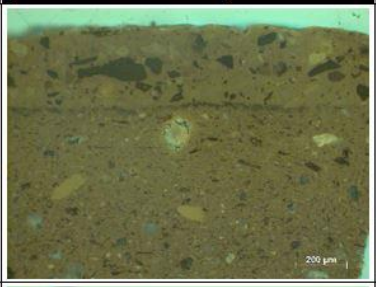	4-5: R1, B1, B2, [B?], B3
2051-S-02		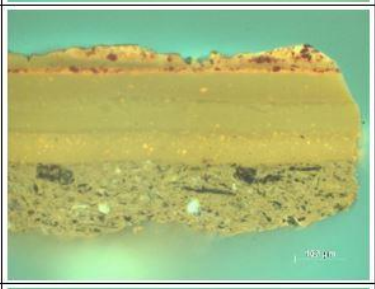	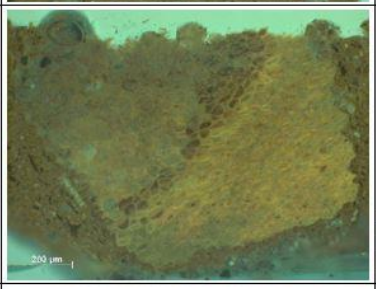	7: R1, B1, R2, B2, B3, B4, B5
2051-S-03		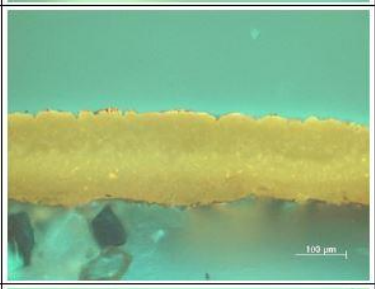		3: R1, B1, G1
2051-S-04				4-5: [R1, missing], B1, R2, B2, B3/Substrate ?
2259-S-01		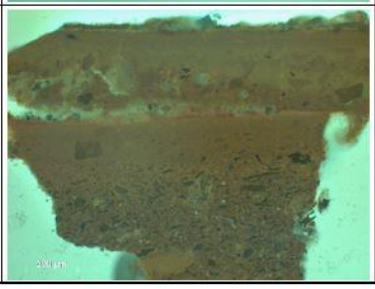		7-10: [Potential green layer], G1, S1, B1, B2, [G2 and S2], R1, B3, B4

	Location Image	X-Section Image, 430nm UV [Top sections]	X-Section Image, 430nm UV [Bottom sections]	Total Layers: Description
2259-S-02		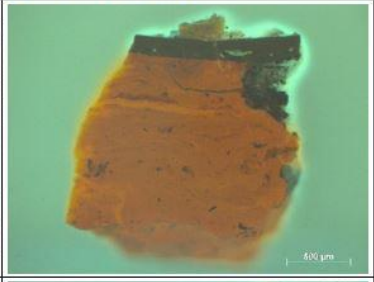		6-7: [Potential green layer], R1, B1, R2, R3, B2, B3, B4
2259-S-03		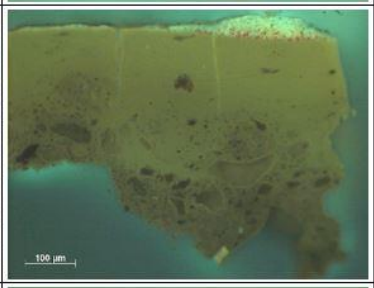		4: W1, R1, B1, B2
2259-S-04		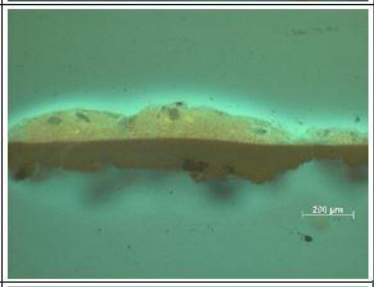		2: R1, B1, [Substrate?]
2259-S-05		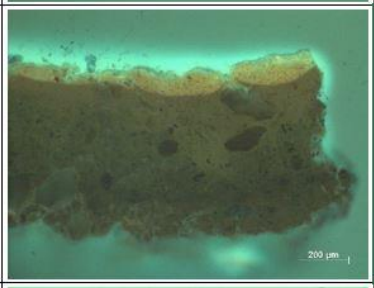		2-3: [Unknown?], R1, B1
N509-S-01 Red		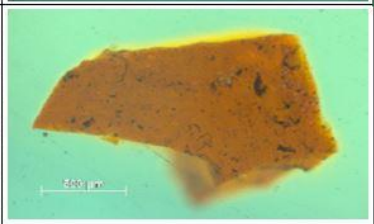		1: B1

	Location Image	X-Section Image, 430nm UV [Top sections]	X-Section Image, 430nm UV [Bottom sections]	Total Layers: Description
N509-S-01 Black		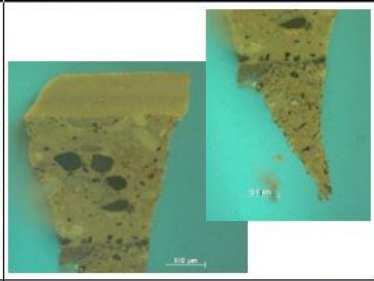		3: B1, B2, B3
N509-S-02		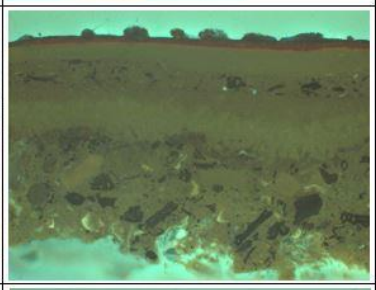	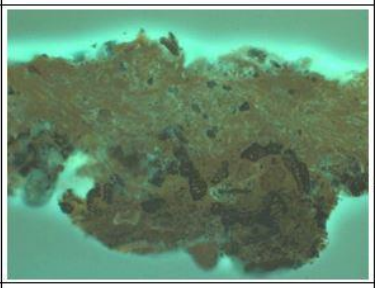	9: G1, S1, R1, B1, B2, B3, B4, Fabric, B5
N509-S-03 Lac				4: R1, B1, B2, B3
N509-S-03 Resin		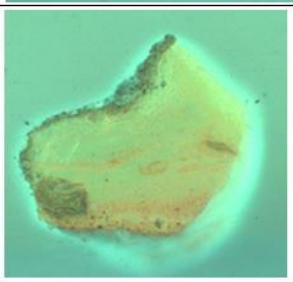		1: R1
N509-S-04		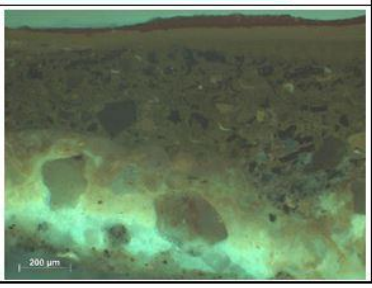		4: R1, B1, B2, B3, Substrate

	Location Image	X-Section Image, 430nm UV [Top sections]	X-Section Image, 430nm UV [Bottom sections]	Total Layers: Description
N1323-W-01		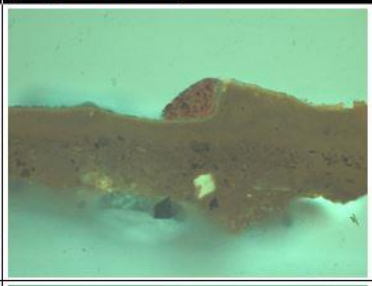	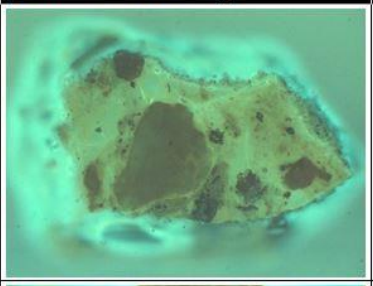	5: R1, S1, B1, B2, B3
N1323-W-02		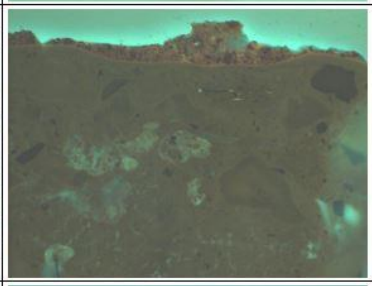	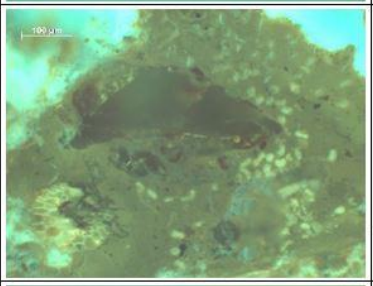	4: [Missing G1] R1, B1, B2
N1323-W-03		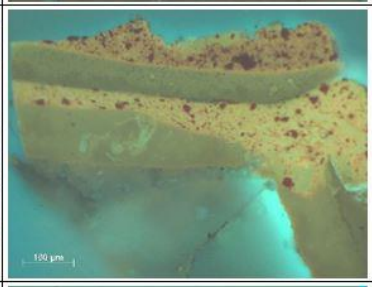	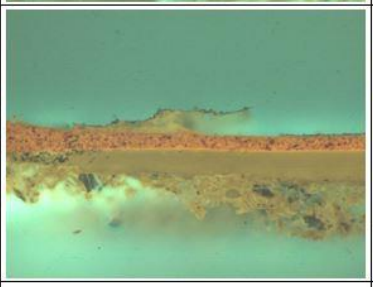	13: [R1 missing], B1, [G1 missing], R2, B2, G2, R3, B3, G3, S1/B4, R4, B5, B6
N1323-W-04		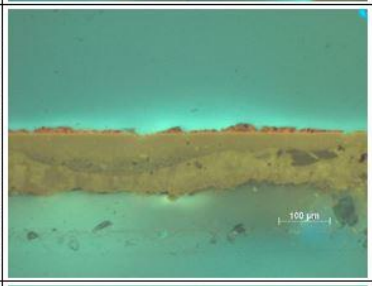		3: R1, B1, B2
N1323-W-05 A		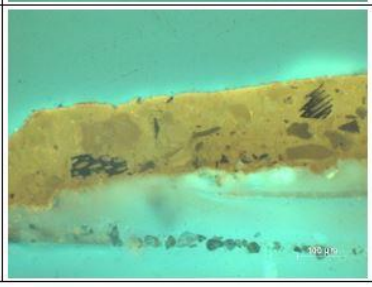		2: R1, B1

	Location Image	X-Section Image, 430nm UV [Top sections]	X-Section Image, 430nm UV [Bottom sections]	Total Layers: Description
N1323-W-05 B		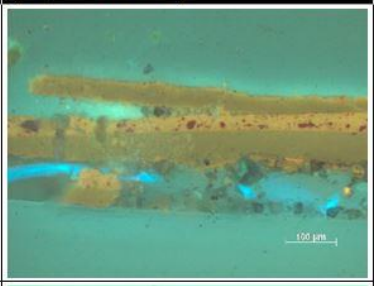		6-8: R1, B1, G1, R2, B2, G2, [R3?], [B3?]
5509-W-01				1: B1
5509-W-02	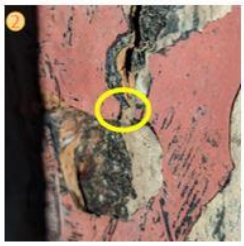	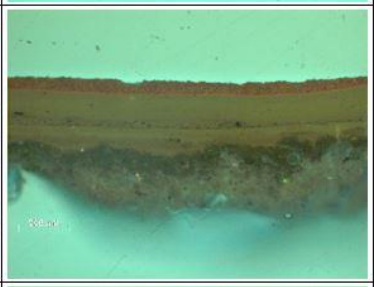		4: R1, B1, B2, W1
5509-W-03		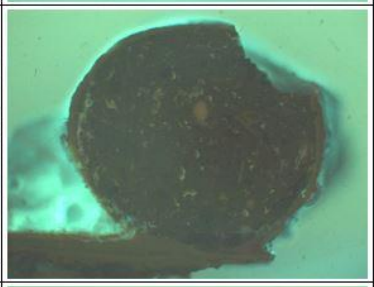	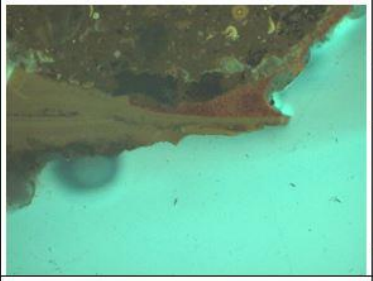	3 and 5: R1, B1, B2 // ON THE FLAT PORTION: R1, B3, B4, B5, W1
5509-W-04		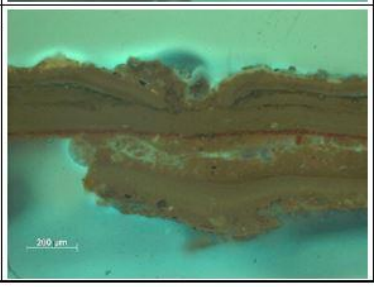		7-9: [G1?], [R1?], S1, B1, B2, B3, R2, B4, B5

	Location Image	X-Section Image, 430nm UV [Top sections]	X-Section Image, 430nm UV [Bottom sections]	Total Layers: Description
N1420-W-01		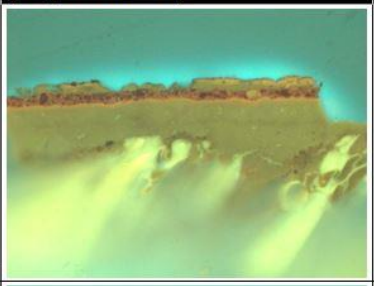		6: [G1 missing], R1, B1, R2, B2, B3
N1420-W-02		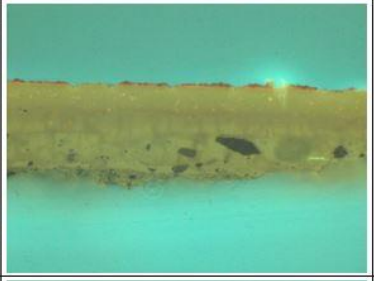		5: R1, B1, B2, B3, B4
N1420-W-03		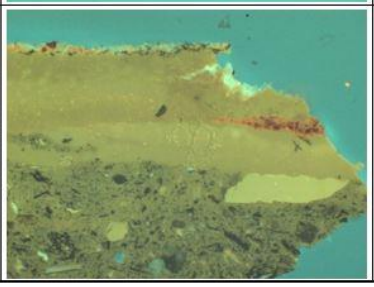	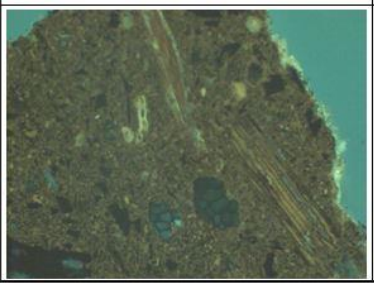	6: R1, B1, R2, B2, B3, B4

Appendix B: Portable X-Ray Fluorescence

Key	Counts
T	<2
X	2-5
XX	5-10
XXX	10-25
XXXX	25-100
E	>100

Sample Number	Si	K	Ca	Ti	Mn	Fe	Ni	Cu	Zn	Au	Hg	Pb
2051-S-01	X	XX	XXXX	X	X	XXXX	X	T	T	-	XXX	-
2051-S-02 Bulk	T	T	XXX	T	T	X	T	T	T	-	T	-
2051-S-02 Surface	T	T	X	T	T	T	X	T	-	-	XXX	-
2051-S-03	T	T	XXX	T	T	X	X	T	T	XXX	XX	-
2051-S-04	X	X	XXXX	T	T	X	X	T	-	-	XXXX	-
2259-S-01	T	T	XX	T	X	XX	X	XXX	X	XX	XX	XXX
2259-S-02	T	X	X	T	T	XX	X	XX	X	-	XXXX	XXX
2259-S-03	T	T	T	T	T	XX	X	T	T	-	T	-
2259-S-04	T	T	T	T	T	XX	X	T	T	-	XXX	-
2259-S-05	X	XX	XXX	T	X	XXXX	X	T	X	-	XXXX	-
5509-W-01	T	T	XX	T	T	XX	X	T	T	-	-	-
5509-W-02	X	T	X	X	T	XXXX	X	T	-	-	E	-
5509-W-03	T	T	XX	X	X	XXX	X	T	-	-	XXXX	-
5509-W-04	T	T	XXX	X	X	XX	X	T	-	-	XXXX	-
N509-S-01 Black	-	-	X	T	-	X	X	T	T	-	-	-
N509-S-01 Red	T	T	X	T	T	XX	X	T	T	-	-	-
N509-S-02 Fabric Layers	T	T	XX	T	T	XX	X	X	T	-	-	-
N509-S-02 Lac Layers	T	T	XXX	T	X	XX	X	X	-	XX	E	-
N509-S-03 Red Lac Layer	T	T	XXX	T	X	XXX	X	T	-	-	XXXX	-
N509-S-03 Resin	T	T	X	T	T	XX	X	T	T	-	XXX	XX
N509-S-04	T	T	XXXX	T	X	XXX	X	T	-	-	XXXX	-
N1323-W-01 Bulk	T	T	XX	T	T	XXX	X	T	T	-	-	-
N1323-W-01 Surface	T	X	XXX	T	T	XXX	X	T	T	T	XX	-
N1323-W-02 Bulk	T	T	XXX	X	T	XXXX	X	T	T	-	-	-
N1323-W-02 Surface	T	T	XXX	T	T	XX	X	T	-	X	-	-
N1323-W-03 Bottom Layer	T	T	XXX	T	T	X	X	T	-	X	XXXX	-
N1323-W-03 Top Layer	T	T	X	T	T	X	X	T	-	XXX	XXXX	-
N1323-W-04	T	T	XXX	T	T	X	X	T	-	-	XXX	-
N1323-W-05 Square Frag	T	T	T	T	T	X	X	T	-	XX	XXX	-
N1323-W-05 Triangle Frag	T	T	XXX	T	T	X	X	T	T	-	X	-
N1420-W-01	-	T	T	T	-	T	X	T	-	T	XX	X
N1420-W-02	T	T	X	T	-	T	X	T	T	-	X	-
N1420-W-03 Bottom Fill	T	T	XX	T	T	XX	X	T	T	-	-	-
N1420-W-03 Lac Layer and Top Fill	T	T	XX	T	T	XX	X	T	T	-	XX	T

Appendix C: Pyrolysis-Gas Chromatography/Mass Spectrometry Results

Sample Number	Layer Number(s)	Layer(s) Description	Anacard	Oils/Fatty Acids	Resins	Proteins	Carbo-hydrates	Pigments	Misc
5509-W-03 (molded)	1	R1, B1	Thitsi					Soot?	Methyl hexadecenoate
5509-W-03 (molded)	2	B2	Thitsi		Various markers but No-ID			Soot	
N509-S-01 Black	n/a	B1, B2, B3	Thitsi	Drying Oil (P/S: 4.22)	Shellac?; Various markers but No-ID				Wax
N509-S-01 Red	n/a	B1			Shellac				Methyl hexadecenoate
N509-S-02 Top	1	G1, S1, R1	Thitsi	Drying oil (P/S: 2.92)	Various markers but No-ID			Sulfur (Cinnabar)	Wax
N509-S-02 Top	2, 3, 4	B1, B2, B3	Thitsi	Drying oil (P/S: 2.13)					
N509-S-02 Top	5	B4	Thitsi					Soot?	
N509-S-02 Bottom	n/a	Fabric and B5	Thitsi	Drying oil (P/S: 1.59)	Various markers but No-ID			Soot	
N1323-W-03 Top	1, 2	R1, B1, G1, R2, B2	Thitsi	Drying oil (P/S: 0.89)				Sulfur (Cinnabar)	
N1323-W-03 Top	3	G2, R3	Thitsi	Drying oil (P/S: 1.07)				Sulfur (Cinnabar)	
N1323-W-03 Top	4	B3	Thitsi	Drying oil (P/S: 1.03)				Sulfur (Cinnabar)	
N1323-W-03 Bottom	1, 2	G3, S1/B4, R4	Thitsi	Drying oil (P/S: 1.38)				Sulfur (Cinnabar)	
N1323-W-03 Bottom	3	B5, B6	Thitsi	Drying oil (P/S: 1.31)	Various markers but No-ID				Trimethyl phosphate
2051-S-04	1	B1	Thitsi	Drying oil (P/S: 1.93)					
2051-S-04	2	R2	Thitsi	Drying oil (P/S: 1.23)				Sulfur (Cinnabar)	
2051-S-04	3	B2	Thitsi	Drying oil (P/S: 1.68)					
2051-S-04	4	B3	Thitsi	Drying oil (P/S: 2.69)					Trimethyl phosphate
2259-S-01	1	G1 and S1	n/a	n/a	n/a	n/a	n/a	n/a	n/a
2259-S-01	2, 3	B1 and B2	Thitsi	Drying oil (P/S: 1.83)	Various markers but No-ID				Methyl hexadecenoate
2259-S-01	4	[G2/S2?] R1	Thitsi					Sulfur (Cinnabar)	Methyl hexadecenoate
2259-S-01	5	B3	Thitsi	Drying Oil (P/S: 1.69)					
2259-S-01	6	B4	Thitsi	Drying oil (P/S: 2.48)	Pinaceae				Methyl hexadecenoate
2259-S-02 Top	1, 2, 3, 4	R1, B1, R2, R3			Pinaceae, Camphor			Soot, Sulfur (Cinnabar)	Trimethyl phosphate
2259-S-02	5	B2	Thitsi		Pinaceae			Soot	Methyl hexadecenoate
2259-S-02	6	B3	n/a	n/a	n/a	n/a	n/a	n/a	n/a
2259-S-02	7	B4			Shellac				Trimethyl phosphate, Methyl hexadecenoate

A note on the layers with no data. Layer 1 of 2259-S-02 included mainly a gilded layer with a potential secondary layer of sizing to adhere it to the lacquer surface. This run returned no peaks and therefore had no information to interpret. Likely, this suggests the layer between the gilding and first black layer was not, in fact, an organic sizing such as animal glue, but does not discount another type of adhesive that is outside the detectable parameters of the instrument. Layer 6 of 2259-S-02 included one of the lower black layers (B3). This analysis began successfully, but the instrument malfunctioned halfway through the run and the analysis could not be completed.

Appendix D: Pyrolysis-Gas Chromatography/Mass Spectrometry Chromatograms

Sample Number	Chromatogram
2051-S-04_01	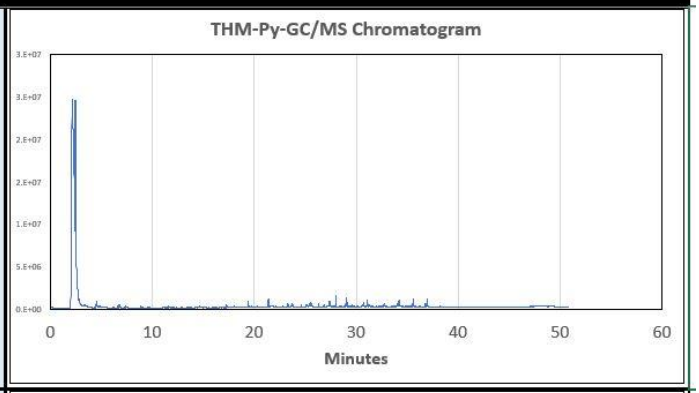
2051-S-04_02	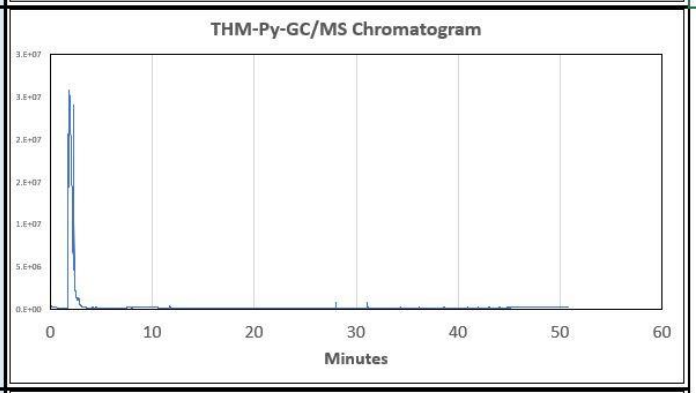
2051-S-04_03	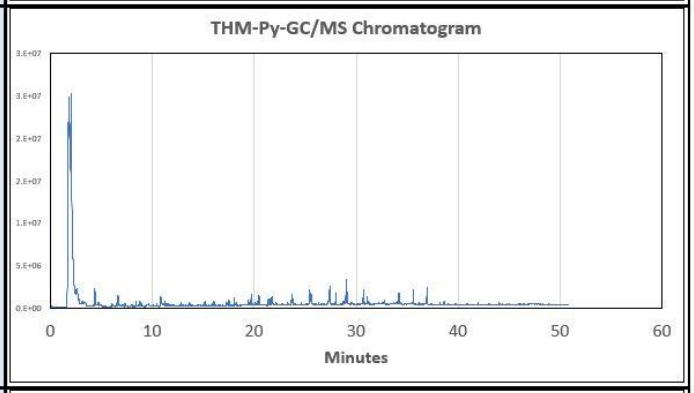
2051-S-04_04	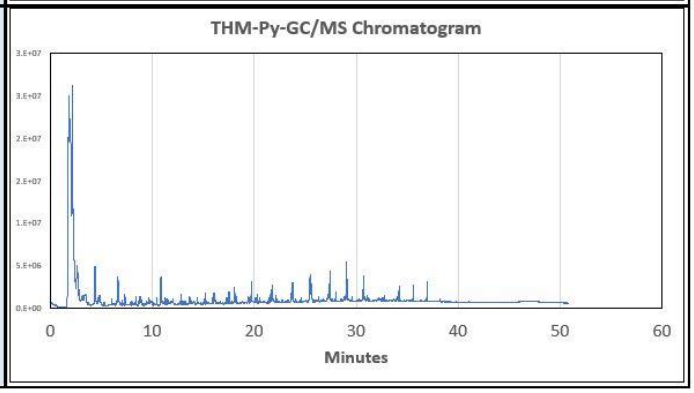

Sample Number	Chromatogram
2259-S-01_02-03	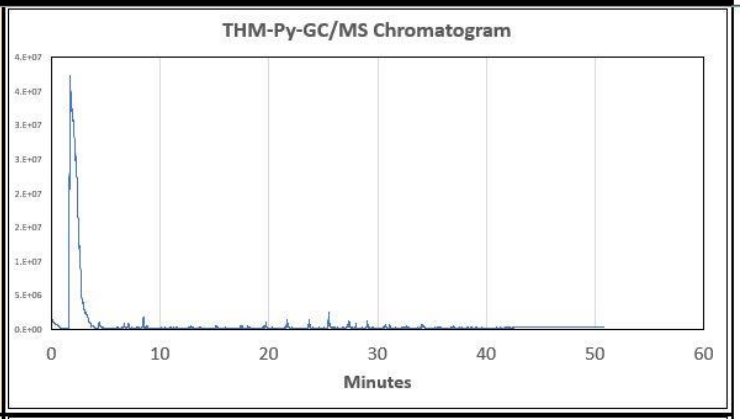
2259-S-01_04	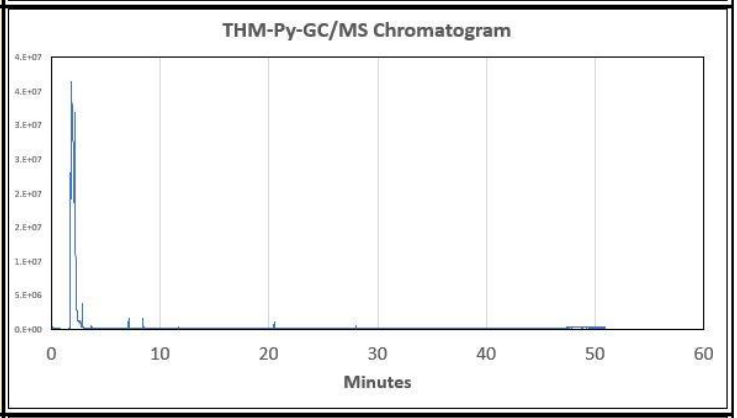
2259-S-01_05	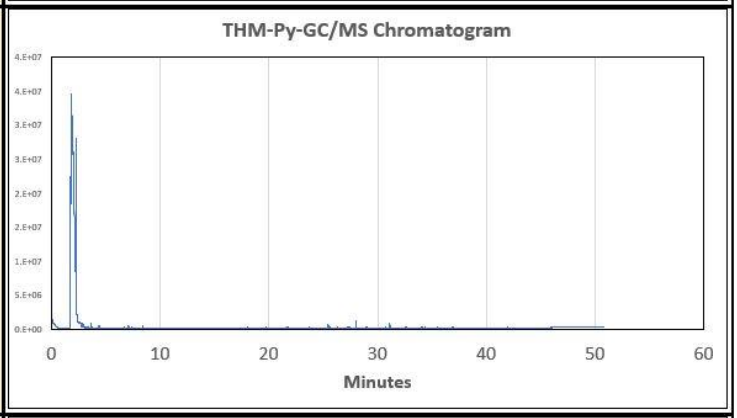
2259-S-01_06	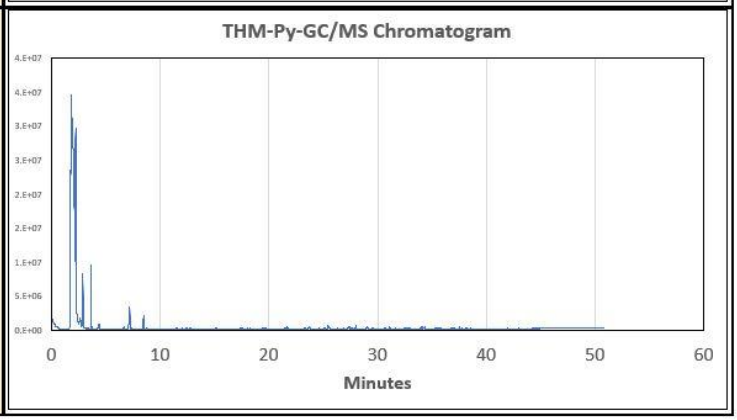

Sample Number	Chromatogram
2259-S-02 Top_01-04	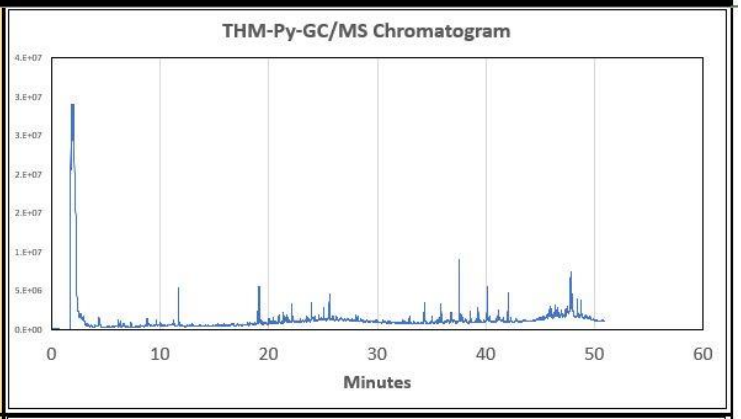
2259-S-02_05	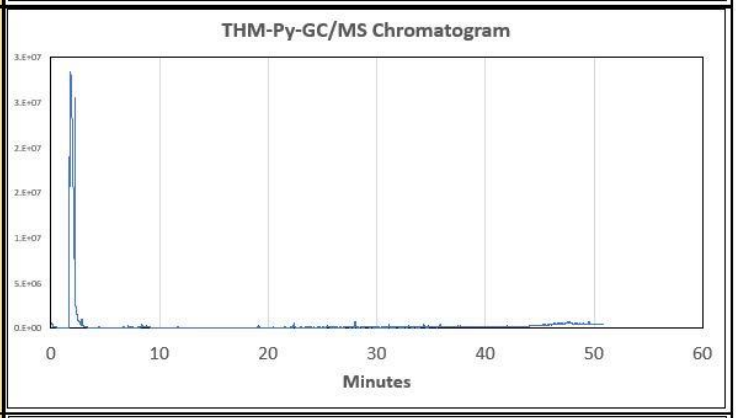
2259-S-02_07	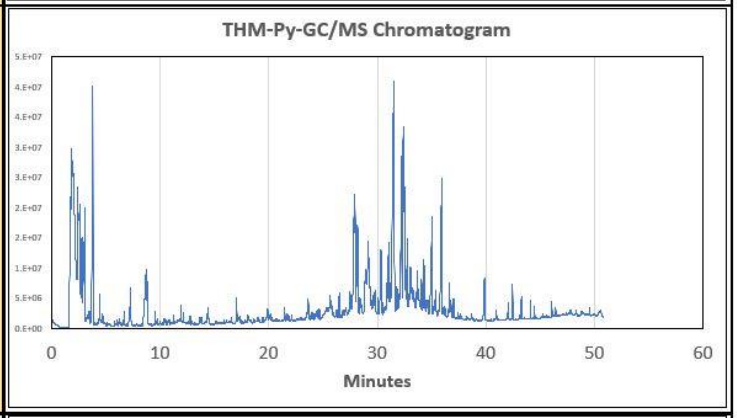
5509-W-03_01	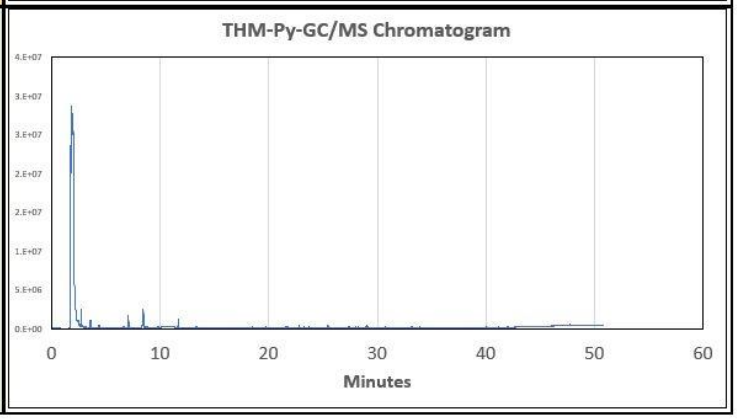

Sample Number	Chromatogram
5509-W-03_02	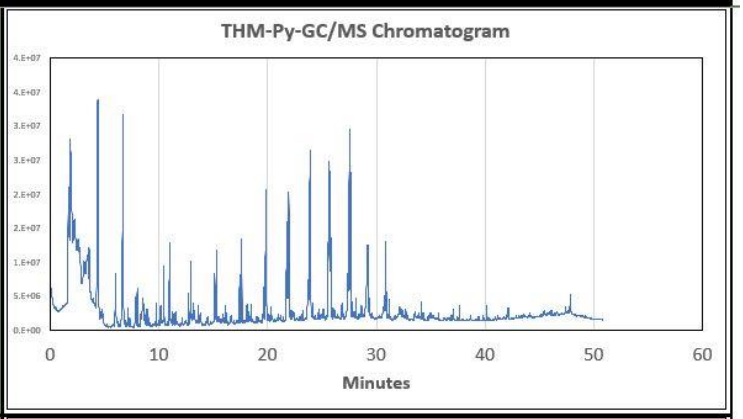
N509-S-01 Black	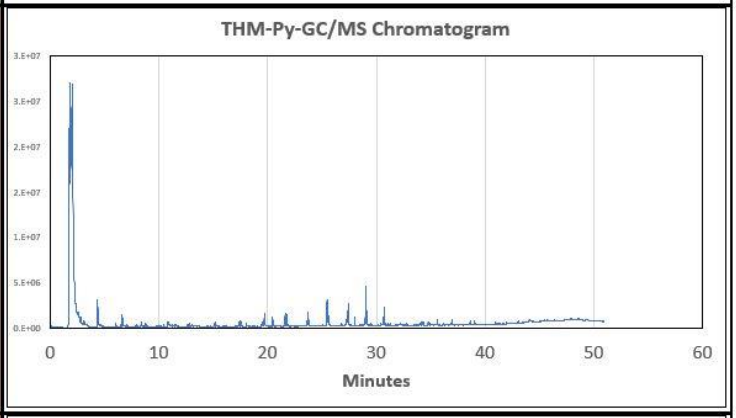
N509-S-01 Red	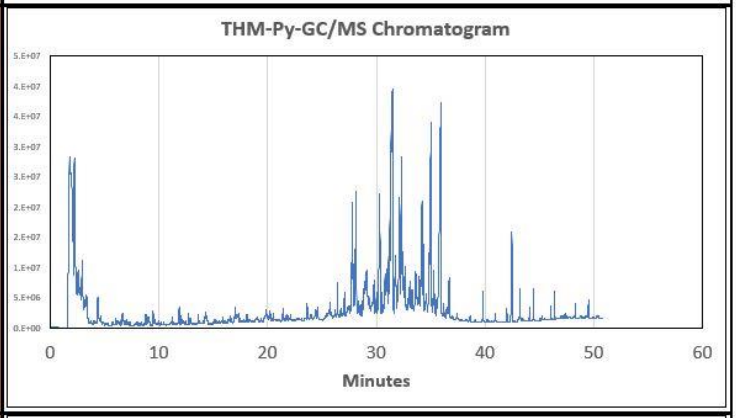
N509-S-02 Top_01	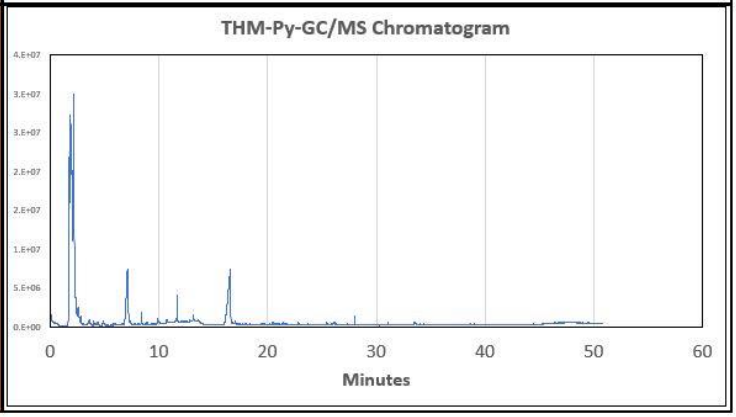

Sample Number	Chromatogram
N509-S-02 Top_02-04	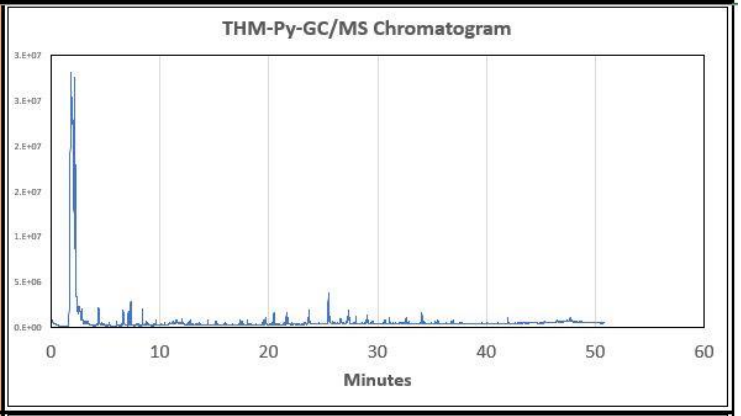
N509-S-02 Top_05	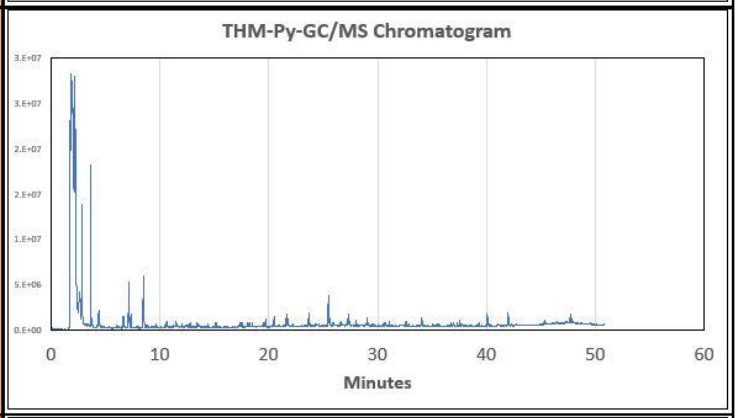
N509-S-02 Bottom	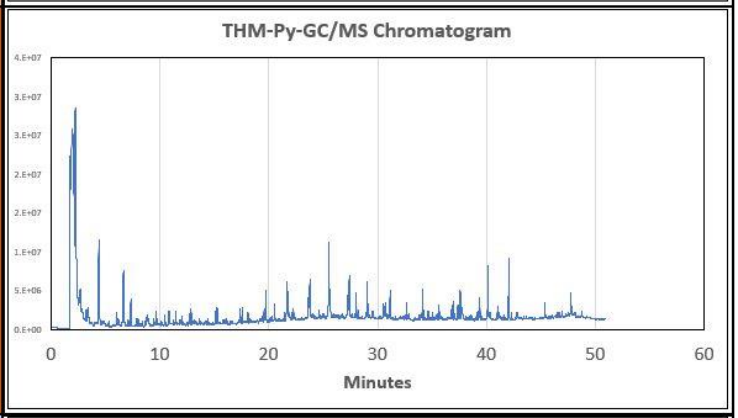
N1323-W-03 Top_01-02	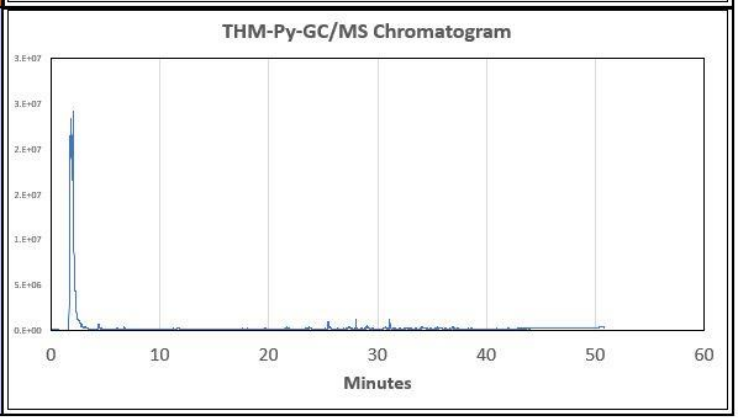

Sample Number	Chromatogram
N1323-W-03 Top_03	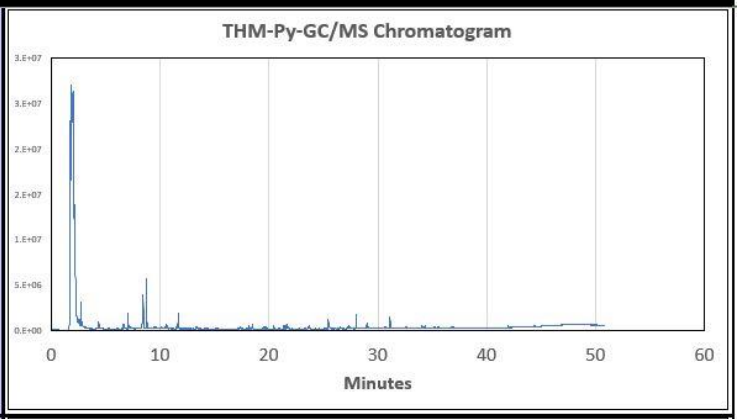
N1323-W-03 Top_04	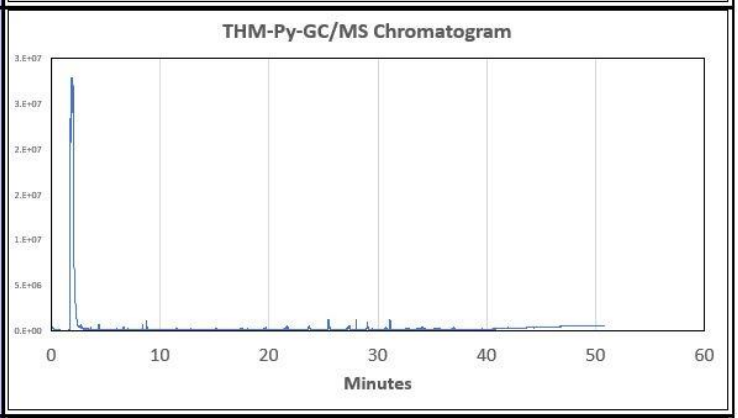
N1323-W-03 Bottom_01	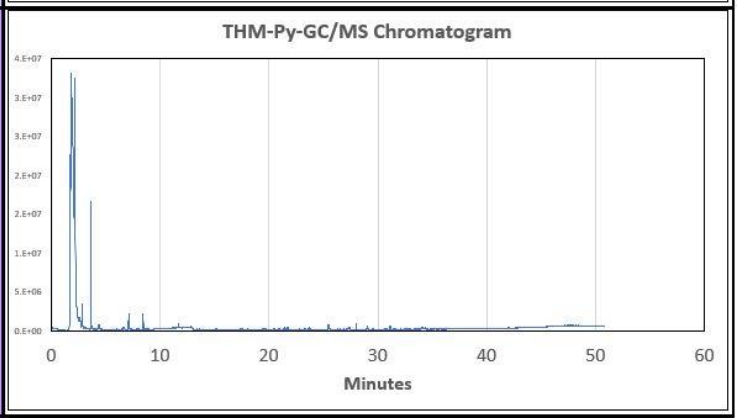
N1323-W-03 Bottom_03	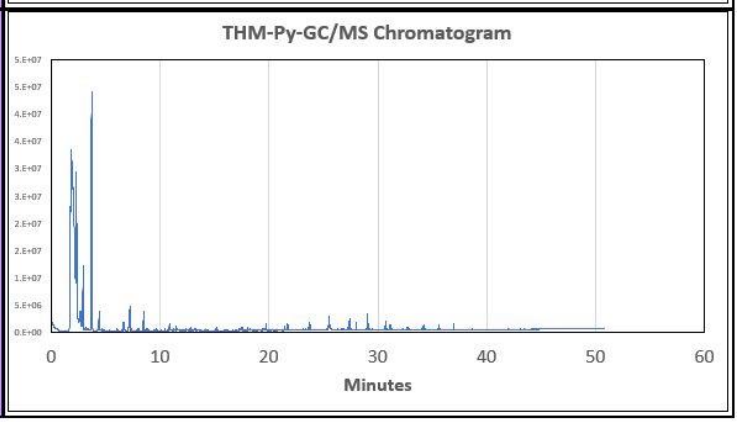

Appendix E: Pyrolysis-Gas Chromatography/Mass Spectrometry Data Visualization Graphs

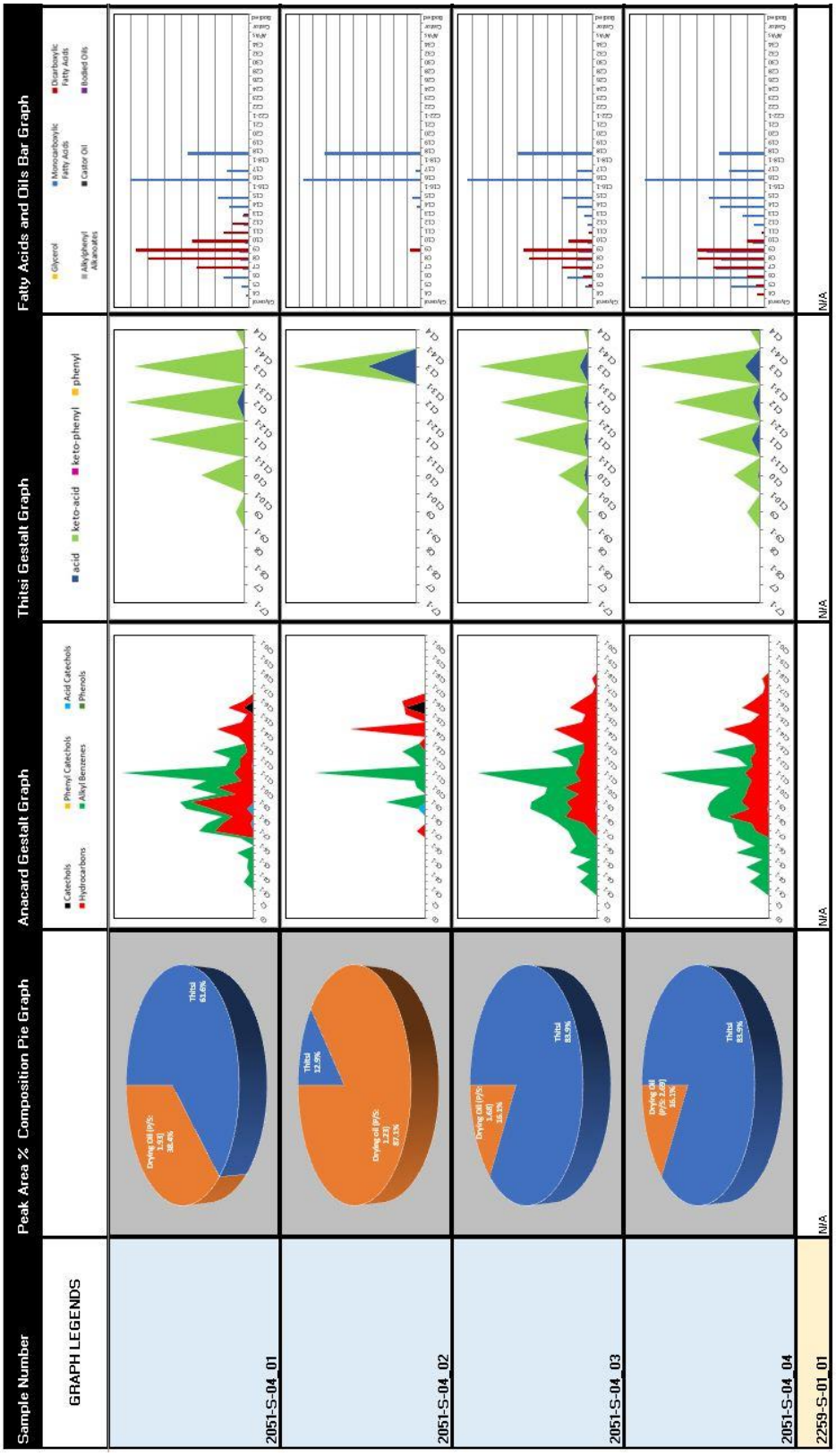

Sample Number	Peak Area % Composition Pie Graph	Anacard Gestalt Graph	Thitsi Gestalt Graph	Fatty Acids and Oils Bar Graph	Resins Pie Graph (if applicable)
GRAPH LEGENDS		■ Catechols ■ Phenyl Catechols ■ Acid Catechols ■ Hydrocarbons ■ Alkyl Benzenes ■ Phenols	■ acid ■ keto-acid ■ keto-phenyl ■ phenyl	■ Glycerol ■ Monocarboxylic Fatty Acids ■ Dicarboxylic Fatty Acids ■ Alkylphenyl Alkanoates ■ Castor Oil ■ Bodied Oils	
2259-S-01_02-03	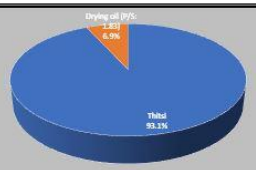	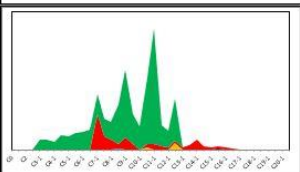	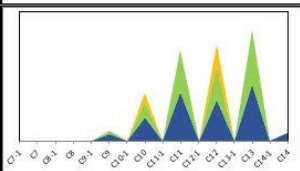	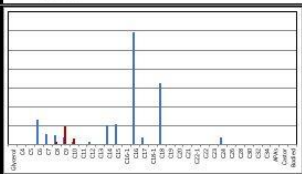	
2259-S-01_04	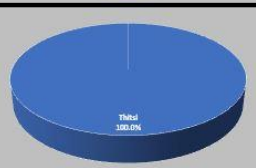	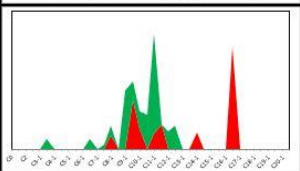	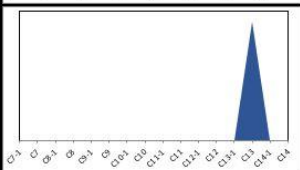	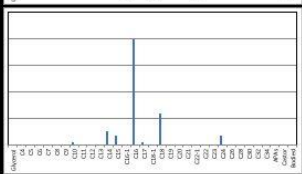	
2259-S-01_05	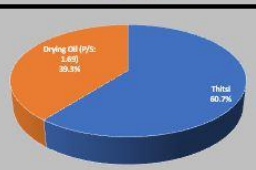	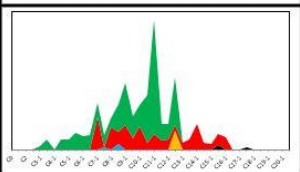	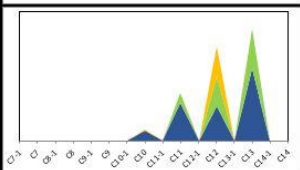	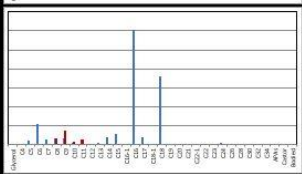	
2259-S-01_06	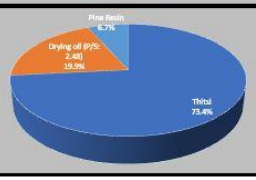	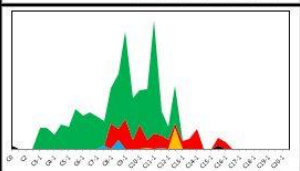	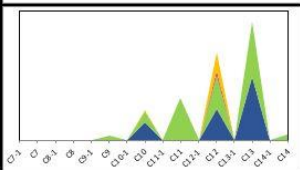	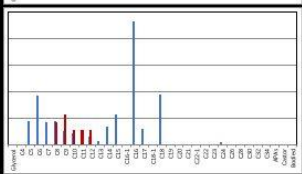	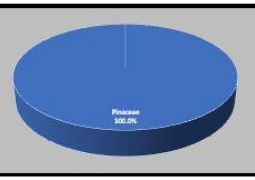

Sample Number	Peak Area % Composition Pie Graph	Anacard Gestalt Graph	Thitsi Gestalt Graph	Fatty Acids and Oils Bar Graph	Resins Pie Graph (if applicable)
GRAPH LEGENDS		■ Catechols ■ Phenyl Catechols ■ Acid Catechols ■ Hydrocarbons ■ Alkyl Benzenes ■ Phenols	■ acid ■ keto-acid ■ keto-phenyl ■ phenyl	■ Glycerol ■ Monocarboxylic Fatty Acids ■ Dicarboxylic Fatty Acids ■ Alkylphenyl Alkanoates ■ Castor Oil ■ Bodied Oils	
2259-S-02 Top_01-04	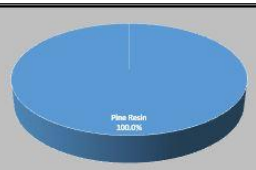	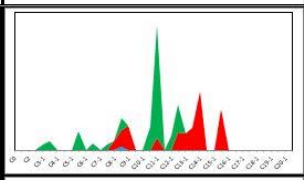	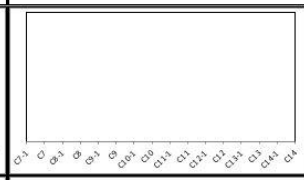	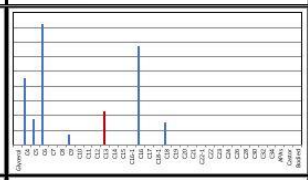	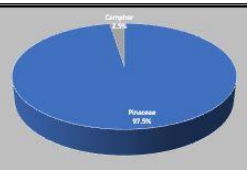
2259-S-02_05	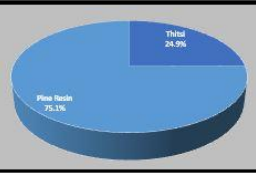	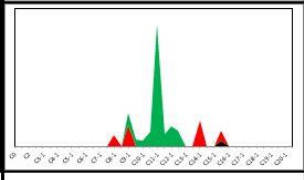	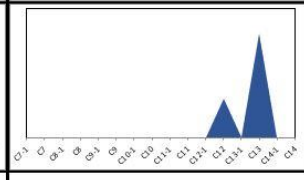	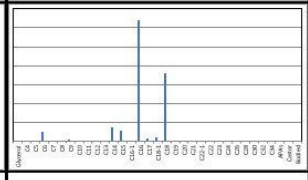	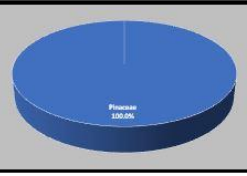
2259-S-02_06	N/A	N/A	N/A	N/A	N/A
2259-S-02_07	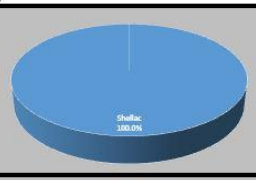	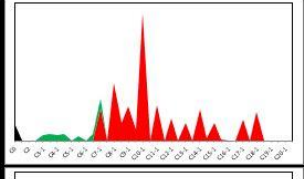	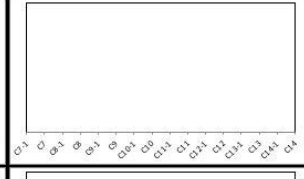	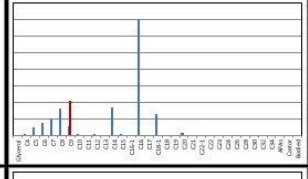	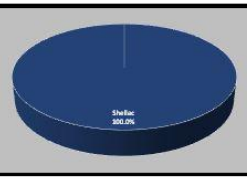
5509-W-03_01	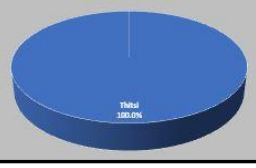	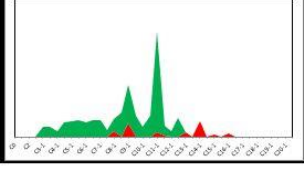	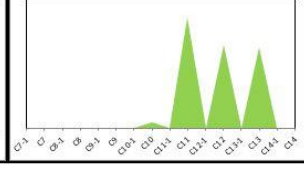	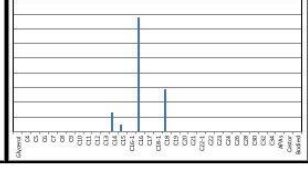	

Sample Number	Peak Area % Composition Pie Graph	Anacard Gestalt Graph	Thitsi Gestalt Graph	Fatty Acids and Oils Bar Graph	Resins Pie Graph (if applicable)	Wax Bar Graph (if applicable)
GRAPH LEGENDS		■ Catechols ■ Phenyl Catechols ■ Acid Catechols ■ Hydrocarbons ■ Alkyl Benzenes ■ Phenols	■ acid ■ keto-acid ■ keto-phenyl ■ phenyl	■ Glycerol ■ Monocarboxylic Fatty Acids ■ Dicarboxylic Fatty Acids ■ Alkylphenyl Alkanoates ■ Castor Oil ■ Bodied Oils		■ Hydrocarbon ■ Ester ■ Fatty Alcohol ■ Hydroxy Fatty Acids
5509-W-03_02	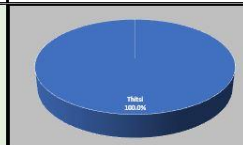	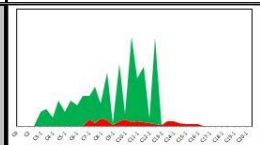	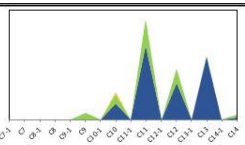	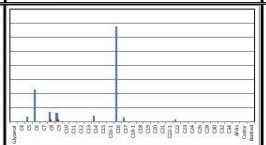		
N509-S-01 Black	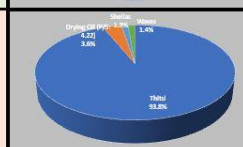	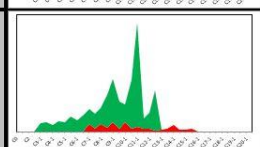	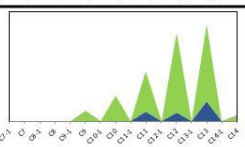	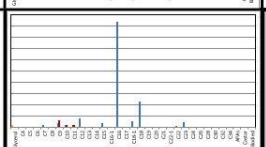	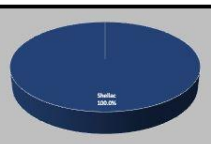	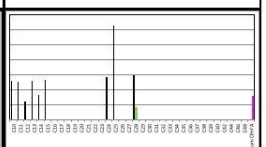
N509-S-01 Red	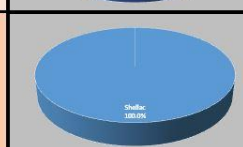	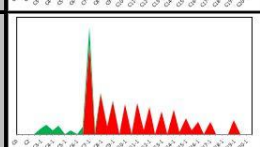	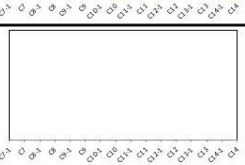	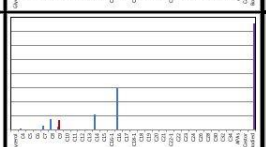	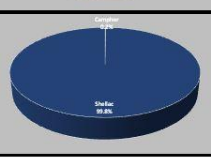	
N509-S-02 Top_01	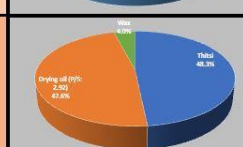	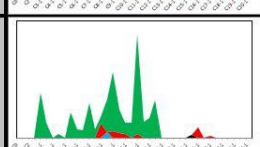	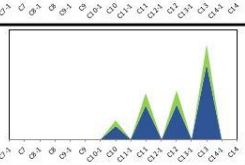	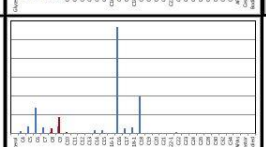		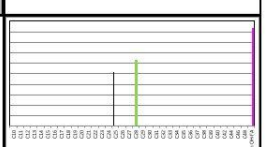

Sample Number	Peak Area % Composition Pie Graph	Anacard Gestalt Graph	Thitsi Gestalt Graph	Fatty Acids and Oils Bar Graph
GRAPH LEGENDS		■ Catechols ■ Phenyl Catechols ■ Acid Catechols ■ Hydrocarbons ■ Alkyl Benzenes ■ Phenols	■ acid ■ keto-acid ■ keto-phenyl ■ phenyl	■ Glycerol ■ Monocarboxylic Fatty Acids ■ Dicarboxylic Fatty Acids ■ Alkylphenyl Alkanoates ■ Castor Oil ■ Bodied Oils
N509-S-02 Top_02-04	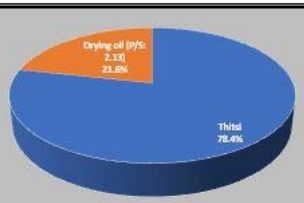	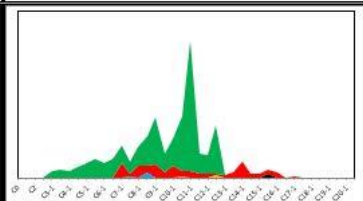	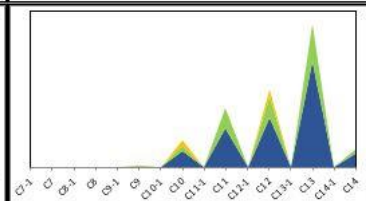	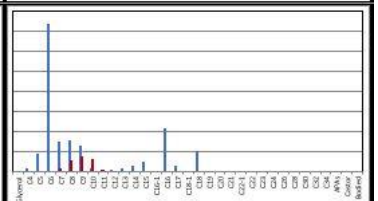
N509-S-02 Top_05	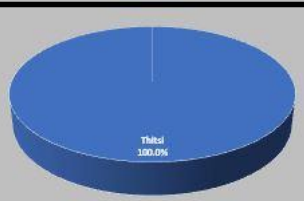	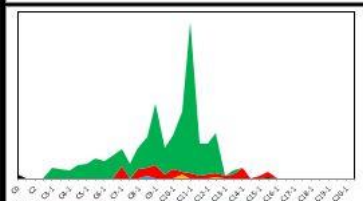	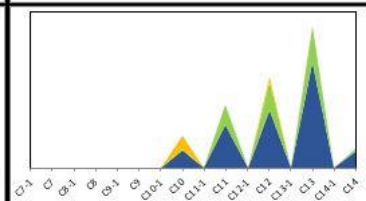	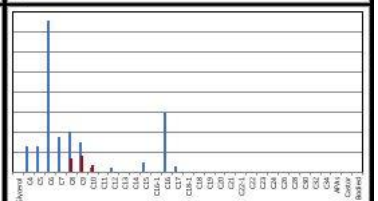
N509-S-02 Bottom	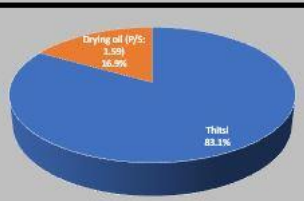	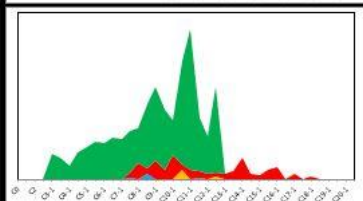	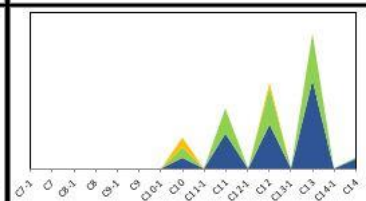	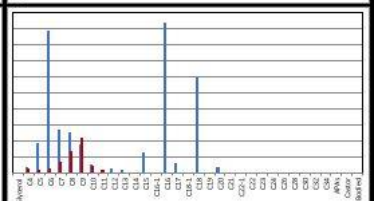
N1323-W-03 Top_01-02	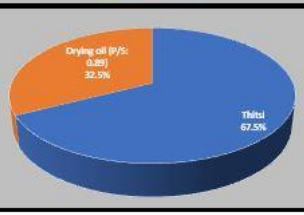	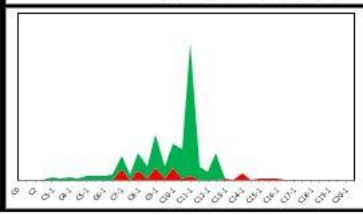	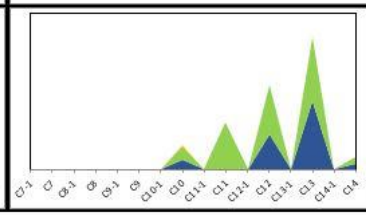	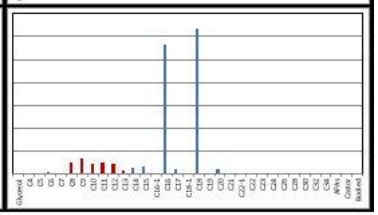

Sample Number	Peak Area % Composition Pie Graph	Anacard Gestalt Graph	Thitsi Gestalt Graph	Fatty Acids and Oils Bar Graph
GRAPH LEGENDS		Catechols; Phenyl Catechols; Acid Catechols; Hydrocarbons; Alkyl Benzenes; Phenols	acid; keto-acid; keto-phenyl; phenyl	Glycerol; Monocarboxylic Fatty Acids; Dicarboxylic Fatty Acids; Alkylphenyl Alkanoates; Castor Oil; Bodied Oils
N1323-W-03 Top_03	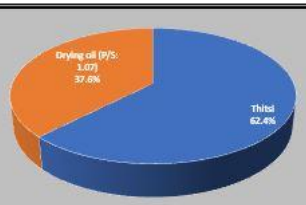	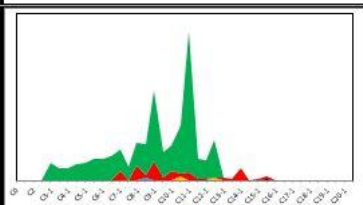	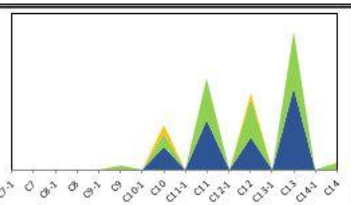	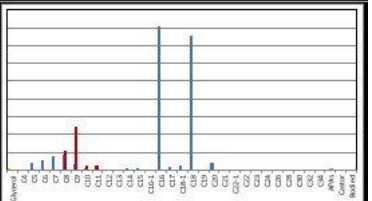
N1323-W-03 Top_04	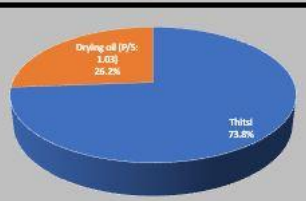	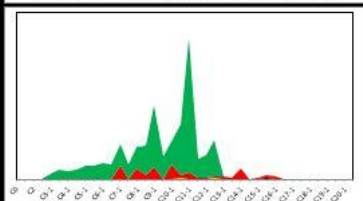	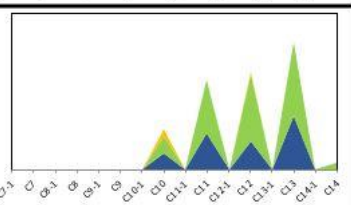	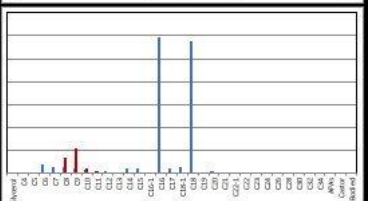
N1323-W-03 Bottom_01-02	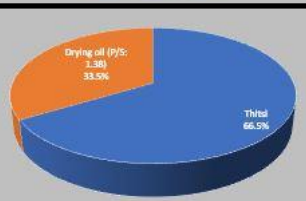	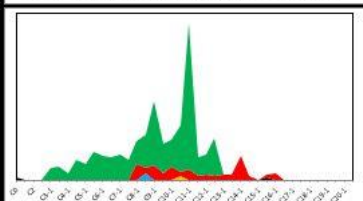	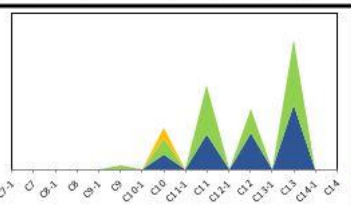	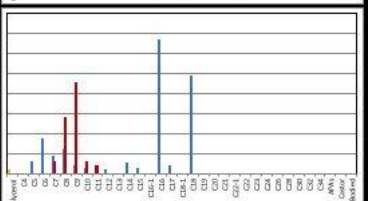
N1323-W-03 Bottom_03	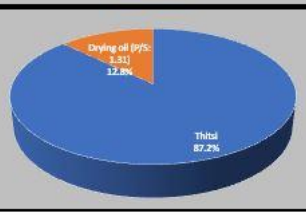	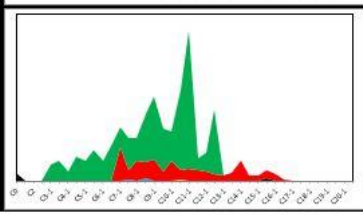	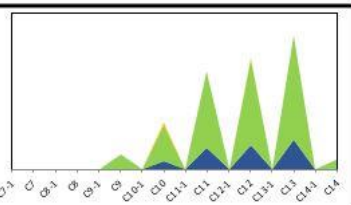	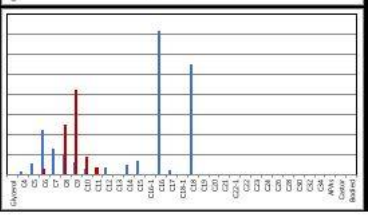

References

Arbace, L., Sonnino, E., Callieri, M., Dellepiane, M., Fabbri, M., Iaccarino Idelson, A., & Scopigno, R. (2013). Innovative uses of 3D digital technologies to assist the restoration of a fragmented terracotta statue. *Journal of Cultural Heritage*, *14*(4), 332–345. https://doi.org/10.1016/j.culher.2012.06.008

Bai, G., Chen, C., Zhao, C., Zhou, T., Li, D., Zhou, T., Li, W., Lu, Y., Cong, X., Jia, Y., & Li, S. (2022). The chromosome-level genome for Toxicodendron vernicifluum provides crucial insights into Anacardiaceae evolution and urushiol biosynthesis. *iScience*, *25*(7), 104512. https://doi.org/10.1016/j.isci.2022.104512

Burgess, M. (2018). *Digitizing Conservation: Incorporating digital technologies to the reconstruction and loss compensation of archaeological ceramics*. University of California, Los Angeles.

Caruso, F., Chillura Martino, D. F., Saverwyns, S., Van Bos, M., Burgio, L., Di Stefano, C., Peschke, G., & Caponetti, E. (2014). Micro-analytical identification of the components of varnishes from South Italian historical musical instruments by PLM, ESEM–EDX, microFTIR, GC–MS, and Py–GC–MS. *Microchemical Journal*, *116*, 31–40. https://doi.org/10.1016/j.microc.2014.04.002

Cooper, C. (2019). You Can Handle It: 3D Printing for Museums. *Advances in Archaeological Practice*, *7*(4), 443–447. https://doi.org/10.1017/aap.2019.39

Daniels, D. (2022, May 19). *Conversation with Doug Daniels, Head of Lux Labs at University of California, Los Angeles* [Personal communication].

Dassault Systèmes. (2023). *3D Printing—Additive*. 3DExperience Marketplace | Make. https://make.3dexperience.3ds.com/processes/binder-jetting

Derry, J. (2012). *Investigating Shellac: Documenting the Process, Defining the Product*. University of Oslo.

Dyrmose, A.-M. H., Turreira-García, N., Theilade, I., & Meilby, H. (2017). Economic importance of Oleoresin (Dipterocarpus alatus) to forest-adjacent households in Cambodia. *Natural History Bulletin: Siam Society*, *62*(1), 67–84.

Farrar, B. (2020, February 15). *Conversation with BJ Farrar, Senior Mountmaker at Getty Villa* [Personal communication].

Garland, K., Spence, S., & North, B. (2018). Loss compensation on ceramics using photogrammetry, digital modeling and 3D printing. *Objects Specialty Group Postprints*, *25*.

Giteau, M. (1975). *Iconographie du Cambodge Post-Angkorian: Vol. C*. Ecole Française d'Extrême-Orient.

Han, J., Webb, M., Hao, X., Khanjian, H., & Schilling, M. R. (2023). Surface appearance and morphology changes of Asian lacquer due to artificial aging: Impacts of traditional additives. *Journal of Cultural Heritage*, *63*, 249–262. https://doi.org/10.1016/j.culher.2023.08.010

Hang, C. (2022, October 4). *Conversation with Hang Chansophea, Conservator at Angkor Conservation Offices* [Personal communication].

Heginbotham, A., Chang (張倚竹), J., Khanjian, H., & Schilling, M. R. (2016). Some observations on the composition of Chinese lacquer. *Studies in Conservation*, *61*(sup3), 28–37. https://doi.org/10.1080/00393630.2016.1230979

Heginbotham, A., & Schilling, M. (2009). *New evidence for the use of Southeast Asian raw materials in seventeenth-century Japanese export lacquer*. https://doi.org/10.13140/2.1.1167.4242

Henriques, F. (2020). Restoration of an 18th century frame: 3D modelling, printing and matching color of decorative flowers elements. *Ge-Conservacion*, *18*(1), 313–322. https://doi.org/10.37558/gec.v18i1.854

Hu, J. (2017). New exploration of the styles and techniques of luodian bronze mirrors. *Zhongyuan Wenwu*, *3*, 88–97.

IDZone. (2019, February 17). *3D Prints Enter the Kitchen – A Guide for Food-Safe 3D Printing*. https://idzoneblog.wordpress.com/2019/02/17/food-safe-3d-printing/

Index of /TAZ/accessories/halibut. (n.d.). Retrieved September 5, 2023, from https://devel.lulzbot.com/TAZ/accessories/halibut/

Ishimura, T., & Yoshida, T. (2015). Polymerization of Oriental Lacquer (Urushi) with Epoxidized Linseed Oil as a New Reactive Diluent. *International Journal of Polymer Science*, *2015*, 1–7. https://doi.org/10.1155/2015/782843

Koumari, L. (2022, April 25). What is Concrete 3D Printing? *Parametric Architecture*. https://parametric-architecture.com/what-is-concrete-3d-printing/

Kumanotani, J. (1995). Urushi (oriental lacquer)—A natural aesthetic durable and future-promising coating. *Progress in Organic Coatings*, *26*(2), 163–195. https://doi.org/10.1016/0300-9440(95)00559-5

Lanaro, M., Desselle, M. R., & Woodruff, M. A. (2019). 3D Printing Chocolate. In *Fundamentals of 3D Food Printing and Applications* (pp. 151–173). Elsevier. https://doi.org/10.1016/B978-0-12-814564-7.00006-7

Lawless, R. (2023, March 20). *Ceramic 3D Printing: Clay 3D Printing Simply Explained*. All3DP. https://all3dp.com/2/ceramic-3d-printing-clay-simply-explained/

Lee, H. S., & Wi, K. C. (2015). Restoration of Earthenware & Porcelain Cultural Assets using 3D Printing. *Journal of the Korean Conservation Science for Cultural Properties*, *31*(2), 131–145. https://doi.org/10.12654/JCS.2015.31.2.06

Liu, W., Liu, X., & Lv, J. (2023). Comparative Study on UV Degradation of Black Chinese Lacquers with Different Additives. *Materials*, *16*(16), 5607. https://doi.org/10.3390/ma16165607

Lu, R., & Miyakoshi, T. (2015). History of lacquer chemistry. In *Lacquer Chemistry and Applications*. Elsevier. https://doi.org/10.1016/B978-0-12-803589-4.00002-X

Lu, R., Yoshida, T., & Miyakoshi, T. (2013). Oriental Lacquer: A Natural Polymer. *Polymer Reviews*, *53*(2), 153–191. https://doi.org/10.1080/15583724.2013.776585

Ly, V. (2021). Traditional Use of Lacquer in Cambodia. *International Journal of Asian-Pacific Heritage Studies*.

MANUFACTUR3D. (2018, February 13). 3D Printing Technology Choice: FDM v/s SLA v/s SLS. *MANUFACTUR3D*. https://manufactur3dmag.com/3d-printing-technology-choice-fdm-v-s-sla-v-s-sls/

Mcsharry, C., Faulkner, R., Rivers, S., Shaffer, M. S. P., & Welton, T. (2007). The chemistry of East Asian lacquer: A review of the scientific literature. *Studies in Conservation*, *52*(sup1), 29–40. https://doi.org/10.1179/sic.2007.52.Supplement-1.29

Neumuller, M., Reichinger, A., Rist, F., & Kern, C. (2014). 3D Printing for Cultural Heritage: Preservation, Accessibility, Research and Education. In M. Ioannides & E. Quak, *3D Research Challenges in Cultural Heritage: A Roadmap in Digital Heritage Preservation* (pp. 119–134). Springer-Verlag Berlin Heidelberg.

Obataya, E., Furuta, Y., Ohno, Y., Norimoto, M., & Tomita, B. (2002). Effects of aging and moisture on the dynamic viscoelastic properties of oriental lacquer (urushi) film. *Journal of Applied Polymer Science*, *83*(11), 2288–2294. https://doi.org/10.1002/app.2321

Okino, E., Ogawa, T., & Oyabu, M. (2016). Charcteristics of Urushiol Film Cured by UV Irradiation. *Journal of The Adhesion Society of Japan*, *52*(12), 365–371. https://doi.org/10.11618/adhesion.52.365

Open Source Syringe Pump—Filament. (2014, August 1). LulzBot. https://forum.lulzbot.com/t/open-source-syringe-pump/678/8

Porte, B. (2002). La remise au jour du Buddha de Vat Kompong Luong. *Arts asiatiques*, *57*(1), 219–222. https://doi.org/10.3406/arasi.2002.1491

Richrap3d. (2012, April 6). Reprap development and further adventures in DIY 3D printing: Universal Paste extruder - Ceramic, Food and Real Chocolate 3D Printing. *Reprap Development and Further Adventures in DIY 3D Printing*. https://richrap.blogspot.com/2012/04/universal-paste-extruder-ceramic-food.html

Runkel, S., Leisen, H., von Plehwe-Leisen, E., & Fuchs, R. (2012). Interior Polychromy and Wall Paintings in Khmer Brick Temples of the 9th and 10th Century in Cambodia. In M. L. Tjoa-Bonatz, A. Reinecke, & D. Bonatz (Eds.), *Connecting Empires and States: Selected Papers from the 13th International Conference of the European Association of Southeast Asian Archaeologists*. https://doi.org/10.2307/j.ctv1ntg9b

Schellmann, N. (2011). Delamination and flaking of East Asian export lacquer coatings on wood substrates. In S. Rivers (Ed.), *East Asian lacquer: Material culture, science and conservation = Tōyō shikki: Sono bunkashi, kagaku to hozon shūfuku* (pp. 107–120). Archetype Books.

Schilling, M. (2023, August 3). *Conversation with Michael Schilling, Head of Materials Characterization research at the Getty Conservation Institute* [Personal communication].

Schilling, M. R., Heginbotham, A., Van Keulen, H., & Szelewski, M. (2016). Beyond the basics: A systematic approach for comprehensive analysis of organic materials in Asian lacquers. *Studies in Conservation*, *61*(sup3), 3–27. https://doi.org/10.1080/00393630.2016.1230978

Schmid, M. (1963). *Note sur la vegetation de la region de Siemreap*. EFEO Paris.

Sitha, A. (2002). Cambodian lacquer art and Khmer lacquerware. In M. Kopplin (Ed.), *Lacquerware in Asia, today and yesterday*. UNESCO.

Sok, S. (2022, October 30). *Conversation with Sok Soda, Stone Sculpture Conservator at National Museum of Cambodia* [Personal communication].

Stocker, E. (2022, September 15). *Conversation with Eric Stocker, Master Lacquerer at Stocker Studios* [Personal communication].

Sung, Y. J., Shin, S. J., & Oh, M.-T. (2009). Chemical Composition of Rice Hull and Morphological Properties of Rice Hull Fibers. *Journal of Korea TAPPI*, *41*(3), 22–28.

Szczepanowska, H., & Ploeger, R. (2019). The chemical analysis of Southeast Asian lacquers collected from forests and workshops in Vietnam, Cambodia, and Myanmar. *Journal of Cultural Heritage*, *40*, 215–225. https://doi.org/10.1016/j.culher.2019.05.015

Tamburini, D., Pescitelli, G., Colombini, M. P., & Bonaduce, I. (2017). The degradation of Burmese lacquer (thitsi) as observed in samples from two cultural artefacts. *Journal of Analytical and Applied Pyrolysis*, *124*, 51–62. https://doi.org/10.1016/j.jaap.2017.02.023

Thompson, A. (2004). Pilgrims to Angkor: A Buddhist «Cosmopolis» in Southeast Asia? *Bulletin of the Students of the Department of Archaeology*, *3*.

Uchida, E., Takubo, Y., Toyouchi, K., & Miyata, J. (2012). Study on the pigments in the Cruciform Gallery of Angkor Wat, Cambodia: Pigments in the cruciform gallery of Angkor Wat, Cambodia. *Archaeometry*, *54*(3), 549–564. https://doi.org/10.1111/j.1475-4754.2011.00634.x

UNSW Making. (2023). *3D Printing: SLA*. UNSW Sydney. https://www.making.unsw.edu.au/learn/3d-printing-with-sla-resin-printers/

Wang, Q., Chen, Y., & Tamburini, D. (2020). Was Lacquer the Key Ingredient for Luxurious *Jinyin Pingtuo* Products in the Tang Dynasty of China (AD 618–907)? *Archaeometry*, *62*(3), 646–659. https://doi.org/10.1111/arcm.12545

Warrack, S. (2011). Learning from Local Leaders: Working Together toward the Conservation of Living Heritage at Angkor Wat, Cambodia. *Change Over Time*, *1*(1), 34–51.

Warrack, S. (2013). Developing Conservation Approaches to Living Heritage at Angkor: The Conservation of the Statue of Ta Reach. In M. Falser & M. Juneja (Eds.), *"Archaeologizing" Heritage?* (pp. 217–233). Springer Berlin Heidelberg. https://doi.org/10.1007/978-3-642-35870-8

Webb, M. (2000). *Lacquer: Technology and conservation: a comprehensive guide to the technology and conservation of Asian and European lacquer*. Butterworth-Heinemann.

Webb, M. (2011). The autofluorescence of Asian lacquer. In S. Rivers (Ed.), *East Asian lacquer: Material culture, science and conservation = Tōyō shikki: Sono bunkashi, kagaku to hozon shūfuku* (pp. 148–158). Archetype Books.

Webb, M. (2022, November 24). *Lacquer behavior on Buddhist statues* [Personal communication].

Webb, M., Schilling, M. R., & Chang (張倚竹), J. (2016). The reproduction of realistic samples of Chinese export lacquer for research. *Studies in Conservation*, *61*(sup3), 155–165. https://doi.org/10.1080/00393630.2016.1227116

Xia, J., Xu, Y., & Lin, J. (2010). UV-induced polymerization of urushiol. II: Effects of hydrogenation degree of urushiol on surface morphology. *Progress in Organic Coatings*, *67*(3), 365–369. https://doi.org/10.1016/j.porgcoat.2009.12.004

Zhao, M., Liu, C., Zheng, G., Wei, S., & Hu, Z. (2013). Comparative studies of bark structure, lacquer yield and urushiol content of cultivated *Toxicodendron vernicifluum* varieties. *New Zealand Journal of Botany*, *51*(1), 13–21. https://doi.org/10.1080/0028825X.2012.731005